Development of a Field Portable Mass Spectrometer for Quantitative Analysis of Volatile Organic Compounds in Air

by

Nicholas G. Davey
B.Sc., Vancouver Island University, 2007

A Dissertation Submitted in Partial Fulfillment of the
Requirements for the Degree of

DOCTOR OF PHILOSOPHY

in the Department of Chemistry

© Nicholas G. Davey, 2016
University of Victoria

All rights reserved. This dissertation may not be reproduced in whole or in part, by photocopying or other means, without the permission of the author.

Supervisory Committee

Development of a Field Portable Mass Spectrometer for Quantitative Analysis of Volatile Organic Compounds in Air

by

Nicholas G. Davey
B.Sc., Vancouver Island University, 2007

Dr. Chris Gill, Co-Supervisor
(Department of Chemistry)

Dr. Tom Fyles, Co-Supervisor
(Department of Chemistry)

Dr. Scott McIndoe, Departmental Member
(Department of Chemistry)

Dr. Erik Krogh, Additional Member
(Department of Chemistry)

Dr. Jay Cullen, Outside Member
(School of Earth and Ocean Sciences)

Abstract

Supervisory Committee

Dr. Chris Gill, Co-Supervisor
(Department of Chemistry)

Dr. Tom Fyles, Co-Supervisor
(Department of Chemistry)

Dr. Scott McIndoe, Departmental Member
(Department of Chemistry)

Dr. Erik Krogh, Additional Member
(Department of Chemistry)

Dr. Jay Cullen, Outside Member
(School of Earth and Ocean Sciences)

The typical strategy for atmospheric analysis of volatile organic compounds (VOCs), is to collect discrete samples which are then transported to a laboratory for analysis. This method has limited spatial and temporal resolution, and can be both costly and time consuming. To overcome these limitations, a mobile monitoring platform was developed for real-time quantitative chemical analysis. This work describes the development of membrane introduction mass spectrometer and identifies the necessary requirements to make a reliable and effective instrument for *in-situ* chemical analysis. These include, the integration of a membrane interface with a miniaturized mass spectrometer, development of a data management strategy, reducing the effects of isobaric interferences and employing an internal standard for quantitative measurements. Furthermore, the negative effects of environmental variables, such as the Earth's magnetic field, were examined and effectively eliminated. In addition, this work demonstrates quantitative mapping of atmospheric VOCs in real-time, which allows rapid identification of chemical plumes and therefore, areas of potential concern. Both lab and field-based comparisons of

membrane introduction mass spectrometer data and traditional whole air sampling canister data were undertaken. The primary field site was near Ft. McMurray, AB where baseline data was collected around a steam assisted gravity drainage (SAGD) facility and surrounding public roads. Monitoring for fugitive emissions at this facility and surrounding bitumen mining and processing operations is demonstrated. Field data were also obtained, near an industrial site in Ft.Saskatchewan, AB, that demonstrate the efficacy of an adaptive sampling strategy. Finally, chemical ionization was investigated as a soft ionization strategy to improve chemical selectivity for the analysis of complex hydrocarbon mixtures. The development of an in-line liquid chemical ionization reagent delivery system is presented and proposed as an effective strategy for eliminating interferences arising from biogenic terpenes and alkyl aromatics. In all, this thesis presents the design and implementation of a mobile membrane introduction mass spectrometer for atmospheric chemical analysis. Results that improve performance and demonstrate the novelty of the data-type are provided, along with avenues for future development.

Contents

Supervisory Committee **ii**

Abstract **iii**

Table of Contents **v**

List of Symbols and Definitions **ix**

List of Tables **xi**

List of Figures **xii**

Acknowledgements **xvi**

Dedication **xvii**

1 Motivations **1**

2 Membrane Introduction Mass Spectrometry (MIMS) **7**

2.1 Introduction 7

2.2 Advances in MIMS instrumentation 9

2.2.1 Membrane improvements–materials and configurations 9

2.2.2 Mass spectrometry improvements – ionization 12

2.2.3 Mass spectrometry improvements – miniaturization 14

2.3 Advances in MIMS for on-site environmental monitoring 14

2.4 Advances in *in vivo* monitoring 19

2.5 Conclusions 20

3 Measurement of spatial and temporal variation in volatile hazardous air pollutants **21**

3.1 Introduction 21

3.2 Materials and methods 23
3.2.1 Sampling Schemes 23
3.2.2 MIMS Instrumentation 26
3.2.3 Statistical Analysis 28
3.3 Results and discussion 28
3.4 Conclusions 36

4 Real-time Quantitation and Spatial Mapping of Atmospheric and Aqueous Contaminants 38
4.1 Introduction 38
4.2 Methods and Materials 41
4.2.1 Overview 41
4.2.2 Membrane Introduction Mass Spectrometer 41
4.2.3 Gaseous Sampling 42
4.2.4 Aqueous Sampling 47
4.2.5 Software Development 48
4.2.6 Field Work Methods 51
4.3 Results and Discussion 51
4.3.1 Field Work–Air Monitoring 51
4.3.2 Field Work–Aqueous Monitoring 59
4.3.3 Implications and Future Work 61
4.4 Conclusions 61

5 Combining Portable Mass Spectrometer and Whole Air Sampling Canister Data for Atmospheric Analysis 63
5.1 Introduction 63
5.2 Materials and Methods 65
5.2.1 Mass Spectrometer System 65
5.2.2 Dynacalibrator Gas Standard Generator 66
5.2.3 Air Sampling Canisters 67
5.2.4 Lab–Based Validation Study 67
5.2.5 Field Studies 68
5.3 Results and Discussion 69
5.3.1 Lab Based 69
5.3.2 Field Based 72

5.4 Conclusions 77

6 The Effect of the Earth's and Stray Magnetic Fields on Mobile Mass Spectrometer Systems 79

6.1 Introduction 79
6.2 Experimental 81
6.2.1 Mobile Mass Spectrometer Relative Response Versus Orientation 82
6.2.2 Electron Beam Deflection Simulations 84
6.2.3 Electron Beam Defocusing Studies 86
6.2.4 Magnetic Field Shielding Effects 87
6.3 Results 89
6.3.1 Mobile Mass Spectrometry Sensitivity Versus Directional Bearing 89
6.3.2 Ion Source Simulations 91
6.3.3 Reducing the Relative Response Variability 94
6.4 Discussion 95
6.5 Conclusions 99

7 Ion–Molecule Reactions for the Reduction of Isobaric Interferences in Ion Trap Mass Spectrometers 100

7.1 Introduction 100
7.2 Experimental 103
7.3 Results and Discussion 105
7.4 Conclusions 112

8 Current status of portable MIMS and directions for future development 113

8.1 Portability 113
8.2 Data management 114
8.3 Isobaric interferences 115
8.4 Controlling environmental variables 116
8.5 Validation and expanding range of analytes 118

A Supplementary Material 120

B Field portable membrane introduction mass spectrometer–early developments 126

B.1 Design of membrane based sampling interface 126

B.2 Calibration 130
B.2.1 Direct calibration and MS/MS 130
B.2.2 Internal standard calibration 133
B.3 Improved sensitivity and response time 134

C Standard Operating Procedures: Field Portable Membrane Introduction Tandem Mass Spectrometer 137
C.1 Description of Application 137
C.2 Instrument Calibration 137
C.3 Pre-Deployment Direct Calibration 138
C.4 In-Field Direct Calibration 140
C.5 Field Sampling 140
C.6 Data Analysis Progression 142

Bibliography 146

List of Symbols and Definitions

Symbol	Units	Description
VOC		volatile organic compound
SVOC		semi-volatile organic compound
PDMS		polydimethylsiloxane
MIMS		membrane introduction mass spectrometry
ppb		part per billion
ppbv		part per billion by volume
MS/MS		tandem mass spectrometry
CID		collision induced dissociation
QIT		quadrupole ion trap
CIT		cylindrical ion trap
m/z		mass to charge ratio
GIS		graphical information system
WAS		whole air sampling
t_{10-90}		10-90% signal response time
GC-MS		gas chromatography mass spectrometry
HFM		hollow fiber membrane
MS		mass spectrometer
EI		electron ionization
CI		chemical ionization
APCI		atmospheric pressure chemical ionization
ESI		electrospray ionization
DCI-MIMS		desorption chemical ionization MIMS
SPI		single photon ionizaiton
ToF		time of flight
GPS		global positioning system
LOD/DL		limit of detection
PM		particulate matter

Symbol	Units	Description
SIM		selected ion monitoring
IS		internal standard
SAGD		steam assisted gravity drainage
R_i/R_o		inner/outer diameter
K_o	cc/mg	analyte constant
E	ng/min	emission rate
F	mL/min	gas flow

List of Tables

Table 3.1 Target VOCs and SVOCs monitored in air by MIMS. 27
Table 3.2 Spatial vatiation in VOC concentrations by route (ppbv) 30

Table 4.1 Summary of Mass Spectrometer Scan Methods and Analytical Performance Characteristics for Target Analytes 49

Table 5.1 Comparison of WAS canister and MIMS data for replicate gaseous standards. 71
Table 5.2 Comparison of WAS canister and MIMS data for isobaric gaseous standards. 73

Table 6.1 Parameters Varied Between Simulations of the CIT Ion Source . 88

Table 7.1 Major product ions and detection limits for a suite of volatile target analytes using different reagent gas ions 107

Table C.1 Griffin 400 operational settings for field deployment. 139
Table C.2 Typical set points for in-field calibration. 141

List of Figures

Figure 1.1 Membrane introduction mass spectrometry schematic. 2

Figure 2.1 Membrane-introduction mass spectrometry (MIMS) versus classical on-line methods 8
Figure 2.2 Membrane-introduction mass spectrometry interface configurations 10
Figure 2.3 Mass spectra for a mini-membrane-introduction mass spectrometry (MIMS) system 13
Figure 2.4 Mobile membrane-introduction mass spectrometry (MIMS) atmospheric monitoring data. 16
Figure 2.5 Underwater mobile membrane-introduction mass spectrometry (MIMS) monitoring data. 18

Figure 3.1 Map illustrating the three woodsmoke sampling routes in Tacoma, Washington, USA. 24
Figure 3.2 Map illustrating the three traffic sampling routes in Tacoma, Washington, USA. 25
Figure 3.3 $PM_{2.5}$ concentrations measured at the three fixed sites 29
Figure 3.4 Box plots illustrating benzene concentration ratios 33
Figure 3.5 Box plots illustrating benzene and toluene concentration ratios 35

Figure 4.1 Schematic of the field portable MIMS system 44
Figure 4.2 Comparison of Dynacalibrator and permeation chamber response. 45
Figure 4.3 Time series of real-time toluene quantitation 53
Figure 4.4 Google Earth snapshot of atmospheric toluene data collected north of Fort McMurray, Alberta, Canada. 56
Figure 4.5 Five-hour time series for atmospheric benzene, toluene, and ethylbenzene + xylenes (EtBz + Xyl). 58
Figure 4.6 In-field analysis of a heavy oil process water sample 60

Figure 5.1 Schematic of MIMS instrumentation and WAS canister configuration for both field and lab based validation studies. 66
Figure 5.2 Schematic of typical sequence of events for WAS canister and MIMS comparison experiment. 68
Figure 5.3 MIMS air data inter–comparison for ethylbenzene/xylene(s) 2012 74
Figure 5.4 MIMS air data inter–comparison for benzene 75
Figure 5.5 Chronograms of toluene, benzene and ethylbenzene concentrations near Ft.Saskatchewan, AB 76

Figure 6.1 SIMION® model approximating the CIT ion souce 85
Figure 6.2 Moving mass spectrometers' response to an internal standard plotted versus directional bearing. 90
Figure 6.3 Simulation of electron transmission of a vertical (a) and a horizontal (b) electron beam 91
Figure 6.4 Density maps indicating the xy location of electrons as they reach the ion trap endplate 93
Figure 6.5 Electron transmission versus Earth's field orientation under varied lens set-points 96
Figure 6.6 Electron transmission versus Earth's field orientation under varied magnetic field conditions. 97

Figure 7.1 Schematic of apparatus and instrument timing diagram for chemical ionization sampling interface 104
Figure 7.2 Comparison of EI and ion–molecule reaction spectra (CI) for mixture of benzene, toluene, toluened_8, ethylbenzene and pinene. 108
Figure 7.3 Effect of reaction time on both chloroform reagent ion (m/z 83) and ethylbenzene adduct ion (m/z 153) abundance. 109
Figure 7.4 Chloroform CI of benzene, toluene, ethylbenzene and –pinene mixture 110
Figure 7.5 Mixture analysis of 500 ppbv benzene (M1), 276 ppbv toluene (M2) and 280 ppbv ethylbenzene (M3) in air using chloroform as a chemical ionization reagent 111

Figure 8.1 Digital Elevation Model (DEM) of toluene–d_8 signal intensity variation with respect to elevation. 117

Figure A.1 Toluene concentrations at satellite sites, relative to the respective central site for each route 120
Figure A.2 Ethylbenzene concentrations at satellite sites, relative to the respective central site for each route 120
Figure A.3 Guaiacol concentrations at satellite sites, relative to the respective central site for each route 121
Figure A.4 Naphthalene concentrations at satellite sites, relative to the respective central site for each route 121
Figure A.5 Benzene concentrations at satellite sites, relative to the respective central site for each route 121
Figure A.6 Instrument response from an underwater mass spectrometer sampling ambient and hydrothermal vent water 122
Figure A.7 Pathways for common positive ion formation from different precursors in EI. 123
Figure A.8 Chloroform CI mass spectrum of benzene and proposed reaction pathway for adduct ion formation with $CHCl_2^+$ 124
Figure A.9 EI mass spectrum for ethylbenzene (50 ppbv). 124
Figure A.10 Chloroform reagent ion ($CHCl_2^+$) population as a function of reaction time with no analytes added to the system. 125
Figure A.11 Chloroform reagent ion (Rg) signal intensity depletion with increased concentration of ethylbenzene 125

Figure B.1 Modification of commercially available GC-MS. 127
Figure B.2 Customized MIMS. 128
Figure B.3 Customized interface housing. 129
Figure B.4 Instrument front panel. 130
Figure B.5 Calibration curve for toluene. 131
Figure B.6 Calibration curve for toluene-d_8. 132
Figure B.7 Chlorobenzene MS/MS with abundant water adduct. 133
Figure B.8 Permeation tube chamber for continuous infusion of an isotopically labelled internal standard. 134
Figure B.9 PDMS membrane with coiled NiCr heating element. 135
Figure B.10 The effect of electrical current on t_{10-90} for the analysis of a 160 ppb naphthalene solution. 135

Figure B.11Triple membrane interface design to increase sensitivity for trace level organics in air. 136

Figure C.1 Schematic of instrument calibration strategy for online analysis of VOCs in air. 138

Figure C.2 Schematic diagram of the instrumentation used for online analysis of VOCs in air. 142

Figure C.3 Sample time series showing conversion of raw counts to calibrated concentration for a toluene MS/MS scan. 145

ACKNOWLEDGEMENTS

This work is the result of tremendous efforts by many people. First, I express much appreciation to my major academic advisers, Dr. Chris Gill, Dr. Tom Fyles and Dr. Erik Krogh. Your guidance and support has fuelled my perseverance and greatly enriched my academic experience. I also express my appreciation to committee members Dr. Scott McIndoe and Dr. Jay Cullen for their valuable feedback. Funding for this research was from the Natural Science and Engineering Research Council of Canada (NSERC) and Statoil ASA. I also acknowledge Dr. Christian Collin-Hansen, for without his interest and efforts much of this work is would not have occurred.

During my time both as an undergraduate and graduate student, many past and present members of the Applied Environmental Research Laboratories (AERL) have helped in numerous ways and on numerous occasions to bring our lab into the field. It has been a great privilege to work with you: Jake Etzkorn, Sandy Thompson, Shakour Ghafouri, Megan Willis, Dana Short, Darien Yeung, Larissa Richards, Kyle Duncan and Dr. Ryan Bell. In particular, I thank Ryan for his willingness to share knowledge and his enthusiasm for the creation (with accompanying debris field) of new instrumentation. I also thank Owen Peer and the VIU Physics department first, for teaching me the basics of metalworking and second, for giving me, and others, free reign in the machine shop.

A special thanks to Morten Martinsen, with whom I have spent many long hours testing instrumentation in remotest northern Alberta; an experience I'm sure neither of us will soon forget.

DEDICATION

To Mom, Dad, Diena, Nissa and Malcolm.

"Nothing tends so much to the advancement of knowledge as the application of a new instrument."
–Sir Humphry Davy

Chapter 1

Motivations

With the development of portable mass spectrometers in recent years, has come new possibilities for environmental chemical analysis. The traditional model involves sampling, shipment to a laboratory, analysis, and finally, reporting an analytical result. This strategy can be extremely sensitive and selective, but generally suffers from low spatial and temporal resolution. In other words, analysts must decide exactly when, where and how often to sample. Also, environmental sampling protocols tend to be time–consuming, costly and often cannot provide information quickly enough to allow on–site decision making. In a dynamic system, like the atmosphere, real–time data collection from a mobile platform would be ideal for filling in data gaps in both spatial and temporal domains.

Mass spectrometers offer a combination of sensitivity, selectivity and high data density. When combined with various sample introduction and ionization strategies, mass spectrometers can provide a wide range of sophisticated chemical sensing possibilities in anything from environmental [1] to *in vivo* [2] applications. Membrane introduction is a sample introduction strategy for mass spectrometry that employs a semi–permeable polymer membrane, typically polydimethylsiloxane (PDMS), that is permeable to non–polar, volatile and semi–volatile organic compounds (VOCs/SVOCs). Figure 1.1 illustrates the typical configuration and versatility of a membrane introduction mass spectrometry (MIMS) system. Of note is the lack of chromatographic separation, which allows continuous sampling.

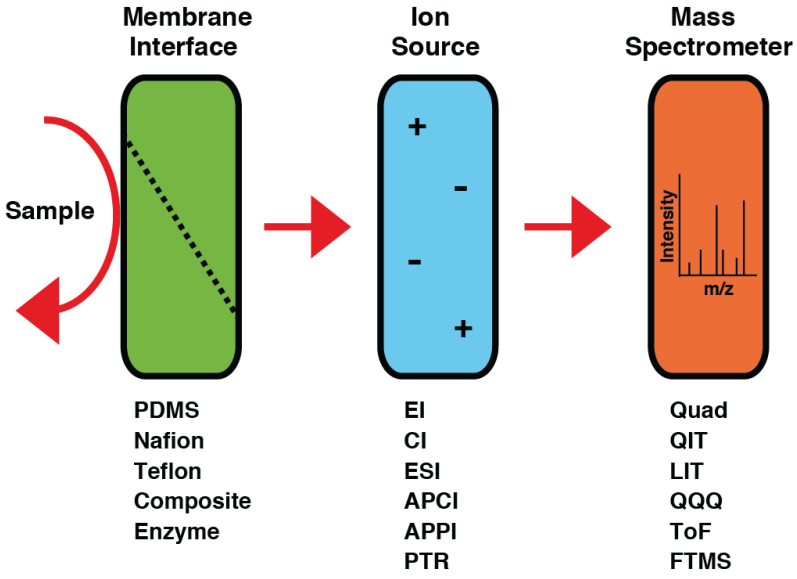


Figure 1.1: Schematic representing transfer of analyte from a sample to the mass spectrometer. Steps include pre–concentration of analyte into a semi–permeable membrane, subsequent ionization and measurement based on mass to charge ratio. Optimizations can be made at the membrane, ion source and mass spectrometer level. Figure reproduced with permission from [3].

One advantage of this introduction strategy, is that the majority of the sample matrix; whether it be air, water or soil; is excluded from, and therefore preserves, the vacuum of the mass spectrometer. At the same time, molecules that permeate the membrane are continuously infused into the mass spectrometer from a sample on the opposite side of the polymer. Of the many membrane introduction configurations that are possible (see Figure 2.2), those that employ flow–through or flow–over cells are the most suitable for a real–time sensors. This type of sampling inlet allows continuous monitoring of atmospheric or aqueous contaminants, over long periods of time (hours to days) without the need for sample pre–treatment. Although the first membrane introduction mass spectrometer appeared in the literature over 50 years ago [4], the limits of the technique have yet to be fully explored. This is, in part, because mass spectrometers are typically large, expensive, power demanding, and delicate. However, with recent technological advances and successes in the miniaturization of mass spectrometers [5], researchers now have new capabilities that did not exist prior to the 21st century.

The objective of the work described *herein*, is the development of a portable MIMS for the detection and quantification of VOCs and SVOCs. Of the many

challenges associated with this endeavour, one that is especially important, is that the instrumentation can be expected to encounter samples of wide ranging complexity and concentration. To address this challenge, a suitable instrument would need a mass spectrometer that is capable of speciating complicated chemical mixtures (anything from pristine aquifers to the air surrounding oil and gas process facilities in summer, when wildfires are commonplace). Furthermore, the analyzer must also be sensitive enough to detect regulated toxins at environmentally relevant concentrations. These concentrations are typically in the low parts per billion (ppb) range, which is certainly well within the capabilities of mass spectrometers.

In essence, all mass spectrometers have the same function; they are used sort ions according to mass to charge (m/z) ratio. In practice, there are a great many ways to both make and sort ions. Of the numerous mass spectrometers on the market at this time, it is the quadrupolar mass analyzers that have been miniaturized to a sufficient extent to make portable mass spectrometry a practical endeavour. Linear quadrupoles are robust, stable, sensitive analyzers that excel at trace gas analysis and, as demonstrated by Wenner *et al.* [6], can be deployed as real–time sensors. The limitation of a single linear quadrupole mass analyser, is that it is a scanning type of instrument and therefore, is inherently incapable of tandem mass spectrometry (MS/MS). In MS/MS experiments, target analytes are ionized and separated from the bulk mixture in the first stage of the experiment within the mass spectrometer. The isolated ions are then fragmented by collision induced dissociation (CID), and the resulting product ions, which are characteristic of the isolated target compound, are analyzed. Tandem mass spectrometry offers enhanced selectivity because isobaric species (ions with the same nominal mass, but different fragments) may be distinguished.

McLafferty's paper in the 1981 issue of *Science* [7], describes tandem mass spectrometry in detail. He illustrates the power of the technique with a long list of successful applications, which all succeed in one way or another at discovering the so called "needle in the haystack". The haystack analogy is a good one, often used to illustrate the challenges associated with trace–level environmental analysis. At the time of McLafferty's publication, the first commercial three dimensional quadrupole ion trap was being developed at Thermo Finnigan by G. Stafford and colleagues (see [8] for Stafford's personal perspective on the development of ion trap mass spectrometry). Pioneering work by W.Paul and H.Steinwedel [9], and later, R.March and J.Todd [10–12], made possible the insights and developments that led

to the 'mass selective ejection' mode of operation (the current standard for trapping and sequentially ejecting ions). In the following years, thanks in large part to the work by Z.Ouyang and R.G. Cooks, ion traps were miniaturized with the clear and focused goal of bringing mass spectrometry into the field (see [5]). For a complete review of *fieldable* mass spectrometers, from both academic and commercial laboratories, the reader is directed to a recent publication from the Cooks group [13].

Miniaturized ion traps, particularly cylindrical ion traps (CITs), offer low power consumption, mass range up to approximately m/z 450, sensitivity in the low parts per billion (ppb), operability at high base pressure ($\sim 10^{-4}$torr), and tandem mass spectrometry (MS/MS) capabilities. MS/MS is particularly useful for confirming molecular structure thanks to well documented and characteristic fragmentation pathways, but also allows innumerate possibilities for studying or employing gas phase ion–molecule reactions for chemical analysis. It is for these reasons that quadrupole ion traps, such as the resonant rectilinear ion traps and cylindrical ion traps, would be practical choices for the development of a mobile, membrane introduction mass spectrometer (MIMS) system for real–time chemical analysis. The application of such a system could support real–time decision making after a critical incident, or for adaptive sampling in combination with traditional environmental monitoring campaigns.

The central goal of this thesis is the development of a reliable mobile MIMS platform for real–time quantitative chemical analysis. To a large extent this development was made possible by funding from an industrial partner, Statoil ASA. Aside from funding for research, Statoil ASA provided access to an industrial steam assisted gravity drainage (SAGD) site both before and after bitumen extraction commenced. This site was to be used as a testing ground following the development of the mobile MIMS. With such a system, the unresolved issue of whether or not a mobile monitoring sensor can provide valuable information that a stationary monitoring sensor cannot. If there is such a benefit, then the additional complexities of a data stream with both spatial and temporal components will need to be addressed. To handle this type of data and determine its value, mapping software and sensor data will need integration followed by visualization. Graphical information systems (GIS) such as ArcGIS and Google Earth are well suited to this type of data analysis as they employ spatio–temporal location as the key variable that relays all other information. In recognizing that the development of a mobile

MIMS for VOC analysis is possible, it will be critically important to determine how the system compares with that of a conventional, high quality sample analysis protocol.

This thesis is based on a series of papers that address individual components of the goals outlined above. Several reference publications on the topic of traditional bench–top MIMS have been published over the years and, in particular, the articles by Johnson [14] and Ketola [1], and the thesis by LaPack [15] are thorough and universally cited works in this field. Chapter 2 of this thesis is a review of the state of the art from the perspective of on–site and *in vivo* applications. It was published in a special edition of *Trends in Analytical Chemistry (TrAC)*, which focused on the wide ranging research strategies that are emerging as a result of benefits associated with performing analysis in the place where sampling occurs. These benefits include, and are not limited to, the potential to reduce sample contamination and analysis time. Furthermore, this article is also intended to be brief update to the MIMS literature since the publications by Johnson [14] and Ketola [1].

The remaining chapters are experimental in nature, each describing a specific development or technical refinement (some anticipated, others serendipitously uncovered) required to make mobile MIMS a reliable technique. Chapter 3 includes comparisons of field MIMS data with fixed point and lab analysis. This addresses the issue of employing sparsely distributed, fixed monitoring stations for the assessment of air toxics in an urban environment. The portable system developed in this study represents mobile MIMS in its nascence.

The integration of membrane introduction with a commercially available, ruggedized cylindrical ion trap is the subject of Chapter 4. This chapter addresses a major bottleneck that was identified in the previous work: that is, real–time MS sensors acquire large amounts of data, and if that data requires weeks of post processing to arrive at final concentrations, then the technique loses much of its relevance. Therefore, beyond simple collection of spatial and temporal data, the development of real–time quantification and visualization software is needed. Chapter 5 confirms the presence of isobaric interferences that result in the over prediction of toluene concentration, and compares both laboratory and field MIMS data with that of a traditional, whole air sampling (WAS) canister analysis protocol for VOCs. Chapter 6 deals with the source (Earth's magnetic field) of an unexpected signal variability uncovered in mobile MS and provides a means to minimize the effect to improve sensitivity. Chapter 7 deals with the isobaric issues

described in Chapter 5 by focusing on MS ionization as a means to improve specificity of mobile MIMS.

As stated above, the central goal of this thesis is the development of a reliable mobile MIMS platform for real–time quantitative chemical analysis. To that end, Chapters 3–7 address key issues that have required research and development. The issues are associated with topics such as power consumption, portability, direct and internal standard calibration, data validation, geospatial positioning, logging of environmental data (wind speed and direction, barometric pressure, temperature), shielding magnetic fields, data visualisation and reduction of isobaric interferences. The final chapter summarizes the research and development of a mobile MIMS and provides a basis on which to evaluate the extent to which the general goals, enumerated above, have been met, and what is still required.

This thesis also includes three appendices. Appendix A unifies additional supplementary figures cross referenced from the text. Appendix B provides a summary of key developments that enabled the research presented in Chapters 4–7. Appendix C provides a standard operating procedure that was developed as a guide for safe and effective field deployment.

Chapter 2

Membrane Introduction Mass Spectrometry (MIMS)

Reproduced from Davey, N.G.; Krogh,E.T.; Gill,C.G. "Membrane Introduction Mass Spectrometry (MIMS)" *Trends Anal.Chem,* **30**, 1477-1485 (2011). Literature review and drafting of manuscript by N.Davey. Editorial contributions by E.Krogh and C.Gill.

2.1 Introduction

Membrane-introduction mass spectrometry (MIMS) uses a semi-permeable membrane as a direct interface between sample and mass spectrometer. The membrane interface acts to separate the bulk sample matrix from the low-pressure environment of a mass spectrometer. Depending on the permselectivity of the membrane, a range of potential analytes is continuously transferred as a mixture to the ion source. Analytes are discriminated and quantified based on their mass-to-change ratio *(m/z)* or by tandem mass spectrometry (MS^2), which affords increased molecular selectivity. The membrane may also extract and pre-concentrate analytes from the sample in an on-line manner, providing increased sensitivity. Because MIMS circumvents sample handling, clean-up and separation steps, it can provide a faster, solvent-less alternative to the discrete sample collection/preparation/analysis associated with chromatographic techniques. In general, MIMS performance is based on its ability to discriminate analytes (selectivity), to detect trace concentrations (sensitivity) and its rapid measurement response time (e.g. t_{10-90} signal-response times).

The ability to directly and continuously measure improved flow and multiple

chemical concentrations provides increased temporal resolution compared to discrete sampling approaches [e.g., gas chromatography with mass spectrometry (GC-MS)]. The temporal resolution of a typical MIMS analysis is limited by membrane transport rates, which are generally considerably less than the duty cycle of conventional chemical analysis for volatile and semi-volatile hydrophobic analytes. Thus, MIMS can provide greater insight into the concentration changes of chemical transients and dynamic processes. For example, MIMS will detect the concentration excursions depicted in Fig. 2.1, whereas a trap-and-purge GC-MS approach integrates them in the measurements or misses them entirely. Furthermore, when MIMS is combined with a mobile power supply and platform, it can yield real-time spatial resolution for analyte concentrations. This can provide a powerful means of characterizing fugitive emissions and source apportionment as well as providing a tool for rapid screening and process monitoring.

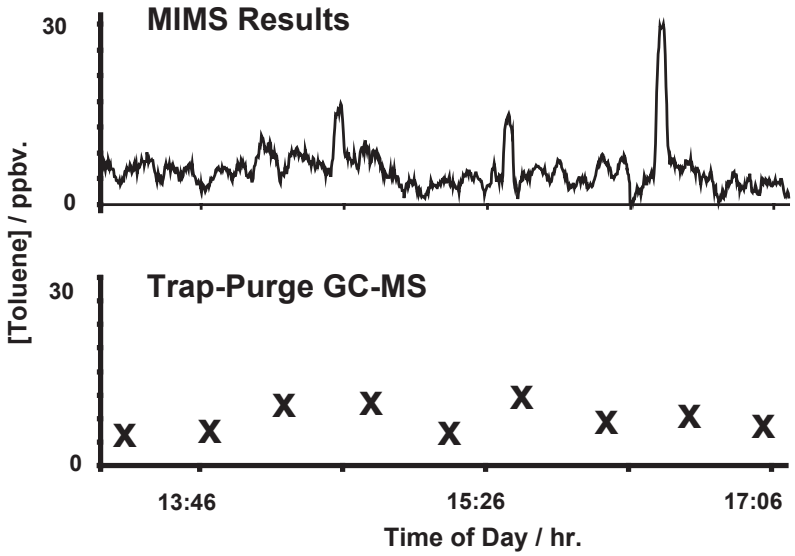


Figure 2.1: Membrane-introduction mass spectrometry (MIMS) versus classical on-line methods. Thematic comparison of MIMS data with that of simulated Trap and Purge GC-MS data for monitoring trace levels of toluene in the atmosphere from a moving vehicle.

MIMS has been used for the direct measurement of analytes from gaseous, liquid and solid samples, including complex heterogeneous and reactive media. Membranes employed to date have been predominantly hydrophobic polymer materials (e.g., polydimethylsiloxane, PDMS, Silicone^{TM}), which are well suited for the on-line analysis of volatile and semi-volatile organic compounds (VOCs and SVOCs). A

number of other membrane materials and modifications have recently been explored in an effort to change the permselectivity and hence extend the technique to a wider variety of analytes. Also, a range of membrane interface variants have been developed, including capillary hollow fiber membranes (HFMs) and sheet membranes. Some interface designs employ an acceptor phase to transfer analytes from the membrane to the MS system, while others interface directly to the vacuum of a transfer line or ion source. Researchers have used HFMs for direct, external probes, with thermally-assisted modes and in a variety of flow-through and flow-over geometries [16–26]. Sheet membranes, available in a wider variety of materials and thicknesses, have also been directly interfaced with flow cells and direct insertion probes [27–32]. Figure 2.2 summarizes a number of the interface variants described in this review. A wide variety of ionization strategies and mass-spectrometer types (e.g., linear quadrupoles, quadrupole ion traps, and time-of-flight) have been coupled to membrane interfaces.

MIMS has been employed in on-line, real-time chemical analysis for over 35 years. Several comprehensive reviews of MIMS appeared a decade ago, reviewing advances in the field including membrane materials and configurations, MS developments, and environmental and other applications for MIMS [1, 14]. Readers are encouraged to review these and the references cited therein for a more detailed description of the MIMS field. A number of new developments since that time have resulted in significant advances and an increasing number of applications. Our aim is to review critically recent developments in MIMS over the past decade, with an emphasis on its use for on-site and *in vivo* applications.

2.2 Advances in MIMS instrumentation

2.2.1 Membrane improvements–materials and configurations

PDMS membranes have dominated MIMS development and application because they are readily available, robust and excellent for the extraction, pre-concentration and transfer of small hydrophobic analytes from various sample matrices. Semi-permeable membrane inlets are well suited to a limited range of chemical analytes because of their physico-chemical properties and the permselectivity of the membrane material. Furthermore, permeants must be effectively removed from the downstream side of the membrane and transferred to an ionization source for MS detection. Several

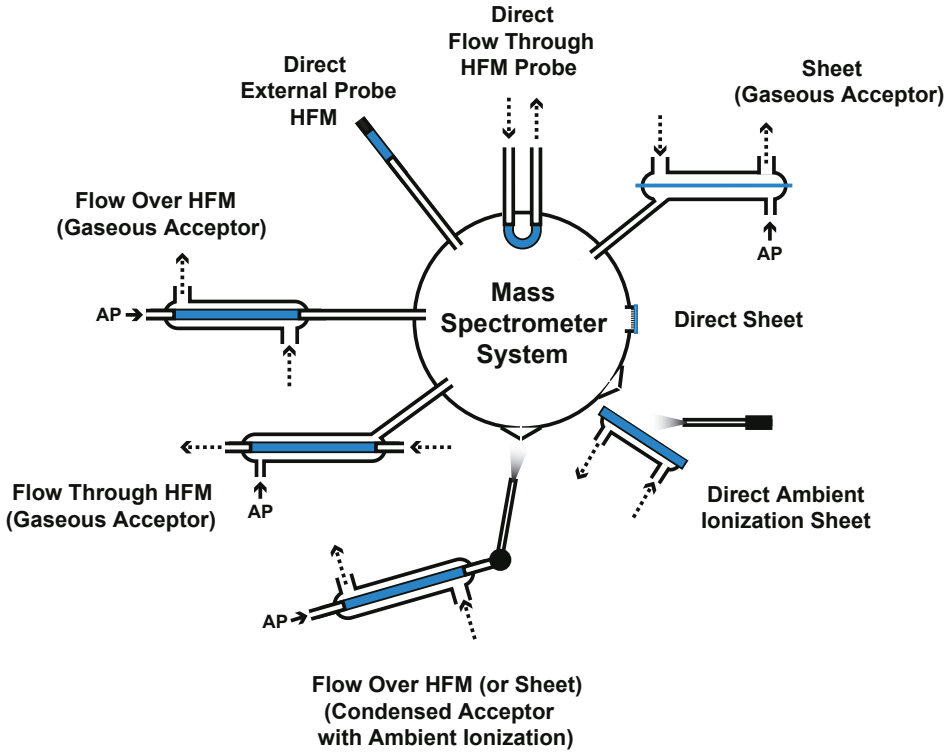


Figure 2.2: Membrane-introduction mass spectrometry (MIMS) interfacing configurations. Multiple variants of sheet and hollow-fiber membrane (HFM) interfacing strategies for MIMS are illustrated, adapted from a variety of sources. The use of an acceptor phase (AP) as well as its flow direction are indicated, as are sample flow direction(s) (dashed arrows), where appropriate.

approaches have been taken to address these limitations (e.g., use of heating strategies and chemical modifications of PDMS membranes, other membrane materials and condensed acceptor phases coupled to appropriate ionization methods).

To extend the application of PDMS membrane interfaces to less volatile SVOCs, various heating strategies have been employed [18, 19, 33–37] and generally increase analyte diffusivity and desorption, reducing the overall signal-response time. This approach works well for the analysis of gas-phase samples, but can lead to problems with aqueous phase samples due to bubble formation and excessive water vapor transfer, degrading overall MIMS performance [1]. This issue has been addressed by drying the membrane after aqueous sample introduction but before heating [36] or by using a coaxially heated HFM [19] in continuous or pulsed heating mode.

Chemical surface modifications can be employed to provide additional chemical

selectivity and to extend the use of PDMS interfaces to non-permeating analytes. For example, Creba *et al.* covalently immobilized *Candida rugosa* lipase on PDMS to detect specific non-volatile esters indirectly by catalyzing the production of alcohols that transport across the membrane [38].

Other materials being used for MIMS include Nafion polymer membranes in both sheet and HFM geometries. Nafion, the copolymer of perfluoro-3,6-dioxa-4-methyl- 7-octene-sulfonic acid and tetrafluoroethylene (Teflon), has unique properties, including being more permeable to ions and polar/hydroxylated species. MIMS systems using Nafion membranes for polar and hydroxylated species have been investigated [39, 40]. Lauritsen has explored the use of various sheet membrane materials with a miniaturized MIMS system (sub-section 2.2.3 below), including the use of cellulose, polyether sulfone and polypropylene for the detection of hydrophilic compounds in hydrophobic solvents [41]. Allen compared the performance of a PDMS HFM to that of an allyl-alcohol polymer on a microporous polypropylene HFM support for the detection of methanol in air and water, and observed $\sim$10$\times$ better sensitivity for methanol with the (more polar) allyl-alcohol membrane [17]. Short recently employed chemical-vapor deposition to generate carbon-nanotube films within the pores of an aluminum-oxide microporous membrane for the analysis of methane in gas mixtures [42]. Eberlin demonstrated the use of cellulose dialysis membranes to measure pharmaceuticals in aqueous solution, using ambient sonic spray ionization of the analytes on the downstream side of the interface [30]. Recently, several groups have begun exploring MIMS systems utilizing condensed (liquid) acceptor phases coupled with ambient ionization techniques (e.g., APCI and ESI) to detect polar molecules in aqueous solutions [20, 25, 27]. Creaser reported the use of a hydrophobic polyvinylidene fluoride microporous sheet membrane to follow the progress of the Michael addition of phenylethylamine and acylonitrile in ethanol [28]. Reactants, intermediates and products were monitored using an acetonitirile/water acceptor phase and an atmospheric pressure chemical ionization (APCI) source. We have recently developed a PDMS and Nafion HFM-based MIMS system employing a methanol acceptor phase and electrospray ionization (ESI) to quantify pesticides, steroids, pharmaceuticals and personal-care products in complex aqueous solutions [25].

2.2.2 Mass spectrometry improvements – ionization

Because the MIMS approach circumvents chromatographic separation, analytes are transferred in an on-line manner to a mass spectrometer as a mixture. Both the selectivity and sensitivity of the technique are influenced by the ionization mode, which determines the type of analyte(s) ionized and the degree of molecular fragmentation. For MS^2 techniques, less fragmentation is desired, yielding more intact analyte ions for collision induced dissociation. We discuss below some of the improvements for ionization that have evolved for MIMS applications.

The development of desorption CI-membrane-inlet MS (DCI-MIMS) was probably the first demonstration of a MIMS system capable of detecting fat-soluble biomolecules, hormones, pesticides and polyaromatic hydrocarbons [16, 36]. DCI-MIMS has been further optimized for ppb-level chlorinated pesticides, using negative-ion CI (NCI) [18]. Vacuum ultraviolet single-photon ionization (SPI) has been combined with a miniature time-of-flight (TOF) MIMS system for the real-time analysis of VOCs [43]. This soft ionization technique produces intact molecular ions without the extensive fragmentation seen in hard ionization techniques (e.g., EI). The high vacuum requirements of TOF analyzers limit the total mass flux (and hence the surface area) of membrane interfaces, which therefore constrain the ultimate sensitivity possible by MIMS-TOF combinations. The use of a buffer-cell, between a direct PDMS sheet-membrane interface and the TOF-analyzer chamber has solved this problem [43]. Also, the use of soft ionization by resonance-enhanced multi-photon ionization (REMPI) has been successfully applied to the MIMS-TOF-MS technique [44].

CI methods have been employed by a variety of researchers, with the objective of reducing analyte fragmentation and mitigating fragmentation-induced isobaric interferences. Allen demonstrated the use of proton-transfer and charge-exchange CI using reagent species directly transferred through a thin PDMS HFM from the sample matrix, removing the need for additional CI hardware within the mass spectrometer, simplifying and improving the method [45]. The limits of detection (LODs) for methanol using a supported allyl-alcohol membrane (Sub-section 2.2), were $\sim 3\times$ lower in water than air, with co-permeating water acting as an in-situ CI gas [17]. Alexander *et al.* coupled proton-transfer reaction mass spectrometry (PTR-MS) with MIMS to resolve isobaric interferences and make measurements of acetone, benzene, toluene and propane in humid air samples [46]. Nitric oxide as a

CI reagent (NOCI/MIMS) was successfully used by Atkinson to improve upon the measurements of non-polar hydrocarbons in gas mixtures [47]. Alwedian *et al.* demonstrated acetonitrile CI for improving the analysis of alkanes, alkenes and aromatic hydrocarbon species by MIMS [48]. Recently, the Gernatova group developed a system using Nafion® and Teflon® sheet membranes for polar, aqueous VOCs and SVOCs at ppb ppm levels, using water transferred through the Nafion® as a CI reagent [40].

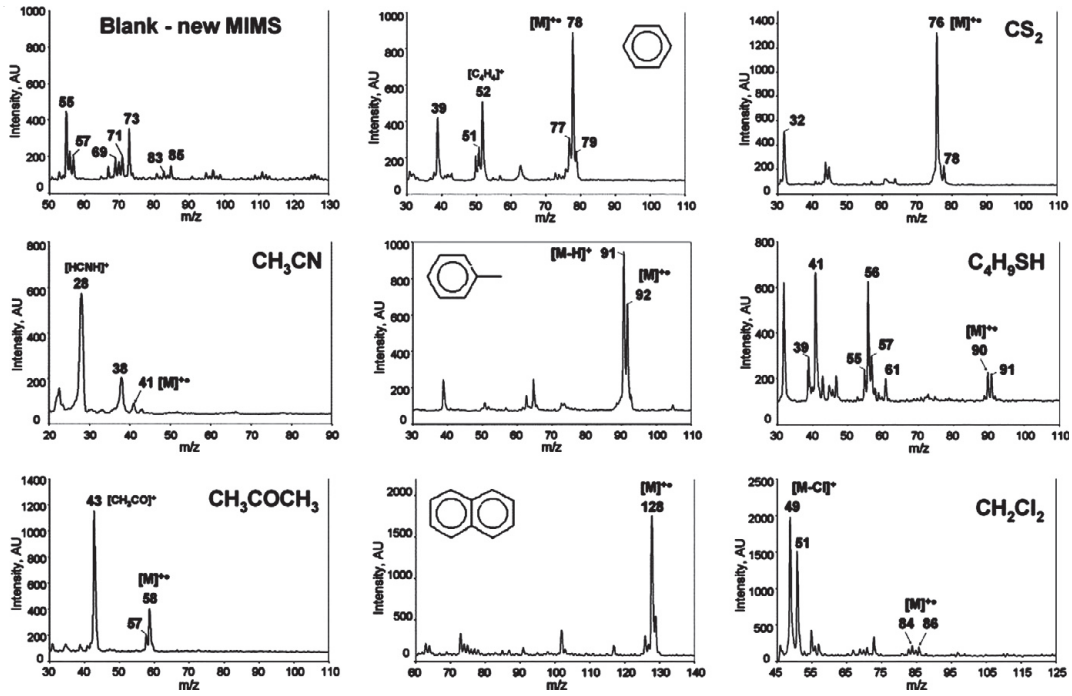


Figure 2.3: Mass spectra for a mini-membrane-introduction mass spectrometry (MIMS) system. Representative electron ionization (EI) mass spectra of blank (new membrane), vapor-phase hydrocarbons and hetero-substituted hydrocarbons: 50 ppm acetone, 45 ppm acetonitrile, 28 ppm benzene, 24 ppm butanethiol, 45 ppm carbon disulfide, 48 ppm dichloromethane, 9 ppm naphthalene, 18 ppm toluene in air obtained using the Mini 10.5 equipped with a PDMS-membrane inlet. In each model compound mass spectrum, one can clearly distinguish characteristic features of the analyte (e.g., the molecular ion of benzene m/z 78, an isotopic chlorine pattern of dichloromethane fragments and m/z 91 and 92 for toluene) [21] (Reproduced with permission from DOI: http://dx.doi.org/10.1039/b805813j).

2.2.3 Mass spectrometry improvements – miniaturization

Until recently, one of the limitations of MIMS systems for in-field and on-site monitoring was associated with the large size, high cost, and delicate nature of mass spectrometers in general. With the development and the commercialization of miniature mass spectrometers, reviewed recently by Ouyang and Cooks [5] , membrane interfaces are being exploited for direct on-line measurements in portable and remote applications.

Cooks *et al.* reported a mini-MIMS with a PDMS HFM capable of real-time analysis for VOC and SVOCs while being carried by hand [49]. As an example, Figure 2.3 illustrates representative, high-quality mass spectra for a range of analytes measured by a mini-MIMS system [21].

Lauritsen has also worked on the development of a small MIMS system [41]. The high-pressure tolerance of that system allowed use of hydrophilic microporous sheet membranes (cellulose and polyether sulfone), which would not be feasible with other systems. This group also developed a portable, hot-cell MIMS (hc-MIMS) to measure SVOC pharmaceuticals and pollutants [31].

Improved selectivity for miniaturized MIMS systems may also be achieved by using ion/molecule reactions to produce adduct ions. For example, the ions of chemical warfare simulants (i.e. nitroaromatics and phosphonates) form characteristic adducts when reacted with gas-phase neutrals, improving selectivity [50]. A recent article by Janfelt *et al.* highlighted the effect of a high background pressure of humid air on the performance of hand held MS systems [22]. Analyte signal intensities were found to decrease and the method of ionization shifted from EI to CI, including the formation of unusual water-adduct ions.

2.3 Advances in MIMS for on-site environmental monitoring

Although bench-top instruments have been successfully deployed for in-field MIMS experiments [23], the smaller size, reduced vacuum/power requirements and robust construction features of miniature mass spectrometers make them more amenable to portable and remote applications. Coupled with membrane interfaces, which obviate the need for sample clean-up and solvents, MIMS is an attractive

option for on-site environmental monitoring. Making timely, on-site chemical measurements can provide mission-critical information on fugitive emissions, human exposure, source apportionment and contamination boundaries. Continuous real-time data provides greater insights into dynamic changes and process monitoring. Although the sensitivity and the mass resolution of portable MIMS systems is generally not quite as good as their bench-top counterparts [5] , their performance characteristics are sufficient for many in-field applications and will undoubtedly improve.

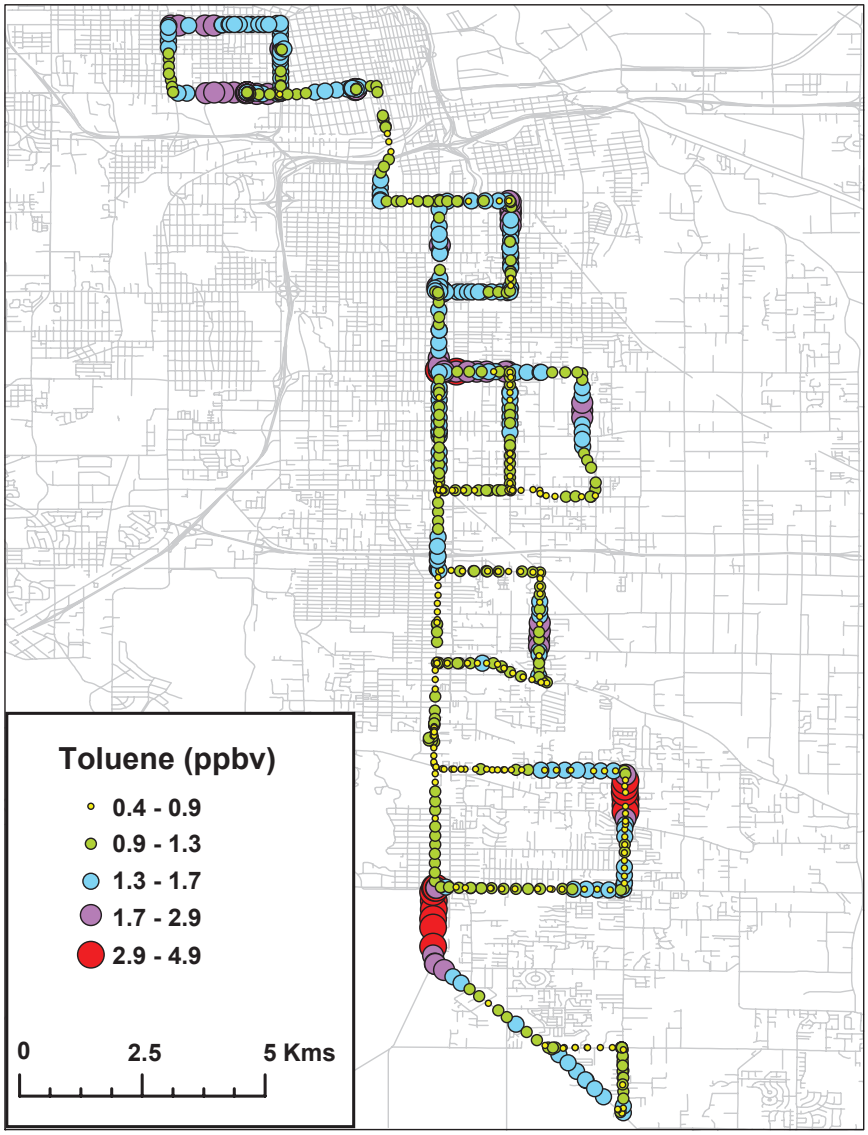


Figure 2.4: Mobile membrane-introduction mass spectrometry (MIMS) atmospheric monitoring data. Typical MIMS-tandem mass spectrometry (MS^2) atmospheric monitoring data (GPS-linked) obtained using a bench-top MIMS system operated in a moving vehicle in the Seattle-Tacoma, Washington, USA, area (January 2009). Contaminant plumes or hot-spots appear to be moving through the monitoring areas, indicated by the observed changes in concentration upon repeated travel over the same measurement paths. Other analytes that were simultaneously measured included BTEX, naphthalene and guaiacol (2-methoxyphenol) (Unpublished data, courtesy of the authors and researchers at the University of Washington, Seattle, WA, USA).

Our group has developed a benchtop quadrupole ion-trap MIMS-MS^2 system for in-field, real-time, atmospheric monitoring [23]. VOCs and SVOCs have been

directly measured in real time at low-ppbv levels in air over multiday–multiweek in-field deployments. For continuous on-line quantitation and long-term performance assessment, an isotopically labelled internal standard is continuously infused in the sample stream (water or air) [23]. The MIMS data can be time stamped and location stamped via the use of an on-board GPS, allowing collection of temporally and spatially resolved quantitative data. Figure 2.4 displays atmospheric toluene concentrations collected from a MIMS system operated in a moving vehicle in an urban environment.

MIMS has been employed for in-field aquatic environmental monitoring primarily for the identification of dissolved gases and VOCs. Tortell used a flat-sheet, flow-through membrane cell for the analysis of dissolved gases directly from seawater in the nmol/L range. This system has been employed during oceanic research cruises, yielding results comparable to those obtained from standard methods [51].

On-line monitoring of the dynamics of trihalomethane concentrations in a public swimming pool has been demonstrated using an unsupervised MIMS system with off-site real-time surveillance [52]. Short developed several underwater MIMS systems [6, 53, 54] to monitor dissolved gases and VOCs in freshwater and saltwater environments. This work has allowed MIMS to provide *in-situ* underwater measurements in a manner not previously possible. Figure 2.5 illustrates representative data showing spatially resolved oceanic methane concentrations. The NERUS/Kemonaut, another underwater MIMS, has also been used to measure underwater concentrations of dissolved gases (including methane) [55].

Because mobile MIMS systems may encounter and pass through analyte plumes, researchers have developed models to help better predict the true concentrations within these "hot-spots" based upon the transient signals obtained [54, 56]. The flow improvement measurement of VOC/SVOCs in soils and sediments and other solids has been accomplished by in-situ measurements of pore waters [57] or gases [58] and by directly heating samples in the MIMS system to measure the evolved analytes [29, 32, 59]. Schluter *et al.* [60] as well as Laing and co-workers [61] have employed MIMS systems to study the distribution and the emission rates of methane in aquatic and other environments. This work represents some of the first attempts to use MIMS to quantify *in-situ* greenhouse gas sources and sinks.

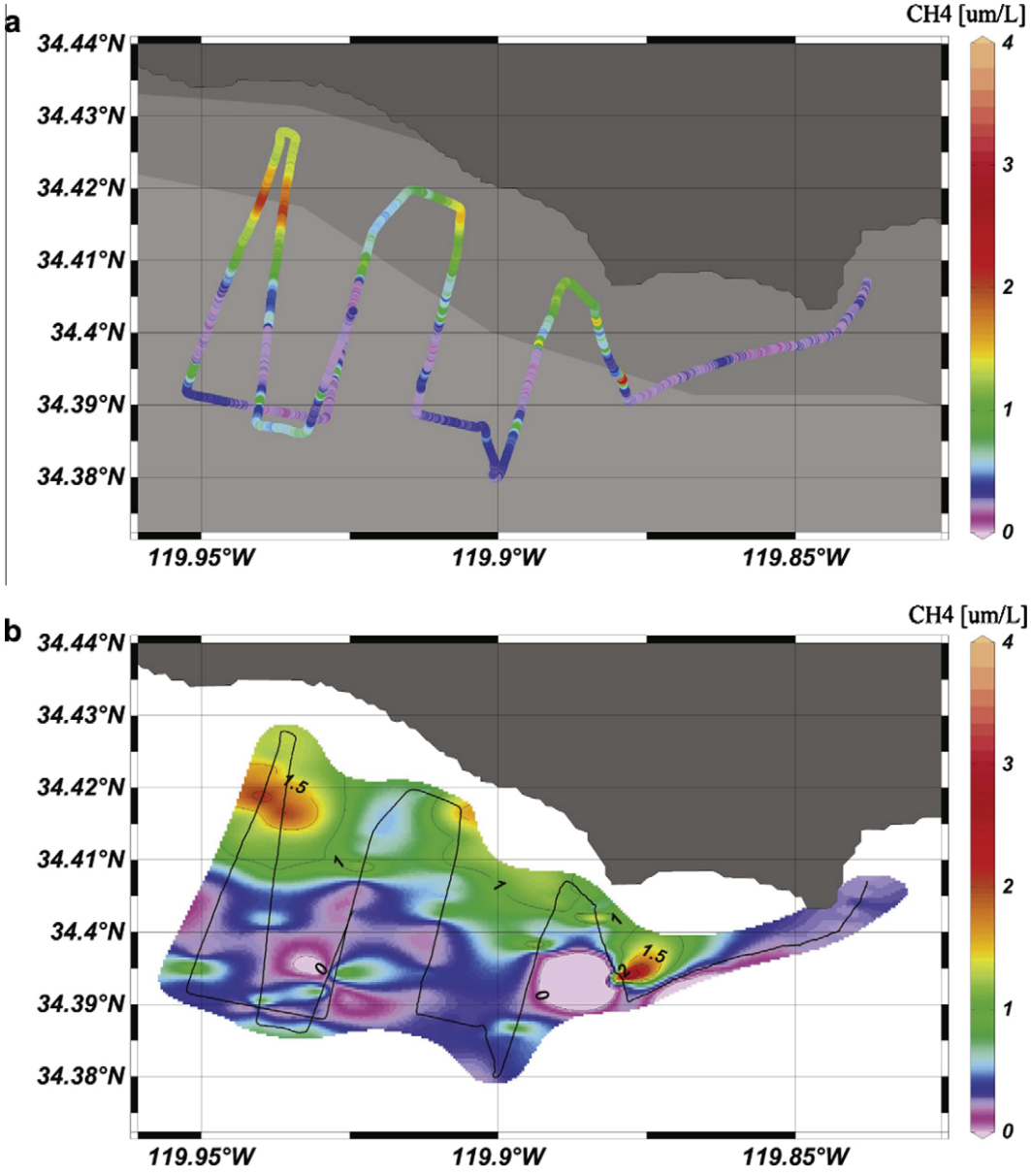


Figure 2.5: Underwater mobile membrane-introduction mass spectrometry (MIMS) monitoring data. Near-surface methane concentrations in the Santa Barbara Channel (California, USA) were determined using a towed membrane-introduction mass spectrometer designed for underwater use (September 2009). (a) Geo-referenced methane concentrations along the track of the towing vessel (R/V Cormorant); (b) Two-dimensional map of methane concentrations obtained by interpolation using data shown in part (a). Data obtained by SRI International personnel in conjunction with University of California at Santa Barbara personnel (Unpublished data, courtesy of R.T. Short, SRI International, St. Petersburg, FL, USA).

2.4 Advances in *in vivo* monitoring

Applications of MIMS that will potentially facilitate the diagnosis/treatment of human disease, detection of physiological deficiencies, and identification of health risks are beginning to appear. Analytical requirements for *in vivo* applications are high sensitivity (i.e. large enrichment factors) and selectivity in diverse biological matrices.

Cooks reported the use of a miniature MIMS system for the direct, real-time analysis of VOCs in human breath obtaining EI-MS^2 spectra for selected VOCs at ppm levels [62].

Total homocysteine concentration (tHcy) in human plasma or serum, a marker for a number of diseases or deficiencies, has been successfully measured at or below physiologically relevant levels using pre-derivatization to form volatile species followed by MIMS [63].

Lauritsen reported the detection of dimethyldiselenide by MIMS during the incubation of hepatocytes with methylseleninic acid, a model compound for selenium anti-cancer drugs [64]. Although this study presents novel *in-situ* data, LODs were relatively high (1 μM) and still need improvement.

The biologically-mediated reduction of dicarbonyl compounds to the corresponding alcohols by immobilized yeast cells was monitored *in-situ* in a continuous plug flow reactor using MIMS, identifying reactants, intermediates and products [26].

Beckman recently reviewed the substantial breadth of MIMS applications in gas-exchange studies for photosynthesis research [65].

Our group has demonstrated MIMS-MS^2 to monitor biogenic VOCs emitted by plants during heat stress and mechanical wounding studies [66].

Dunges recently examined the use of MIMS employing a microporous membrane interface to measure gases in breath as a simplified route for diagnosing lung disease [67]. The application of MIMS for directly measuring VOCs in breath [62] as well as biomarkers in biological fluids (e.g., serum [63] and urine [25]) represent potentially groundbreaking new directions that will pave the way for future *in vivo* applications.

2.5 Conclusions

MIMS was developed for high-frequency, real-time measurement of dissolved gases in 1963 [4]. Since then, most applications have been limited to the analysis of gases, volatile hydrocarbons and halogenated organics in air, water and slurry samples without the need for discrete sampling, clean-up and chromatography.

Recent advances in membrane materials and interface configurations have significantly broadened the range of analytes to include less volatile compounds, including polyaromatic hydrocarbons, bio-molecules and pharmaceuticals. New interfaces have been designed for optimum mass transfer, compatible with various ionization strategies and mass analyzers. Most notably, the use of condensed acceptor phases, coupled to ambient pressure ionization techniques, opens significant new territory in direct chemical analysis of polar and charged analytes of environmental and biomedical importance.

The miniaturization of mass spectrometers over the past 10 years has resulted in MIMS systems with reduced power requirements, greatly facilitating mobile and remote operation. A number of in-field environmental monitoring studies are emerging to exploit the temporal and spatial resolution afforded by MIMS.

The use of MIMS for *in vivo* applications is in its nascent stages, with relatively few papers published to date. We anticipate considerable growth in this area.

Chapter 3

Measurement of spatial and temporal variation in volatile hazardous air pollutants

Reproduced in part from Davey, N.G.; Fitzpatrick, C.E.; Etzkorn, J.M.; Martinsen, M.; Crampton, R.S.; Onstad, G.D.; Larson, T.V.; Yost, M.G.; Krogh, E.T.; Gilroy, M.; Himes, K.H.; Saganic, E.T.; Simpson, C.D.; Gill, C.G."Measurement of spatial and temporal variation in volatile hazardous air pollutants in Tacoma, WA using a mobile membrane introduction mass spectrometry (MIMS) system" *J. Environ. Sci. Health A* **49** 1199–1208 (2014). MS data collection by N. Davey, J. Etzkorn and M. Martinsen. Data for summer/winter comparisons were collected over a period of time overlapping with my entry into the graduate program. GPS data collection by C. Fitzpatrick, G. Onstand, and C. Simpson. Editorial contributions to the manuscript from T. Larson, M. Yost, M. Gilroy, E. Krogh, C. Simpson and C. Gill. MIMS hardware assembly, calibration, data collection, data analysis and final manuscript preparations performed by N. Davey.

3.1 Introduction

Air toxics encompass a diversity of chemicals, including both particulate and vapor phase components. Traffic exhaust and woodsmoke are two important sources of air toxics. Both of these sources emit complex chemical mixtures including particulate and vapor phase air toxics. A wealth of literature demonstrates associations between air pollution and adverse health outcomes [68–70].

A number of recent studies have suggested that fine scale spatial variation in pollutant concentrations may be an important determinant of exposure to air pollution and adverse health outcomes. Significant associations have been reported

between roadway proximity and various health outcomes [71–73]. Fine scale spatial variability tends to be greater for specific air toxics, than it is for particulate matter (PM) in general [74, 75]. Therefore, it is important to develop and evaluate *in–situ* monitoring tools and strategies that are able to measure multiple air pollutants simultaneously, with high spatial resolution.

Membrane introduction mass spectrometry (MIMS) is a technique that is well suited for rapid and simultaneous measurement of volatile chemicals. MIMS is an on–line (continuous) analytical technique with sensitivity in the low ppbv range for volatile compounds. Because MIMS introduces analytes to the MS as a mixture, the use of tandem mass spectrometry (MS/MS) confers higher specificity for mixture resolution [23]. Although MIMS has been known for almost four decades [76], in the mid 1990s there was a resurgence in the use of MIMS for real–time trace analytical measurements in both air [77] and water samples [78].

There are several reviews of the MIMS technique, including trends [14], environmental applications [1] and recently its use for environmental and in–situ measurements [79]. Several groups have been applying MIMS as an on–line monitor for environmental contaminants. As examples, Feilberg and co–workers [80] used MIMS as an on–line monitor to study the removal of malodorous compounds in air by livestock air filtration systems, and Norgard *et al.* [81] used a compact MIMS system to study the release of VOCs during the application of nanofilm spray products. Thompson *et al.* used MIMS as a method for monitoring the release of biogenic VOCs from wounded plants [66] and Etzkorn *et al.* have shown its potential use as an in–situ, mobile measurement strategy for investigating anthropogenic VOCs in both terrestrial and marine environments [23].

The objective of the current study is to demonstrate the use of a mobile MIMS system to characterize seasonal and spatial variability of selected volatile hazardous air pollutants. This study was part of a larger project that investigated seasonal and spatial gradients for a broad range of toxic air pollutants in the cities of Seattle and Tacoma, WA USA. The United States Environmental Protection Agencys (USEPA) National Air Toxics Assessment (NATA) places the Seattle and Tacoma urban areas of Washington State in the top 5^{th} percentile of US municipalities for potential health (cancer) risk from air toxics. The Tacoma urban area, connected to Seattle via the Interstate 5 corridor, is host to many of the same air toxics sources as the Seattle urban area, including a major port, highways, some industry, and neighborhood woodstoves and fireplaces. Census tracts in the Tacoma area were among those ranked highest

in the 1999 NATA for potential cancer risk of any census tracts in the Puget Sound area (King, Snohomish, Pierce, and Kitsap counties) [82]. Additionally, in 2009, the USEPA classified parts of Tacoma and Pierce County as a "nonattainment area" for fine particle pollution (or $PM_{2.5}$) under the federal Clean Air Act [83].

3.2 Materials and methods

3.2.1 Sampling Schemes

Fixed site

Three existing fixed location air monitoring sites in Tacoma, operated by the Puget Sound Clean Air Agency (PSCAA) were included in this study. These sites were the Tacoma Tideflats, Portland Avenue and South L St. Data from these fixed sites provided reference levels of pollutants for historical comparison, and served to anchor the mobile measurements for the analysis of fine scale spatial variation of pollutant concentrations.

Mobile routes

Monitoring took place in the neighborhoods adjacent to the three fixed air toxics sites in Tacoma, WA during two periods, one in summer and one in winter. The winter monitoring was undertaken during an atmospheric stagnation event January 15–21, 2009. During this period, the PSCAA issued a stage 1 burn ban on January 17, and a stage 2 burn ban on January 19. The bans were cancelled on January 20th as the air quality began to improve. Summer monitoring took place July 23–24, 2009 and July 28–30, 2009. Although there were no smog watches called, there was an atmospheric stagnation event during this period.

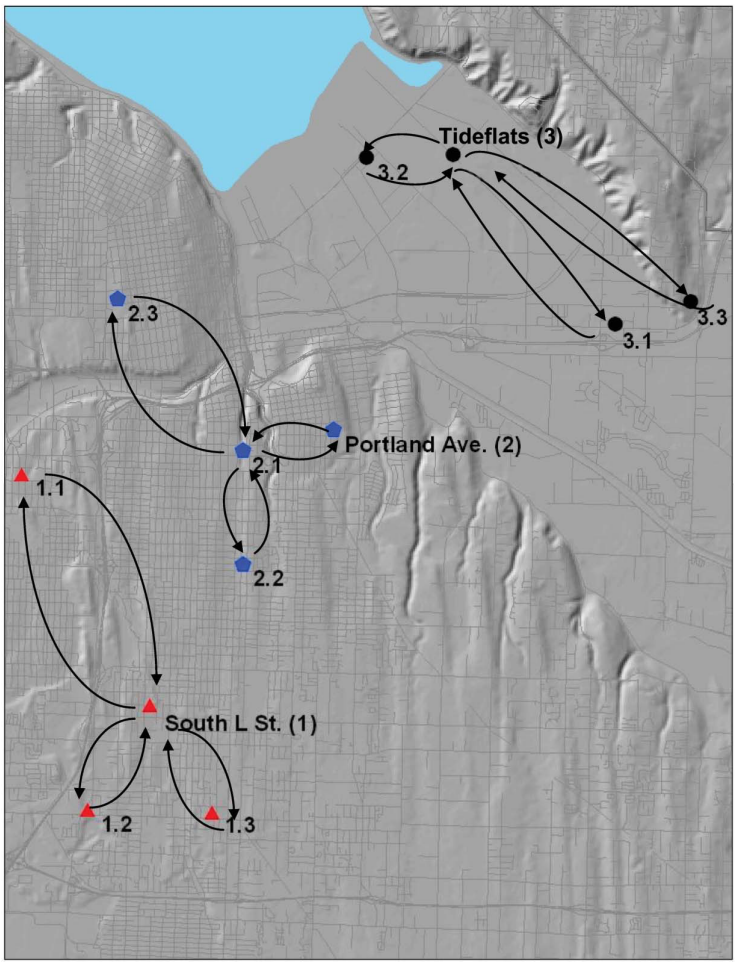


Figure 3.1: Map illustrating the three woodsmoke sampling routes in Tacoma, Washington, USA.

Two separate strategies were used to identify spatial and temporal variation in select VOCs associated with traffic–related and woodsmoke–related pollution respectively. For woodsmoke–related air pollution, three separate monitoring routes were identified, each consisting of a central site (one of the three PSCAA fixed sites for routine air quality monitoring) and three satellite sites (see Fig.3.1). The mobile MIMS monitoring system began each route by slowly driving (∼15–20 mph) around the central site for that route and sampling air quality for 15–20 minutes. The mobile system then drove out to the first satellite location and data was acquired in the same manner over another 15–20 minute period.

The route continued with the mobile system moving from the satellite location back to the central site to sample for a further 15–20 minutes, prior to moving to the next satellite site. In this way, the sampling design was able to tightly control

for variations at the urban scale in contaminant concentrations over time that could otherwise confound analysis of the spatial variability across sites. One route was completed each evening, between 8pm–1am, when wintertime impact from woodsmoke was expected to be greatest. The satellite locations for each route were chosen *a priori* as likely to have consistently higher or lower air pollutant concentrations than the corresponding central site, and were identified based on land–use characteristics including residential and vegetation density as well as elevation, estimated from satellite photography.

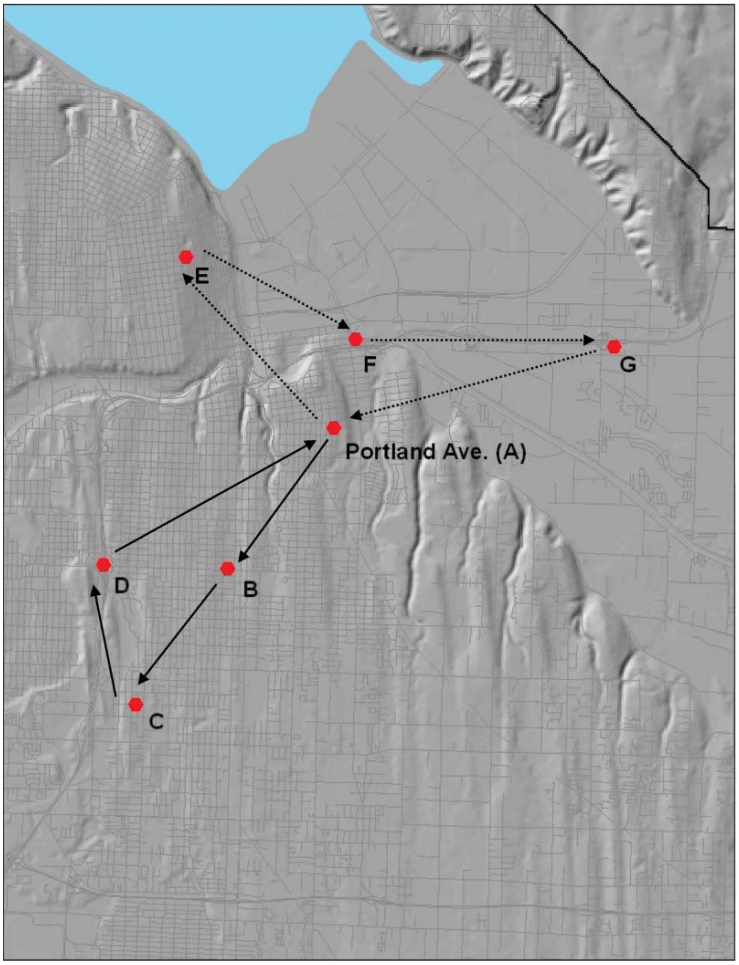


Figure 3.2: Map illustrating the three traffic sampling routes in Tacoma, Washington, USA.

For traffic related pollution, seven locations were selected, which included two sites used by PSCAA for routine air quality monitoring (Sites A (Portland Ave) and C (South L St) in Figure 3.2, and five additional satellite sites which were located near major roadway intersections (see Fig.3.2). The seven sites were divided into

two routes (four sites/route), with the Portland Avenue site (Site A) being common to both routes. Traffic Route 1 comprised sites A, B, C and D, whereas Traffic Route 2 comprised sites A, E, F and G. On each sampling day, the mobile MIMS system completed two circuits of one of the routes, circling each of the four sites per route [84] (typically in a clover–leaf pattern) for 15 minutes to accumulate air quality data, before moving on to the next site. Sampling for traffic related pollutants took place during the afternoon rush hour, between 2pm–6pm when impacts from traffic related air pollutants were anticipated to be greatest.

3.2.2 MIMS Instrumentation

The experimental apparatus used for this work has been described in detail elsewhere [23]. Briefly, the MIMS system used consisted of a hollow fibre polydimethylsiloxane silicone (Dow–Corning Silastic, Midland, MI) membrane (10.0 cm X 0.94 mm OD X 0.51mm ID), mounted inside a 0.25 in OD stainless steel flow cell interface. A gas chromatograph (Thermo Trace GC, Austin, TX) was used to supply helium gas (1.0 mL/min, 99.999% pure, Praxair, Seattle, WA) through the inside of the hollow fibre membrane (HFM) and to heat the membrane (70°C). The He sweep gas transferred analytes from the HFM to a quadrupole ion trap tandem mass spectrometer (Thermo GCQ, electron ionization (EI) mode, 175°C ion source, 175°C transfer line, 10 μTorr base pressure). Except where noted, MS/MS scans were operated continuously in an interlaced manner, in addition to a full scan experiment (m/z = 50 to 250, data not shown). Table 3.1 lists the relevant response factors, MS/MS transitions and detection limits for the target analytes in air samples investigated by this work.

For this study, 0.25 in OD Teflon tubing (Cole Parmer, Montreal, QC, Canada) was used for air sampling lines, and was heated (70°C) via a flexible heating tape sheathing wrap (Omegallux Model CN 7500, Stamford, CT). PTFE membrane filters (2.0 μm, 37 mm, SKC Corp., Eighty Four, PA) were used in line for particulate removal prior to MIMS measurement.

A diaphragm pump regulated by a precision ball float meter (Model FM4334, Advanced Specialty Gas Equipment, Middlesex, NJ) was used to maintain a sample flow of 4.0 L/min. Toluene–d_8 internal standard was infused via a gravimetrically calibrated permeation tube (6.1 μg /min at 70°C) installed downstream from a 5 m in–line, coiled stainless steel heat exchanger, with both upstream from the MIMS interface.

Table 3.1: Target VOCs and SVOCs monitored in air by MIMS.

Analyte	Molecular Weight	MS/MS Transition[a] (m/z)	Response Factor[b]	Detection Limit[c] (ppbv)
Toluene–d_8	100.19	100→ 70	–	–
Toluene	92.14	91→ 65	1.75	0.08
Benzene	78.11	78→51	1.22	0.44
Ethylbenzene/Xylene	106.17	106→79, 106→91	0.94	0.19
Guaiacol	124.14	124→81, 124→109	2.13	0.06
Naphthalene	128.17	102, 128[d]	2.10	0.15

[a]Precursor ion→ monitored product ion.
[b]Response relative to toluene–d_8 internal standard.
[c]Detection limit defined as 3 × signal/noise
[d]Naphthalene concentration determined based on extracted ion signal for m/z 102 and 128.

Gas standards for the calibration and determination of interference factors were generated using a commercial gas dilution apparatus (Model 450 Dynacalibrator, VICI Metronics, Poulsbo, WA) equipped with gravimetrically calibrated permeation tubes, with the exception of naphthalene, for which a permeation tube was not available at the time of the study. Instead, naphthalene was calibrated in a separate experiment by using dilute aqueous standards of naphthalene and toluene–d_8, directly introduced to the MIMS system at varying concentrations as a re–circulated liquid sample. The MIMS system was housed in a small moving van that was retrofitted for the field experiments with an in–house constructed shock absorbing bench to support the instrument, associated gas cylinders, computer and vacuum/sampling pumps.

A diesel generator towed behind the moving van (MQ Power WisperWatt 25 kW, Lewisville, TX) supplied all electrical power for this work. Air samples were drawn into the MIMS on the left hand side of the moving van approximately 2m above the ground (the exhaust was on the right hand side of the vehicle). Qualitative examination of the MIMS data showed no evidence of a response due to exhaust emissions from the generator or the moving van, provided the vehicle was moving in a forward direction (as was the case during the sampling runs). A global positioning system (Trimble Juno ST GPS, Sunnyvale, CA) was used to track the travelled routes for the system over the course of the study.

3.2.3 Statistical Analysis

All raw MIMS signals were background corrected by subtracting the averaged zero–air baseline values for each trace. Toluene and benzene raw signals were also numerically corrected for interference from ethylbenzene/xylene by subtracting 1.32 times the ethylbenzene/xylene signal from the toluene signal and 0.4 times the ethylbenzene/xylene signal from the benzene signal, based upon previously determined interference factors for each compound and from the ratios of ethylbenzene/xylene in the Seattle–Tacoma Airshed previously measured using by EPA method TO–15 using SUMA canisters and GC/MS [70].

The interference arises from common fragment ions being produced by ethylbenzene/xylene under EI conditions at the parent m/z values used for both toluene and benzene. This is a potential source of error, especially for toluene, as it may result in slight over or under correction of the toluene signal, depending upon the variability in the relative concentrations of ethylbenzene and xylenes. Contributions from other unidentified chemical species in the air pollutant mixture that create isobaric interferences (e.g. pinenes) may also generate a positive bias for the results for benzene, toluene and related molecules. Although such compounds are not suspected to be major contributors to interference (based upon full scan data), their effect on the data cannot be entirely ruled out.

The background–corrected MIMS signals were first smoothed by applying a moving boxcar averaging filter (7 datapoint window). Instrument responses corresponding to the five target compounds were then converted to concentrations using previously determined response factors relative to the toluene–d_8 signal, which was continuously infused as the internal standard in all experiments. The internal standard signal was stable throughout the runs except when there was dramatic variation in air sampling flows or transient signal drops that occurred as a result of large bumps–the instrument was located in a moving vehicle operated on sometimes rough road surfaces. In cases where this occurred, evidenced by disrupted internal standard signals, the compromised data was censored.

3.3 Results and discussion

Figure 3.3 illustrates variation in $PM_{2.5}$ concentrations at the three fixed-site locations in the Tacoma area, during the winter and summer intensive monitoring periods.

During the summer campaign, $PM_{2.5}$ data were not available for the tideflats site, due to technical problems with the Agency monitor. We planned monitoring around meteorologically stagnant episodes to capture high pollution levels. Both monitoring sessions had light winds and temperature inversions that prevented vertical mixing. The average and 1-hour peak $PM_{2.5}$ concentrations were similar across all three sites, and were consistently higher in winter (21 μg m^{-3}, mean of 24-hr average $PM_{2.5}$ concentrations) compared to summer (9.7 μg m^{-3}).

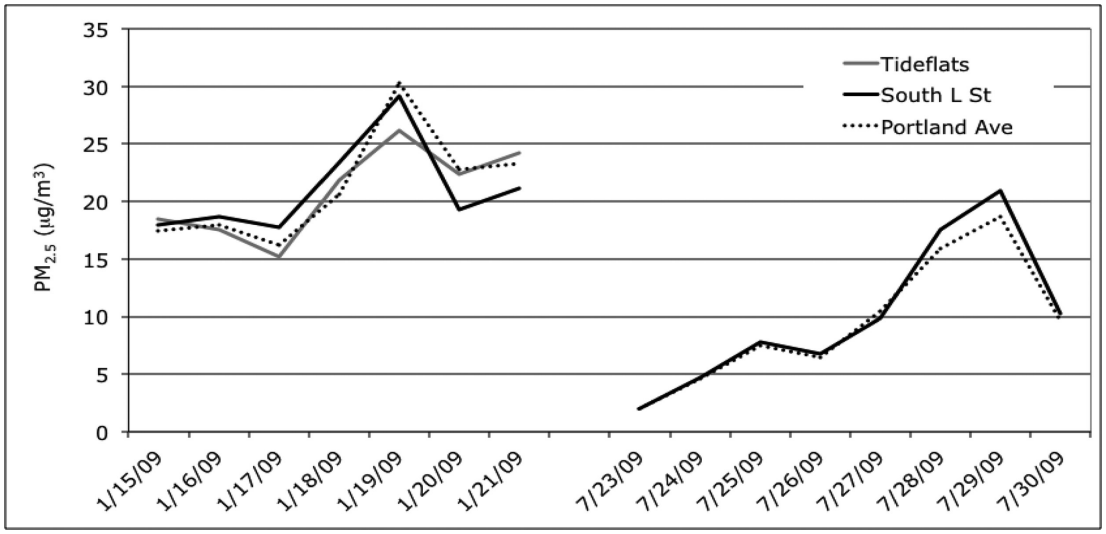


Figure 3.3: $PM_{2.5}$ concentrations measured at the three fixed (central) sites during the winter and summer monitoring periods (x axis indicates the sampling date). Data are 24-hr average values obtained from $PM_{2.5}$ Partisol monitors operated by the Puget Sound Clean Air Agency.

The winter session had higher concentrations than the summer session due to increased wood burning activity attributable to the cold evening temperatures on January 18–20, 2009. The summer session was during a record breaking heat wave that led to an all–time high temperature for Tacoma of 39.4°C (103°F) on July 29th. The winter session had typical midday mixing, when the surface inversion breaks until the evening hours, when it reforms and causes pollution to rebuild. Conversely, the summer session saw a gradual buildup of pollution with little to no diurnal pattern.

Table 3.2 summarizes concentrations of five specific compounds measured using the MIMS system at each of the central site and satellite locations. Paired t-tests were used to evaluate whether there were significant seasonal differences in analyte concentrations.For the woodsmoke routes, toluene and benzene were significantly higher in winter vs. summer, whereas guaiacol and naphthalene were significantly

Table 3.2: Spatial vatiation in VOC concentrations by route (ppbv)

			Toluene		Benzene		Ethylbenzene		Guaiacol		Naphthalene	
			Summer	Winter	Summer	Winter	Summer	Winter	Summer	Winter	Summer	Winter
Woodsmoke Route 1	Central	Mean	1.08	1.05	4.36	3.71	1.55	1.10	0.20	0.15	3.44	2.02
		SD	0.99	0.42	4.68	1.02	1.03	0.35	0.11	0.09	2.91	0.55
	Satellite 1	Mean	0.63	1.03	4.34	3.66	1.28	1.06	0.19	0.16	3.86	1.94
		SD	0.25	0.23	4.02	0.83	0.48	0.39	0.09	0.09	2.34	0.52
	Satellite 2	Mean	1.10	1.30	4.99	4.67	1.75	1.25	0.21	0.14	4.31	2.36
		SD	0.76	0.35	5.44	1.85	0.78	0.42	0.11	0.10	3.41	0.91
	Satellite 3	Mean	1.13	1.02	4.99	3.68	1.95	1.09	0.21	0.14	3.51	2.11
		SD	0.83	0.28	5.58	0.74	1.44	0.34	0.14	0.08	3.34	0.57
Woodsmoke Route 2	Central	Mean	0.74	1.60	2.20	3.75	0.93	1.89	0.18	0.15	1.78	2.11
		SD	0.26	1.26	0.58	1.58	0.32	0.66	0.08	0.07	0.82	0.39
	Satellite 1	Mean	1.08	2.41	2.13	4.48	1.63	2.24	0.16	0.17	1.37	2.04
		SD	0.34	1.48	0.54	2.14	0.55	0.82	0.08	0.07	0.47	0.63
	Satellite 2	Mean	0.98	1.56	1.88	3.98	0.89	2.06	0.18	0.19	2.17	2.26
		SD	0.28	1.48	0.45	1.63	0.22	0.48	0.03	0.08	0.31	0.38
	Satellite 3	Mean	0.53	0.92	2.14	3.30	0.70	1.34	0.16	0.20	2.89	2.49
		SD	0.25	0.73	0.29	1.07	0.21	0.20	0.07	0.08	0.36	0.33
Woodsmoke Route 3	Central	Mean	0.96	1.85	2.92	4.28	1.38	1.32	0.19	0.15	3.94	1.81
		SD	0.64	0.82	1.30	0.90	0.64	0.55	0.08	0.06	1.25	0.38
	Satellite 1	Mean	1.31	1.58	3.21	3.86	1.95	1.19	0.24	0.16	3.99	1.67
		SD	0.69	0.67	1.21	0.62	0.38	0.52	0.10	0.07	1.49	0.20
	Satellite 2	Mean	0.70	1.66	2.34	4.05	0.92	1.15	0.17	0.12	3.76	1.73
		SD	0.28	0.70	0.61	0.46	0.29	0.50	0.08	0.06	0.66	0.20
	Satellite 3	Mean	1.13	1.40	1.99	3.56	1.05	0.99	0.15	0.13	2.81	1.61
		SD	0.51	0.66	0.43	0.54	0.45	0.48	0.09	0.07	0.44	0.23
		Overall mean	0.69	1.17	1.57	2.35	0.76	0.90	0.13	0.11	2.00	1.11
		t-test[a]	**0.002***		**0.048***		0.772		**0.011***		**0.003***	
Traffic Route	Central (Site A)	Mean	1.09	1.17	6.38	3.92	1.82	1.13	0.25	0.14	10.69	2.31
		SD	0.57	0.56	5.01	1.33	0.66	0.49	0.14	0.06	9.44	0.89
	Site B	Mean	0.85	1.85	4.83	5.08	2.38	2.05	0.17	0.16	6.63	3.00
		SD	0.37	0.88	1.03	1.37	0.79	0.85	0.07	0.06	1.39	0.71
	Site C	Mean	0.55	1.14	4.19	4.61	1.43	1.56	0.15	0.16	6.06	2.84
		SD	0.27	0.59	0.49	0.83	0.38	0.58	0.07	0.06	0.73	0.43
	Site D	Mean	0.51	1.08	4.37	4.96	1.57	1.80	0.15	0.15	6.36	3.05
		SD	0.21	0.59	0.51	1.01	0.28	0.54	0.06	0.06	0.62	0.45
	Site E	Mean	1.57	1.72	10.31	5.43	2.47	1.59	0.32	0.15	18.92	2.74
		SD	0.77	0.88	4.50	1.81	0.64	0.89	0.14	0.07	8.90	1.17
	Site F	Mean	2.33	1.73	12.48	6.29	3.11	1.59	0.34	0.18	22.03	3.72
		SD	1.74	0.76	3.88	1.97	3.05	1.02	0.13	0.09	9.03	1.46
	Site G	Mean	1.88	2.30	12.80	6.48	3.28	1.76	0.39	0.17	22.13	3.88
		SD	0.58	1.35	2.14	2.45	0.93	1.00	0.11	0.08	5.64	1.40
		Overall mean	1.30	1.33	6.66	3.63	1.97	1.20	0.21	0.11	12.47	2.12
		t-test[a]	0.149		0.067		0.053		**0.034***		**0.009***	

[a] P value for paired-test, comparing summer vs winter.
Bold text signifies statistically different seasonal differences.

higher in summer compared to winter. For the traffic routes, only guaiacol and naphthalene showed significant seasonal differences (higher in summer vs. winter). Ethylbenzene concentrations did not differ significantly by season for either the woodsmoke or the traffic routes.

Guaiacol (2-methoxyphenol) concentrations measured in both seasons were close to the limit of detection for this compound when using the MIMS system (Table 3.1). Guaiacol is a pyrolysis product of lignin, and it was therefore anticipated that the primary source of guaiacol would be wood combustion, and hence that guaiacol concentrations would be higher in winter compared to summer. Our observation that guaiacol concentrations were in fact higher in summer compared to winter, therefore runs counter to our *a priori* expectations.

Levoglucosan (another tracer for wood combustion) was measured contemporaneously with the MIMS measurements [85]. Average levoglucosan concentrations were 170 ng m^{-3} during the winter session, consistent with a substantial contribution from residential wood combustion. However, during the summer monitoring period, levoglucosan levels were below our limit of quantitation (80 ng m^{-3}), indicating that woodsmoke (e.g., due to wildfires) was not a significant source of air pollution during this period.

To remove the potential for temporal variation in contaminant concentrations confounding the spatial analysis, a temporal correction was applied to data from the woodsmoke routes as follows. For each analyte, the median concentration at a satellite site during each 15–20-min sampling period was divided by the median concentration for that analyte measured at the central site for the time periods 10 min before and after the satellite site measurement. This expresses the analyte concentrations at each satellite site as a ratio in relation to the central site. Box plots illustrating the spatial variation in benzene relative to the central sites for the three woodsmoke routes are shown in Figure 3.4.

Similar plots for the other four analytes are included in the supporting information. A ratio of 1.0 indicates the benzene concentration at a specific satellite site is the same as for the central site. As can be seen in Figure 3.4, the benzene concentration ratios for all satellite sites are close to one (range 0.7–1.4). This suggests that community-scale spatial variation in benzene concentrations was relatively small for the locations and time periods studied, and that the central sites provide a reasonable representation of benzene levels within each of these communities. This finding is consistent with the hourly PM data illustrated in

Figure 3.3, which showed that $PM_{2.5}$ concentrations were highly correlated amongst the three central sites.

These results are perhaps not surprising given that both the summer and winter sampling took place during periods of air stagnation, and sampling of the woodsmoke routes took place at night, when direct traffic emissions were at a minimum. A study by Gilroy *et al.* [85] reported that during the heating season, a strong association existed between 24-hr benzene concentrations measured at the fixed sites and levoglucosan–which is a specific tracer for woodsmoke. The same study also reported a strong association between benzene measured by the MIMS instrument, and mobile measurements of light scattering coefficient.

Based on these observations, Gilroy and Yost concluded that a substantial amount of the benzene measured at these sites is due to residential wood combustion [85]. Similar, to benzene, community-scale spatial variation was relatively small for the other gas-phase pollutants measured by the MIMS instrument (see supporting information). Greater spatial variation may exist at other times of the year when wind currents may lead to rapid dilution of air pollutants, and steeper concentration gradients between source and receptor.

Similar to the woodsmoke routes, a correction was applied to data from the traffic routes to remove the potential for temporal variation in contaminant concentrations to confound the spatial analysis. For each analyte, the median concentration for all data from a specific satellite on a given day was divided by the median concentration measured for that analyte at the central site (Portland Ave. Reservoir) on the same day. This expresses the analyte concentrations at each satellite site as a ratio in relation to the central site. Because the Portland Ave site was common to both traffic routes, it is possible to compare all traffic sites in a single figure. Box plots illustrating the spatial variation in benzene and toluene relative to the Portland Ave site are shown in Figure 3.5.

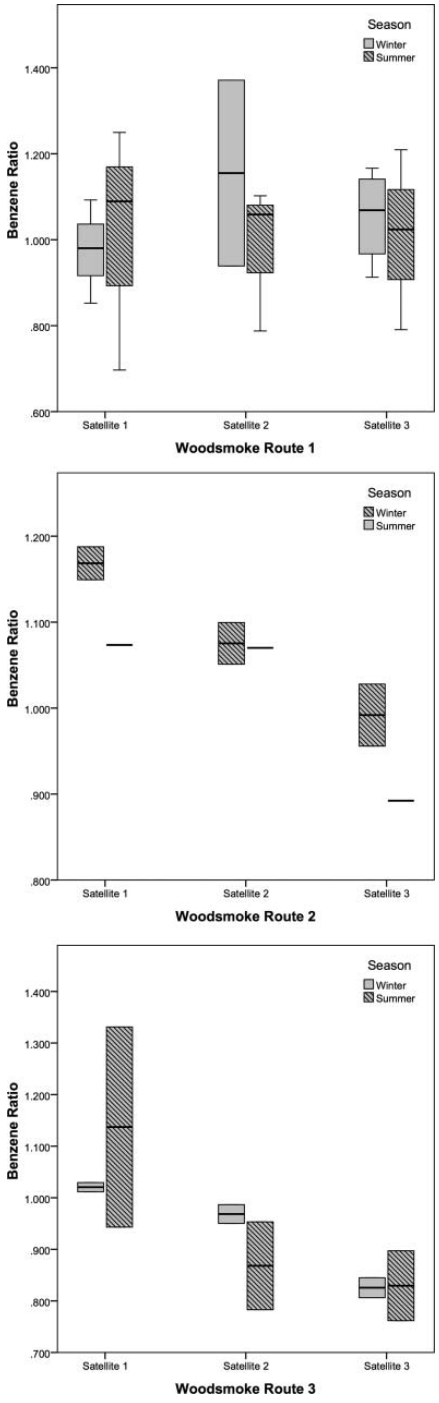


Figure 3.4: Box plots illustrating benzene concentration ratios at satellite sites, relative to the central site for each route. Some routes (e.g., route 2, summer) were only sampled on one day. On these occasions only a single concentration ratio is reported. For other routes, the variation in the concentration ratio is shown as the 25th–75th percentiles (box) and the 5th–95th percentiles (whiskers).

Benzene concentrations at sites B, C and D were similar to the Portland Ave Central site in both summer and winter (ratios close to 1.0, Fig. 3.5). In contrast benzene concentrations at the other traffic sites E, F and G are substantially higher than the Portland Ave site, especially during the summer (average concentration ratios 1.5–3, 3.5). The spatial pattern for toluene is somewhat different compared to benzene: toluene concentrations at sites B, E (winter only), F and G are approximately 50% higher than the Portland Ave Central site, whereas at sites C, D and E (summer) toluene concentrations are similar to the Portland Ave Central site. Additional box plots from woodsmoke routes for toluene, ethylbenzene, guaiacol, naphthalene and benzene are presented in the supplementary material (Figures A.1–A.5 respectively).

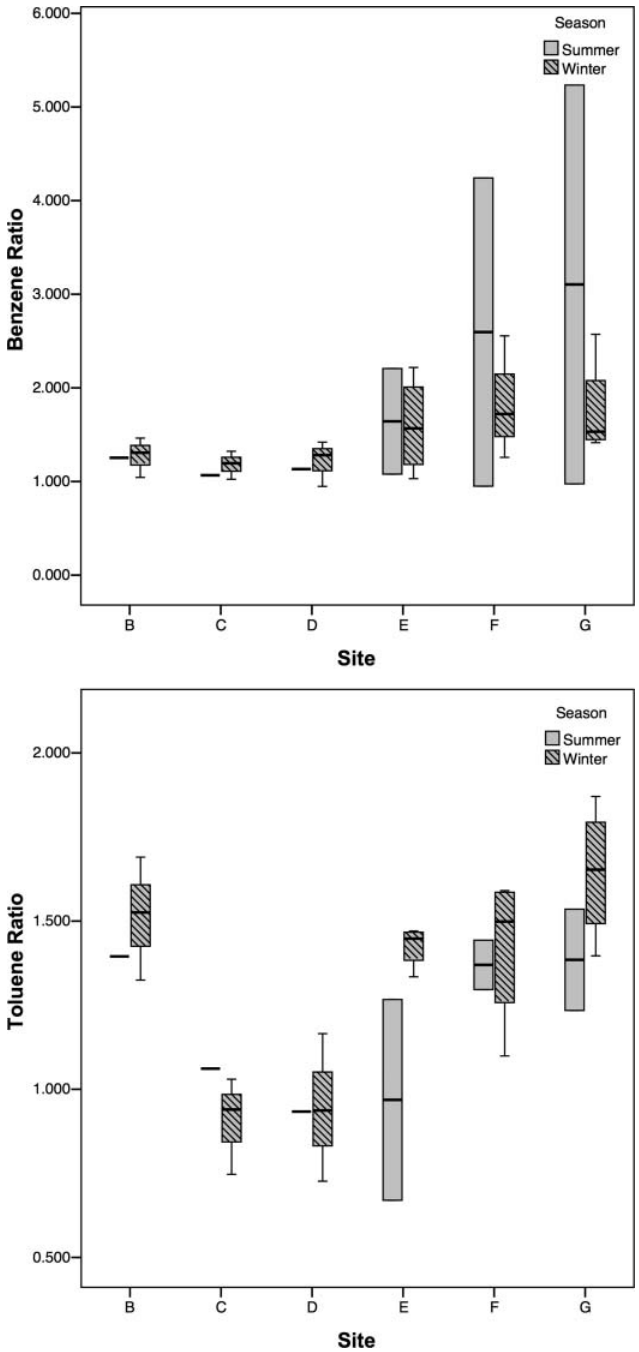


Figure 3.5: Box plots illustrating benzene and toluene concentration ratios measured at the traffic sites, relative to the Portland Ave Reservoir central site. For some sites (e.g., B, C, and D, summer) the route was only sampled on one day. On these occasions only a single concentration ratio is reported. For other sites, the variation in the concentration ratio is shown as the 25th–75th percentiles (box) and the 5th–95th percentiles (whiskers).

For the traffic sites, in contrast to the woodsmoke sites, substantial spatial variation was observed for some target compounds. In these cases, measurements made at the central site tended to underestimate concentrations measured at the other locations. This may reflect differences in sampling strategies between the woodsmoke and traffic routes. Compared to the Portland Ave Central site, many of the traffic sites were close to major intersections and highways, and were sampled during the evening commute period when traffic emissions were near their peak. In contrast, the woodsmoke sites were sampled at night when traffic emissions were at a minimum. Furthermore, sources of woodsmoke (primarily residential combustion) are likely to be more uniformly distributed over space compared to traffic, resulting in smoother spatial surfaces for the woodsmoke measurements.

For selected compounds, VOC concentrations as measured by the MIMS instrument can be compared to VOC measurements reported previously by Gilroy and Yost [85]. PSCAA data were obtained using EPA method TO–15. These values represent annual average concentrations obtained from 24–hr integrated samples that were collected on a 1 in 6 day collection cycle and were as follows (mean $\pm$ SD): benzene 0.38 $\pm$ 0.12 ppbv; toluene 0.71 $\pm$ 0.25 ppbv and ethylbenzene 0.10 $\pm$ 0.03 ppbv.

The comparison of the fixed site integrated sampling analysis results with the MIMS data indicates that for some compounds (e.g., toluene) there is relatively good agreement between concentrations measured by the two techniques. However, for other compounds (e.g., benzene), there are notable differences. In part these discrepancies likely arise from the fact that the integrated sampling strategy will underestimate short–term concentration levels that will, by nature of the measurements, be detected by an online technique such as MIMS. The goal of this study was to use the MIMS system to assess localized spatial and temporal variabilities for air toxics, and although the comparison of absolute concentrations between MIMS and fixed site integrated sampling methods is not completely congruent, the comparison is non–ideal because of the differences between the measurement strategies and data averaging times.

3.4 Conclusions

An in–house developed, mobile MIMS system was deployed for real–time, in–field use to provide fine–scale temporally and spatially resolved quantitative

measurements of selected hazardous air pollutants. Although most of the pollutants measured are common to both traffic exhaust and residential wood combustion, selection of sampling times and locations allowed us to differentiate features of the air pollution associated with wood combustion or traffic exhaust. Data indicated that fine-scale spatial variation associated with woodsmoke sources is far less pronounced than for traffic related air pollution. For traffic related air pollution, the central site data tended to underestimate air pollutant concentrations measured at the other locations–presumably because the satellite locations were closer to major roadways than the central site. Comparison of MIMS data to historical VOC data from the fixed sites showed reasonable agreement in some cases (e.g., toluene), but for other compounds (e.g., benzene), MIMS measurements were substantially higher than the reference method.

These discrepancies are likely in part the result of our MIMS measurements being made during periods of poor air quality, whereas the historical measurements represent annual averages. The MIMS data we report indicates the promise of this technique for environmental monitoring applications where spatial or temporal variability of hazardous air pollutants is suspected. However, the current limitations of this instrument include its size, power requirements, and marginal sensitivity towards some of the less volatile analytes of interest (e.g., guaiacol). A more compact instrument specifically engineered for field use would greatly facilitate increased use of mobile MIMS for air pollution monitoring. To increase sensitivity for SVOC measurements, a coaxially heated membrane interface could be employed to achieve low pptr detection limits for guaiacol in air samples [19]. A ruggedized and portable system would also increase the potential utility of the technique for a diversity of applications such as aqueous monitoring of streams, rapid screening of contaminated samples, and mapping of chemical plumes or boundaries.

Chapter 4

Real-time Quantitation and Spatial Mapping of Atmospheric and Aqueous Contaminants

Reproduced from Bell, R. J.; Davey, N. G.; Martinsen, M.; Collin-Hansen, C.; Krogh, E. T.; Gill, C. G. "A Field-Portable Membrane Introduction Mass Spectrometer for Real-time Quantitation and Spatial Mapping of Atmospheric and Aqueous Contaminants" *J. Am. Soc. Mass Spectrom.* **26**, 212–223 (2015). Development of MIMS interface, MS method development, MS calibration and gas sample handling by N. Davey. Details of this development are included in this thesis as Appendix B. A standard operating procedure for this instrument is also included in Appendix C. Aqueous sample introduction and calibrations by M. Martinsen (graduate student, Norwegian University of Science and Technology) . Software development, hardware development, data presentation and manuscript preparation by Ryan Bell (VIU post-doctoral fellow). Data collection by N. Davey, M. Martinsen and R. Bell. Editorial contributions by N. Davey, C. Collin-Hansen (industry partner), E. Krogh and C. Gill.

4.1 Introduction

Many processes, both natural and anthropogenic, are associated with the release of volatile and semivolatile organic compounds (VOC/SVOCs) to the environment [86]. When considering hydrocarbon extraction and processing, these emissions may be atmospheric [87] or aqueous [88], can be from point or diffuse sources [89], and are potentially harmful to nearby residents, biota, and workers [90]. Additionally, contaminant concentrations in the environment can be very dynamic as plumes migrate, especially under the influence of mixing events

driven by meteorological and hydrological processes [91, 92]. Grab sample collection (e.g., bottles, canisters, and sorbent traps) are often the primary sampling method used for current environmental monitoring programs and, although quantitative in nature, measured concentrations reflect a single point in space and time (or integrated over a specific time window), predominantly in an off-line manner. The time and expense required by these strategies often results in monitoring programs with relatively low data density that are limited in scope, and that can fail to provide information for making timely corrective decisions. Furthermore, improper documentation of baseline concentrations to compare industrially affected areas can lead to controversial situations that are difficult to assess [93, 94]. As a result, grab sample collection programs are often very limited and frequently serve only to meet current regulatory compliance requirements.

The advent of portable chemical sensing technology has enabled a new framework for environmental monitoring, where it is possible to take high precision, high accuracy chemical measurements to the field [23, 95–102]. Many of these analytical techniques, such as membrane introduction mass spectrometry (MIMS), can provide continuous monitoring time series data that resolve multiple analyte concentrations simultaneously [6, 23, 31, 79, 101, 103–105]. When operated on a mobile platform, these instruments can track transient concentration excursions in both spatial and temporal domains that may be missed by grab sampling strategies [105]. Continuous datasets allow the analyst to better understand the spatial boundaries of contaminant plumes as well as temporal changes due to dilution, mixing, and/or processing. For example, directly comparing plume intensities and background intensities in a single dataset can reduce the possibility of obtaining both false negative and/or positive measurements made in dynamic environments. Furthermore, with this information collected in real-time, sampling decisions and corrective actions can be made in a timely manner, helping to mitigate liability for both resource management and environmental stakeholders.

Our research has involved the development of a portable MIMS system for the continuous analysis of VOCs and SVOCs in both atmospheric and aqueous samples that greatly improves upon our early work in this area [23, 79, 101]. In general, MIMS systems allow continuous sampling of VOC/SVOC analytes as they diffuse through a semi-selective membrane, whereupon simultaneous quantification of multiple co-permeating molecules occurs by mass spectrometry [1, 14, 79]. The use of hydrophobic membranes, such as polydimethylsiloxane (PDMS), impedes the

diffusion of ionic and hydrophilic compounds, while pre-concentrating hydrophobic compounds, enhancing their permeation. Thus, MIMS systems employing PDMS membranes yield sensitive and selective determinations of VOC/SVOCs in both aqueous and gaseous samples. Because the membrane allows analytes to pass simultaneously as a mixture, it is important for quantitative analyses that the mass spectrometer can resolve each analyte without interference. Analyte interferences can be reduced through the use of tandem mass spectrometric (MS/MS) techniques. In addition, corrections for known interferences can be applied by using simultaneous measurements for these interfering compounds and through inspection of analyte response times [106].

The collection of continuous real-time datasets affords additional challenges and opportunities for data storage, presentation, and interpretation. In-field data collection is eased through the use of cellular networks and cloud-based storage. These systems allow any user with an internet connection to inspect the data at any time, while simultaneously creating an integrated data backup system. Data presentation and interpretation is eased through the use of free Geographic Information System (GIS) applications, such as Google Earth. Using mass spectrometric data that is both time- and location-stamped, we are able to provide real-time chemical concentrations that are geospatially mapped. In addition to providing environmental protection through rapid screening and continuous monitoring applications, this approach can be used to inform intelligent adaptive sampling strategies, delineate plumes or contaminated sites, identify point sources, quantify fugitive emissions, monitor process efficiencies, and provide discrete molecular information about complex mixtures (e.g., chemical fingerprinting).

In summary, we present the development and application of a field portable, battery operated MIMS system based upon a quadrupole ion trap that utilizes MS/MS for direct, on-line, low level (e.g., ppbv/ppb) analyte measurements in air and water samples. This flexible measurement system is compact and can be operated in an automobile for mobile measurements. Since volatile and semivolatile analytes pervaporate through the membrane interface from a sample as a mixture, the full resolution of isobaric isomers may not be possible, and other techniques involving chromatographic separations may be more appropriate. Additionally, higher sensitivity for analytes in gaseous samples can be achieved via methods such as proton transfer reaction mass spectrometry (PRTMS) [102, 107] and selected ion flow tube mass spectrometry (SIFT-MS) [108, 109]. Despite these potential

drawbacks, we have successfully employed mobile MIMS to provide continuous geospatially resolved quantitative information for target analytes in both air and water, using in-house developed data management software to process and visualize the data in real-time using cellular network communications.

4.2 Methods and Materials

4.2.1 Overview

A commercially available, portable cylindrical ion trap mass spectrometer system (Model Griffin 400; FLIR, West Lafayette, IN, USA), was modified in-house for in-field measurements by the addition of a MIMS sampling interface and internal standard (IS) infusion system, similar to that described previously [23]. In addition to the MIMS sampling system (which is described in detail below), the system also included several peripheral monitoring devices. A global positioning system (GPS, QStarz, Model BT-Q1000XT; Taipei, Taiwan) was used for geo-location and accurate time-stamping of all collected data. A cellular network card installed in the data system computer (Model M6600; Dell, Round Rock, TX, USA) was used to provide cloud data storage (Dropbox, San Francisco, CA, USA) and continuous data backup in the field. A portable weather meter (Kestrel, Model 4500; Birmingham, MI, USA) was used periodically to determine meteorological data, including wind speed, wind direction, humidity, temperature, and barometric pressure. Although not utilized for the present study, a video camera (Model HERO2; GoPro Inc., San Mateo, CA, USA) was incorporated to allow the potential creation of a video log of the surrounding environment during data collection events, to allow retrospective assessment of the data collection environment.

4.2.2 Membrane Introduction Mass Spectrometer

The cylindrical ion trap utilizing electron impact ionization (EI) was selected for use as the mass analyzer because of its compact, ruggedized, and field-portable design, and its ability to perform MS/MS for increased selectivity. Furthermore, the system is capable of multiple types of mass scan techniques in an interlaced series, allowing cycled quantitative analyte scans to be performed in sequence with general survey (full) scans. The entire mass spectrometer was encased in approximately 1.6 m^2 of

0.1 mm thick nickel alloy foil, or mu-metal ($\mu \approx 50{,}000$) (product number 8912 K32; McMaster Carr, Elmherst, IL, USA) to reduce the effects of the earth's magnetic field upon instrumental sensitivity. For additional information regarding the influence of magnetic fields upon portable EI mass spectrometers, the reader is directed to Chapter 6 in this thesis. The instrument was equipped with a temperature-controlled MIMS interface that replaced the supplied gas chromatograph system. For this work, the MIMS interface was constructed using a PDMS hollow fiber membrane (0.94 mm o.d., 0.51 mm i.d., 10 cm length, Silastic brand; Dow Corning, Midland, MI, USA) and a flow-over sample cell design. A similar experimental arrangement has been described previously [23], though a major difference in design is the use of an in-house constructed aluminum block heater to maintain a constant membrane temperature. The lumen (permeate side) of the membrane was swept with a helium carrier gas (1 mL/min), provided by a miniature 16 L helium cylinder (Model 49617HE; Leland Ltd., South Plainfield, NJ, USA). In addition to acting as the membrane acceptor phase for analyte transport to the mass spectrometer, helium was also used as a buffer gas by the mass spectrometer. A schematic of the entire apparatus is given in Figure 4.1. For choosing desired sample flows, two three-way valves (Figure 4.1, valves A1, A2) were located on either side of the membrane inlet to facilitate convenient switching between aqueous or atmospheric samples (vide infra).

4.2.3 Gaseous Sampling

Sample was drawn into the MIMS system via two solvent cleaned microporous stainless steel inlet filters in series (15 and 5 m) (Model SS-6 F; Swagelok, Solon, OH, USA), and 1/4in. o.d. Teflon transfer lines (Cole Parmer). The air-sampling inlet was mounted on the roof rack of a sport utility vehicle, approximately 30 cm above the roof line. Upstream from the MIMS inlet system, gaseous samples flowed through a temperature regulated chamber housing a toluene-d_8 permeation tube to allow the continuous on-line infusion of IS (Figure **??**). Since the permeation of analytes through the membrane is temperature-dependent, for the experiments described below the MIMS interface, permeation chamber, transfer lines, and inlet filters were independently temperature-regulated to 50°C. To utilize the system for SVOC analyses (data not shown), the inlet filter and transfer lines could be maintained at temperatures up to 200°C. The sample flow rate was set to the desired value using a rotameter equipped with a precision, 10-turn needle valve

(Model FM4312(4); Advanced Specialty Gas Equipment, Middlesex, NJ, USA) and maintained by a mechanical diaphragm pump (Model B-Series Dia-Vac; Air Dimensions, Deerfield Beach, FL, USA) located after the membrane. A pressure gauge (Model PX209-30V15G5V; Omega, Laval, Canada) located on the sample flow line immediately following the membrane interface was used to monitor pressure changes (e.g., resulting from a clogged inlet filter). A second pressure gauge (Model PX209-030G5V; Omega), located between the diaphragm pump and rotameter, was used to monitor possible changes in sample flow rate. A pressure decrease here would suggest a leak in the sampling system, most notably a failure in the sampling pump diaphragm. Pumps and pressure transducers were controlled and monitored using a custom micro controller (Arduino UNO, Torino, Italy) and in-house developed software (Labview 2011; National Instruments, Austin, TX, USA). While under way, the system was powered by a bank of four 6 V lead acid batteries (2011) (Model T-145 Plus; Trojan Battery Company, Santa Fe Springs, CA, USA) or smaller footprint Li-polymer batteries (2012) (Model 4784 AA; Portable Power Corp, Richmond, CA, USA), using the mass spectrometers on-board 24 V voltage regulator to ensure a steady voltage supply to critical components.

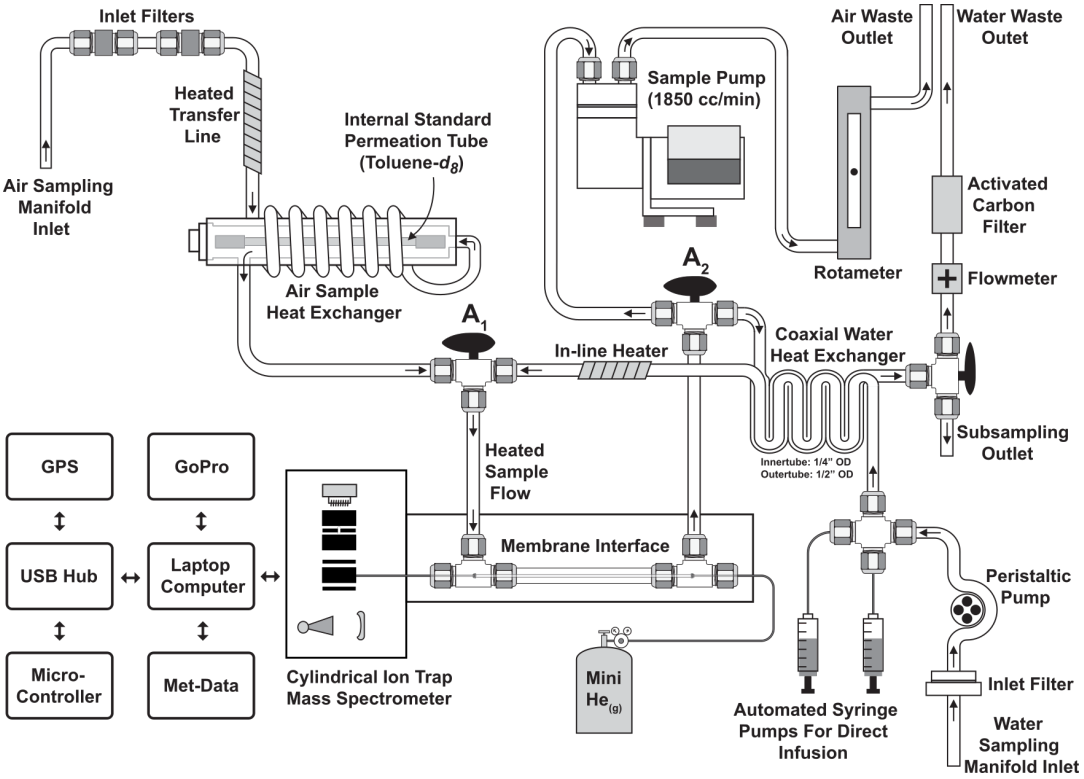


Figure 4.1: Schematic of the field portable MIMS system. Two flow selection valves (A1 and A2) are used to quickly switch between either the air or aqueous sample introduction manifolds. Figure courtesy of G.W. Vandergrift.

Prior to field deployment, the system was calibrated for a variety of target analytes (Table 4.1). Tandem mass spectrometryscans (MS/MS) were optimized for suitable target analytes, and selected ion monitoring (SIM) scans where used in cases where analytes did not fragment well in the cylindrical ion trap (e.g., reduced sulfur compounds), or for those that were highly fragmented under EI conditions (e.g., pinene). A full scan was also performed to survey for any unexpected analytes (see Table 4.1). Performing each measurement in an interlaced series resulted in a total scan cycle time of 13.5 s (averaging 10 replicate scans per measurement). Continuous flow gas standards were produced using certified permeation tubes (KinTek, La Marque, TX, USA) housed in a Dynacalibrator gas dilution apparatus (Model 340; VICI Metronics Inc., Poulsbo, WA, USA), with hydrocarbon scrubbed air used for the dilution gas. At an air sampling flow rate of 1850 mL/min, the inline toluene-d_8 permeation tube produced a constant IS concentration of 75 ppbv throughout calibration. Response factors for each analyte (relative to the IS) were obtained by flowing individual gas standards prepared using the Dynacalibrator

through the in-line permeation chamber (Table 4.1). Detection limits reported for each analyte were based upon three times signal to noise ratio.

The satisfactory performance of the in-line permeation tube chamber and sample heat exchanger was confirmed by comparing calibration standards made using the in-line permeation chamber to those made externally using the Dynacalibrator. Figure 4.2 illustrates the results for gas phase ethylbenzene. Each point on the calibration curve was measured as the mean of 90 scans and fit with a weighted leastsquares solution, using the inverse of the variance as the weighting factor. Importantly, the slopes of each calibration curve are in excellent agreement (within 0.4%). This indicates that the in-line permeation chamber and sample heat exchanger perform as anticipated, and field calibrations utilizing the inline chamber for on-line IS addition can be trusted and directly compared with laboratory-based calibrations performed using the Dynacalibrator. A small offset (380 counts) was observed (Figure 4.2) as a result of minor instrumental background shifts occurring overnight between the calibration runs, suggesting the necessity of daily background signal checks.

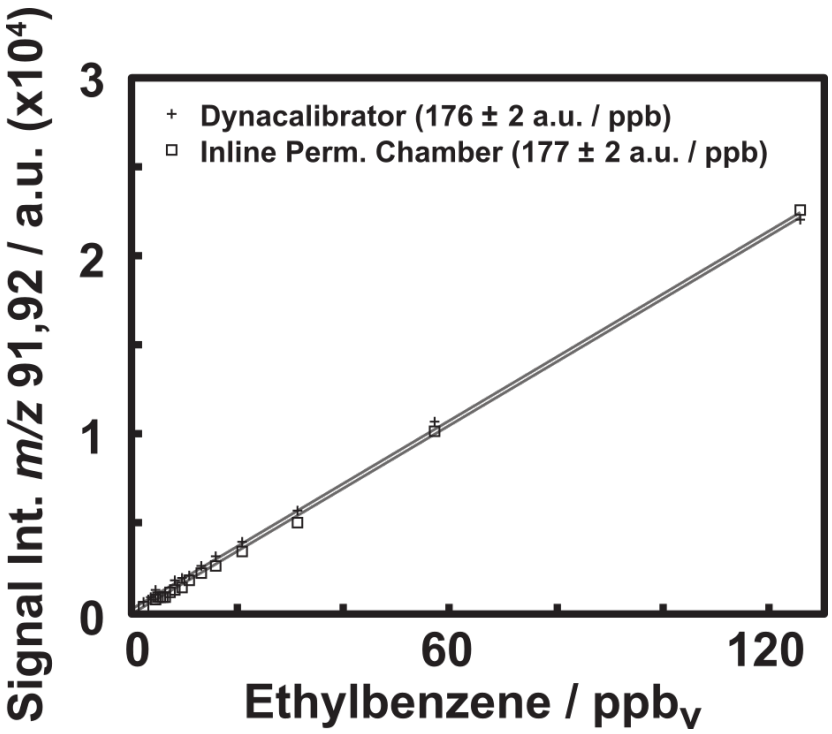


Figure 4.2: Direct comparison of the instrumental response for gas phase ethylbenzene concentrations with the permeation tube standard located in the Dynacalibrator versus the inline permeation chamber. Instrumental signal intensities are given in arbitrary units (a.u.).

Interference correction factors were also calculated and employed for selected, known isobaric interferents. For example, ethylbenzene EI fragment ions trapped by the MS/MS scan for toluene result in isobaric interference. The fragmentation of ethylbenzene ($M^{\cdot+}$, m/z 106) under EI conditions yields the stable aromatic tropylium ion ($C_7H_7^+$, m/z 91), which is also used for toluene quantitation via MS/MS (m/z 91 $\rightarrow$ 65). This positive isobaric interference of ethylbenzene upon toluene was numerically corrected by using the ratio of isobaric interference between the ethylbenzene (m/z 106$\rightarrow$91) and the toluene MS/MS scans (m/z 91 $\rightarrow$ 65) obtained during the analysis of a gaseous ethylbenzene standard. In this manner, signal contributions from the EI fragment ions of known interferents were numerically corrected. Although a similar, unaccounted for interference from xylene may result in a positive bias for toluene, the low xylene concentrations typically observed (data not shown) will lead to small biases. Future work will focus on resolving additional interference factors using more advanced spectral analysis or soft ionization techniques (e.g., CI) [110].

Experimentally, we have observed that with this system, reproducible measurements are possible for air sampling flow rates of 1000 mL/min (data not shown). In the field, the air sampling flow rate was maintained at 1850 mL/min (well above this threshold), yielding a constant 75 ppbv toluene-d_8 IS concentration in the sample flow. This resulted in a sufficient IS signal from which analyte concentrations could be calculated using the experimentally determined response factors (Table 4.1). A sensitivity coefficient was also calculated, giving the user an indication of the overall instrument performance level. For example, if the IS response during an analysis is observed to be 80% of its response measured during pre-deployment calibration, a correction factor of 0.8 could be applied to the external calibration coefficients. Drift in the instrumental sensitivity was monitored continuously, allowing for corrective actions (e.g., replace the EI filament, optimize the detector voltage, etc..) when necessary. Thus, continuously infused IS allowed for both real-time calibration and instrument performance monitoring. Variations in operational parameters are also detected by observation of the correction coefficient. For example, if the sample temperature, pressure, or flow rate changes, the concentration of the IS will also change, signalling potential problems to the operator during in-field measurements. For this study, we limited our measurements to relatively flat terrain, minimizing pressure variations arising from altitude changes. Sampling parameters were closely monitored and stored as interlaced

meta-data to enable post-deployment data interrogation. Prior to daily deployments during field monitoring campaigns, instrumental background values were re-established after a 1 h warm up, using a small cylinder of zero air (Model AI 0.0UM; Praxair, Mississauga, ON, Canada). Periodic calibration checks were performed using toluene and benzene permeation tubes added to the in-line permeation chamber and varying sample gas flow rate from the zero air cylinder.

4.2.4 Aqueous Sampling

MIMS analysis of aqueous samples was carried out with the same instrumentation by changing the position of valves A1 and A2 (Figure 4.1). Aqueous sampling was performed at a sample flow rate of 150 mL/min using a battery-operated peristaltic pump (Model Masterflex E/S; Cole Parmer, Montreal, Canada) and monitored with a flow meter (Model FLR1000-8; Omega, Laval, Canada). Experimentally, we have observed with this system that reproducible measurements are possible for aqueous sample flow rates of >100 mL/min (data not shown). Incoming aqueous samples were maintained at 35°C using a flexible heating tape (thermocouple regulated) wrapped around the sample inlet tubing upstream of the MIMS interface. To reduce the power consumption required for sample heating before measurement, an in-house constructed coaxial tubing heat exchanger (70% efficient) was used to recycle thermal energy from the exiting sample flow (Figure 4.1). Continuously infused IS was added to the aqueous sample stream, (e.g., toluene-d_8) using a software-controlled syringe pump (Model C24000; Tricontinent, Grass Valley, CA, USA). Additionally, a second syringe pump was incorporated to allow on-line analyte infusions for lab experiments, in-field calibration checks, and standard addition calibrations. The exiting sample flow was passed through an in-house constructed activated carbon filter trap (1000 g of activated carbon suspended between glass wool plugs in a 3 in. diameter plastic casing) before discharge from the system.

Prior to field deployments, the MIMS system was calibrated for a variety of aqueous analytes using closed 1-L glass recirculation flasks equipped with a Teflon lined septa in a manner similar to that described previously [19, 111]. Deionized water (maintained at 35°C by a constant temperature water bath) was recirculated through the MIMS interface at 150 mL/min, and stepwise injections of combined analyte stock solutions in methanol were used to generate low ppb (μg/L) aqueous concentrations (e.g., 3 to 30 ppb) for calibration. To avoid isobaric interferences

during aqueous calibrations, two analyte suites were employed: Suite 1: benzene, toluene, chloroform, methyl iodide, dimethyl sulfide; Suite 2: ethylbenzene, chlorobenzene, naphthalene, guaiacol, iso-octane, 1-chloronaphthalene. Toluene-d_8 was included in both suites and used as an IS for the determination of response factors. Using these data, instrumental background, analyte sensitivity, detection limits, and response factors were determined for each target analyte (Table 4.1).

For in-field quantitation, incoming aqueous samples were continuously infused with toluene-d_8 at low ppb levels via a syringe pump, allowing on-line analyte quantitation by response factors as well as affording the continuous monitoring of overall instrument performance. For example, an infusion flow rate of 0.20 mL/min of 14 ppm toluene-d_8 (in methanol) into 150 mL/min on-line sample flow rate produced an on-line toluene-d_8 concentration of 19 ppb. The second syringe pump injection port was used to infuse analyte standards in the field for periodic target analyte calibration checks. Some of the aqueous samples were also calibrated by using standard additions methodology, whereupon a calibration solution containing toluene-d_8 and the desired target analytes was infused into the sample stream immediately following a sample measurement. Field samples included 4-L grab samples collected in amber glass bottles (Scientific Specialties Inc., Hanover, MD, USA) and also the continuous sampling of water directly drawn from rivers and streams over multi-hour sampling periods with the peristaltic pump. Extended periods of stationary aqueous monitoring in the field (>12 h) were enabled by switching to supplementary power, provided by a small gasoline-powered generator (EU2000i; Honda, Tokyo, Japan) located at least 100 m downwind from the sampling location. This prevented the complete depletion of the battery systems, and ensured uninterrupted data collection.

4.2.5 Software Development

Mass spectrometric scan methods were developed and executed using the mass spectrometers operating software (Griffin System Software, GSS, v3.9; FLIR Systems, West Lafayette, IN, USA). Calibration software to quantitate the raw data and automate the handling of the associated meta-data was written in-house using Labview. Calibration results were stored in a custom file format that was subsequently employed by additional Labview-based software designed for real-time data collection and analysis. Briefly, the real-time software extracted quantitative

Table 4.1: Summary of Mass Spectrometer Scan Methods and Analytical Performance Characteristics for Target Analytes

Analyte	Vapor Pressure at 25°C (Pa)	Mass Spectrometer scan method (m/z)	Response times (t_{10-90})		Detection limits[d]		Response factors	
			Air at 50°C (min)	Water at 35°C (min)	Air at 50°C (ppb_v)	Water at 35°C (ppb)	Air at 50°C	Water at 35°C
Survey Scan		Full Scan 40–150	n/a	n/a	n/a	n/a	n/a	n/a
Toluene-d_8 (Internal Standard)		98→ 69,70	0.5	2	0.5	0.5	–	–
Toluene	3,715[a]	91 → 64,65	0.5	2	0.5	0.5	1.5	2.7
Benzene	12,590[a]	SIM 77, 78	0.5	2	2	1	0.3	0.17
Ethylbenzene/Xylenes	1,230/630[a]	106 → 91,92	0.5	2	0.75	1	1.0	0.04
Chloroform	25,120[a]	SIM 83,85	0.5	2	2	1	2.8	n/a
Chlorobenzene	1,580[a]	112 → 76,77,78	1	2	10	5	0.08	0.06
Naphthalene	200[a]	128 → 102	2	10	10	5	3.9	0.29
2-Methoxyphenol	20.9[a]	124 → 108,109	2	10	20	50	n/a	n/a
Pinene	582[b]	SIM 121	2	10	20	50	n/a	n/a
Dimethyl Sulfide	64,460[b]	SIM 62	1	5	20	50	0.03	n/a
Methyl Mercaptan	196,200[b]	SIM 47,48	1	5	20	50	n/a	0.04

[a]Reference [112]
[b]Reference [113]
[c]Selected reaction monitoring(SRM) denoted with →; selected ion monitoring (SIM) and full scan data acquired as noted.
[d]Detection limits based upon signal/noise = 3.

ion signals from the raw GSS data files and applied the calibration data file, producing real-time quantitative results. These results were then plotted as multiple time series and as color proportional tracks on a map. Maps were downloaded as needed using Google Maps API. All data were automatically stored on Dropbox servers via the cellular data connection. After all mobile data were collected, data workup and re-analysis were performed using in-house developed MATLAB code (Mathworks, Natick, MA, USA). Meta-data and final result files were stored as time series for inspection and quality control. Final results were saved as .kmz files for presentation in Google Earth. These self-contained data files enable inspection of data both geospatially and temporally, are easily networked, and contain hierarchal data structures to enable the presentation and sharing of the large complex datasets in a clear and concise way.

The field monitoring examples presented were obtained in Northern Alberta in early July, 2012. Air sampling data sets were obtained in and around a Steam Assisted Gravity Drainage (SAGD) pilot facility (Statoil Canada Ltd.) located roughly 200 km south of Fort McMurray, and on public roads north of Fort McMurray along Highway 63. The MIMS system was operated in a sport utility vehicle (GMC Yukon). Stationary air sampling data sets were collected with the vehicle engine off and correlated with meteorological data determined at the sampling site. Aqueous sampling included the analysis of grab samples of on-site processed and ground water as well as measurements made by continuously sampling from nearby natural surface waters.

An example air monitoring dataset, presented here (vide infra), was generated during travel north of Fort McMurray on Highway 63 through areas adjacent to active oil sand recovery operations. Frequent stops (with the vehicle engine off) were performed to allow the collection of meteorological data and to obtain periods of stationary MIMS data. The example dataset was collected on July 7, 2012. The day was warm (27°C) and dry (30% relative humidity), with gentle wind speeds ranging between 4 and 7 m/s.

Aqueous samples of both on-site process water and off-site natural (stream, river, and ground) water were also collected during this field trip. An example dataset shown here was collected July 3, 2012 from an active steam generation system used by a Statoil Canada Ltd. oil recovery operation (vide infra). The SAGD site has been operational since 2010, and the small settling pond is used for holding recovery water prior to reuse in the steam injection process.

4.2.6 Field Work Methods

The field monitoring examples presented were obtained in Northern Alberta in early July, 2012. Air sampling data sets were obtained in and around a Steam Assisted Gravity Drainage (SAGD) pilot facility (Statoil Canada Ltd.) located roughly 200 km south of Fort McMurray, and on public roads north of Fort McMurray along Highway 63. The MIMS system was operated in a sport utility vehicle (GMC Yukon). Stationary air sampling data sets were collected with the vehicle engine off and correlated with meteorological data determined at the sampling site. Aqueous sampling included the analysis of grab samples of on-site processed and ground water as well as measurements made by continuously sampling from nearby natural surface waters.

An example air monitoring dataset, presented here (vide infra), was generated during travel north of Fort McMurray on Highway 63 through areas adjacent to active oil sand recovery operations. Frequent stops (with the vehicle engine off) were performed to allow the collection of meteorological data and to obtain periods of stationary MIMS data. The example dataset was collected on July 7, 2012. The day was warm (27°C) and dry (30% relative humidity), with gentle wind speeds ranging between 4 and 7 m/s.

Aqueous samples of both on-site process water and off-site natural (stream, river, and ground) water were also collected during this field trip. An example dataset shown here was collected July 3, 2012 from an active steam generation system used by a Statoil Canada Ltd. oil recovery operation (vide infra). The SAGD site has been operational since 2010, and the small settling pond is used for holding recovery water prior to reuse in the steam injection process.

4.3 Results and Discussion

4.3.1 Field Work–Air Monitoring

Data collected with the mass spectrometer operating continuously in a moving vehicle is presented as a time series in Figure 4.3, and the progression of data workup is presented in each subpanel. The raw data for toluene measurement is shown in Subpanel A and indicates several toluene detections throughout the day. Generally, the data consists of long periods where toluene was not detected, punctuated periodically by transient excursions to higher signal levels. For example,

at 16:02, a very strong signal was observed (14,240 counts) when the vehicle passed over a stretch of road that had been very recently paved with fresh asphalt. At 16:24, a sustained signal was detected while the vehicle was stationed downwind of a tailings settling pond used by an active heavy oil extraction operation. Several other minor concentration excursions above detection limit levels may have been the result of passing vehicle exhaust emissions or air masses influenced by other settling ponds. Detections of vehicle exhaust were rather infrequent because of the elevated sampling intake, the very large dilution that rapidly occurs in the turbulence behind a moving vehicle (roughly estimated to be 25,000:1 at highway velocity), and the effective catalytic conversion of hydrocarbon emissions that occurs for hot, underway vehicles [114].

As noted above, ethylbenzene readily fragments under EI to yield m/z 91, and this can lead to a positive bias in the toluene concentration as determined by m/z 91→65. To compensate for this, we independently measure ethylbenzene by measuring m/z 106 → 91 and applying an interference factor calculated during pre-deployment calibration.

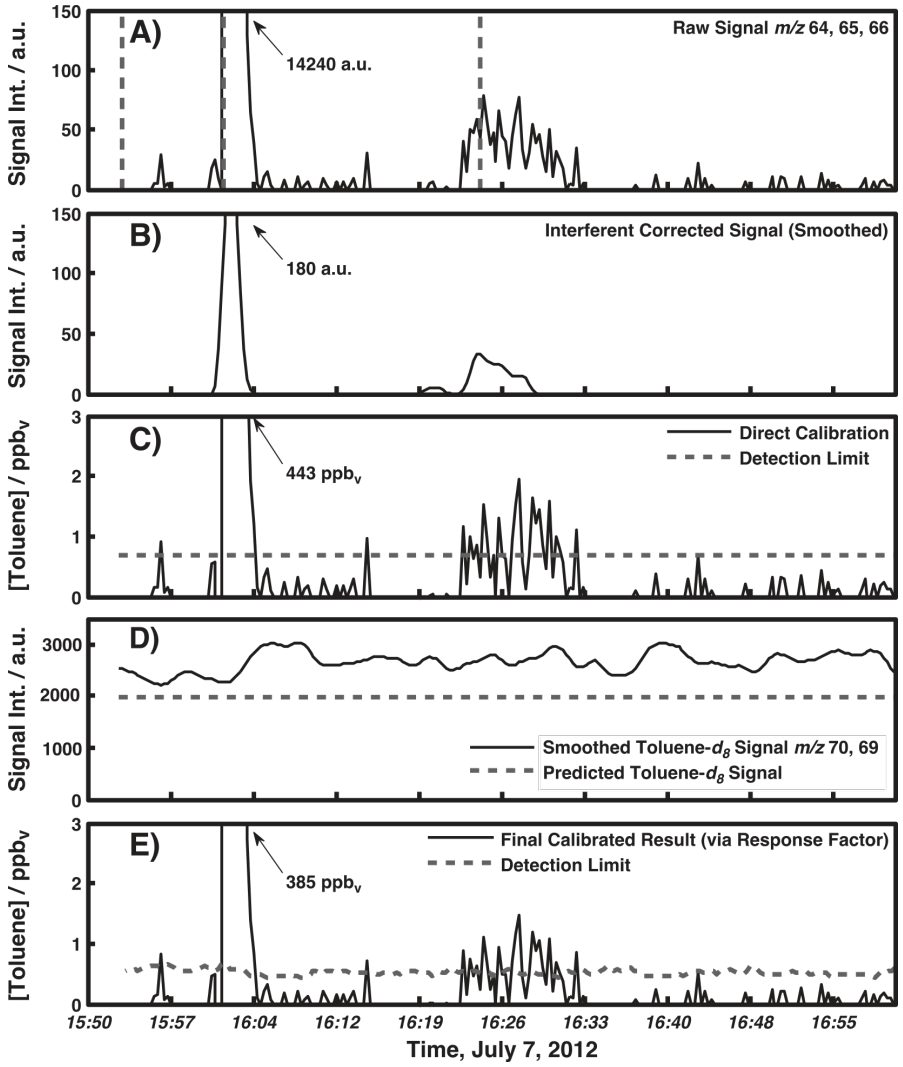


Figure 4.3: Time series representation of the instrumental data used for real-time toluene quantitation collected north of Fort McMurray, Alberta, Canada. The x-axis represents the time of day when the data was collected. Subpanels show data progression through the data workup process and the final data time series result is given in subpanel **E**.

The interference contribution data were smoothed (five-point boxcar) prior to being subtracted from to the analyte signal. Smoothing prevents the inclusion of additional instrumental noise into the signal data and allows signal corrections to be made on a time scale comparable with the MIMS response time for ethylbenzene (Table 4.1). The contribution of ethylbenzene to the m/z 91→65 signal is typically small (e.g., during the detection of emissions from fresh asphalt, 1.2%, 16:02), but can in some instances be significant (e.g., during detection of settling pond off

gassing, 40%, 16:24). The variability, of course, is strongly dependent on the particular sample composition. We cannot rule out positive interference in the toluene quantitation arising from other alkylbenzenes and hydrocarbons likely present near fresh asphalt paving [115]. Therefore, we caution the reader not to over-interpret the displayed toluene concentrations, even after correction for specific interferences such as those arising from ethylbenzene. Although EI is relatively simple to implement, it is a hard ionization strategy, resulting in the extensive fragmentation of many analytes, especially alkyl hydrocarbons. Further improvements in the use of interference factors as well as on-line standard addition strategies and softer ionization sources are currently being investigated to address the challenges of resolving isobaric interferents.

The ethylbenzene corrected toluene signal is converted to concentration in Subpanel c (Figure 4.3) using direct calibration factors from gaseous calibration standards prepared pre-deployment. Displaying this data along with the calculated detection limits is an additional quality control check and allows the user to quickly assess any signal deviations in the final data time series (Subpanel E).

Subpanel d (Figure 4.3) shows the instrumental signal for the continuously infused IS, toluene-d_8 (m/z 98 $\rightarrow$ 70), and is compared with the expected response to the IS given the sample flow rate and laboratory pre-deployment calibration (predicted toluene-d_8 signal). The IS concentration was calculated from the analyte constant, K_0 (cc/mg), derived from molecular weight and the ideal gas constant, permeation tube emission rate, (E , ng/min), and sampling gas flow rate (F, mL/min at STP) (Eq. 4.1). Expected IS response is calculated as the product of IS concentration[IS] and instrumental sensitivity to the IS ($m_I S$). The ratio of actual response to expected response provides a sensitivity coefficient that is a real-time measure of the instrument performance (Eq. 4.2). For example, rapid changes in the sensitivity coefficient may be indicative of transient events that can impact instrument sensitivity (e.g., due to a matrix interference or space-charge effects resulting from a highly contaminated sample or from membrane rupture/fouling). Long-term changes are useful in reporting drift in the instrumental state (e.g., filament or electron multiplier wear). As can be seen in Subpanel D (Figure 4.3), the instrument was slightly more sensitive to toluene-d_8 on this deployment than during pre-deployment lab-based calibrations. The IS data was also boxcar smoothed with a moving average (n =5) to reduce the addition of unnecessary electrical noise to the analyte signals, while allowing sensitivity corrections to be made on a time scale

that is comparable to the MIMS signal response times (Table 4.1).

$$[IS] = \frac{Ko * E}{F} \tag{4.1}$$

$$SensCoeff = \frac{Counts_{IS}}{m_{IS} * [IS]} \tag{4.2}$$

Subpanel E (Figure 4.3) shows the toluene concentration time series calibrated from an instrumental response factor (e.g.,toluene/toluene-d_8) determined during lab calibration, the raw analyte counts and the smoothed IS counts along with the sensitivity adjusted detection limit (DL_{Adj}, Eq. 4.3). As the instrumental sensitivity declines during multi-day deployments, the adjusted detection limit will increase. This can happen, for example, when the EI filament is nearing failure. When the detection limit crosses a predetermined threshold, the user can be warned by the software interface and corrective actions (e.g., replace the filament) can be taken. It is important for the instrument field operator to have real-time knowledge of the detection limit for immediate assessment of anomalous signals and to ensure the detection limits are adequate for the collection of meaningful data.

$$DL_{Adj} = DL * SensCoeff \tag{4.3}$$

As a final data assessment, Subpanel a (Figure 4.3) indicates two distinct detections. These detections are marked with vertical dashed bars (16:02 and 16:24) and for these intervals, the 30 s of full scan data following the vertical bar were averaged and presented as insets in Figure 4.4. The spectra were normalized using the IS signal (measured at *m/z* 98), then corrected by subtracting the spectrum for the IS. The IS spectrum was determined immediately prior to collection of this time series, and this time stamp is also marked with a vertical bar in Subpanel a (Figure 4.3, 15:54 h). The spectra indicate a complex suite of analytes permeating the membrane. The spectra insets in Figure 4.4 are distinctly different and suggest that MIMS full scan *m/z* data can be used in multivariate statistical approaches, such as Principal Component Analysis (PCA) for source apportionment and tracking. They also emphasize the importance of employing selective techniques such as MS/MS for quantitation.

The response factor calibrated toluene mass spectrometric data (*m/z* 91→65) collected north of Fort McMurray, Canada (Figure 4.3, Panel e) was time-matched

to GPS data and meteorological data, and is presented in Figure 4.4.

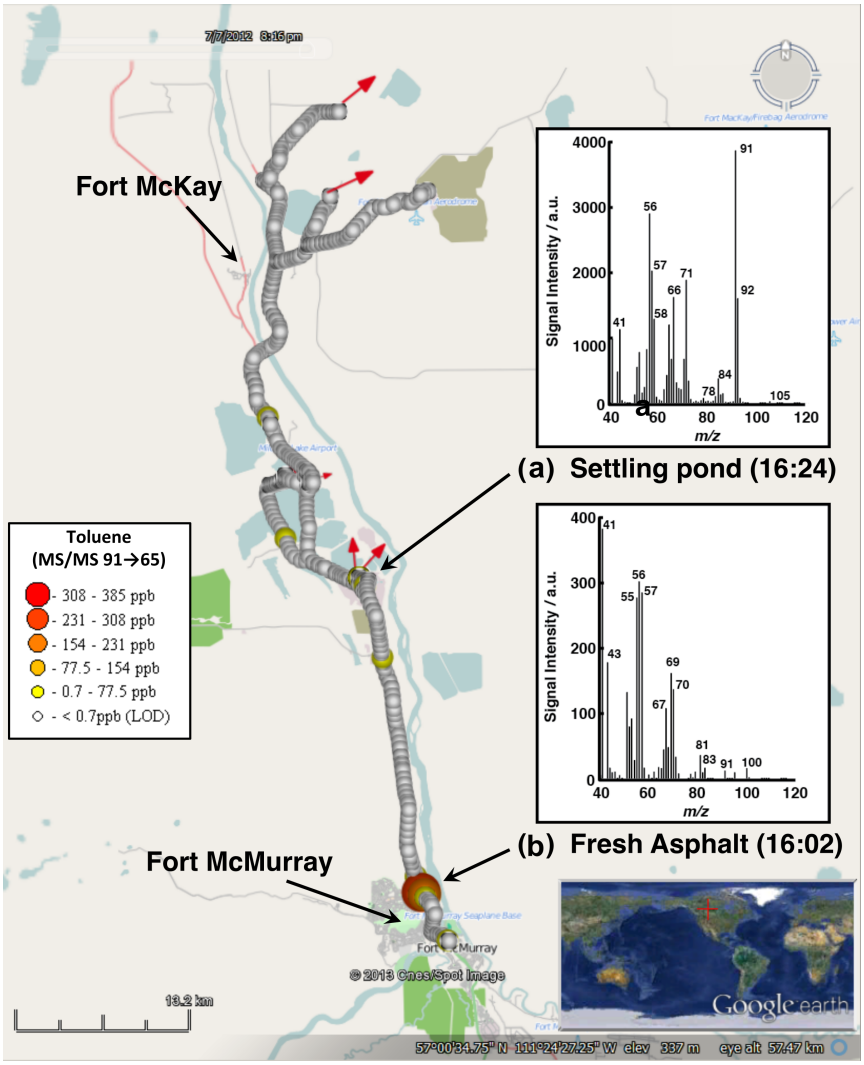


Figure 4.4: Google Earth snapshot of atmospheric toluene data collected north of Fort McMurray, Alberta, Canada. Data are multidimensional and time-stamped, allowing for a fully navigable data environment and video creation. The insets illustrate full scan mass spectra of selected survey data obtained during detection events. Inset (a) shows the mass spectrum of the air space downwind of a waste-water settling pond (16:24) and (b) shows the mass spectrum for atmospheric monitoring while travelling on a freshly paved asphalt roadway (16:02). Both spectra were normalized to the toluene-d_8 IS, with background and IS spectra subtracted.

White dots represent data collected that were below the detection limit. Wind vectors are represented by the red arrows and can be queried (with a computer mouse click) in Google Earth to inspect the data file source, wind direction, wind speed, temperature, humidity, barometric pressure, time, latitude, and longitude.

The 16:02 detection discussed above is noticeable as a large dot just north of Fort McMurray, and the 16:24 detection is labelled at Settling pond 16:24. The data track presented in Figure 4.4 is a small subset of a much larger dataset navigable by Google Earth.

Multiple analyte concentrations are embedded in the Google Earth *.kml data file(s) and can be depicted as individual tracks for inspection in real-time or post-deployment. Figure 4.5 shows a 5 h continuous time series collected while driving and parked in a discrete pattern (termed a Rosette) at strategic locations in and around a SAGD demonstration facility, similar to the methodology employed in other work by our group [101].

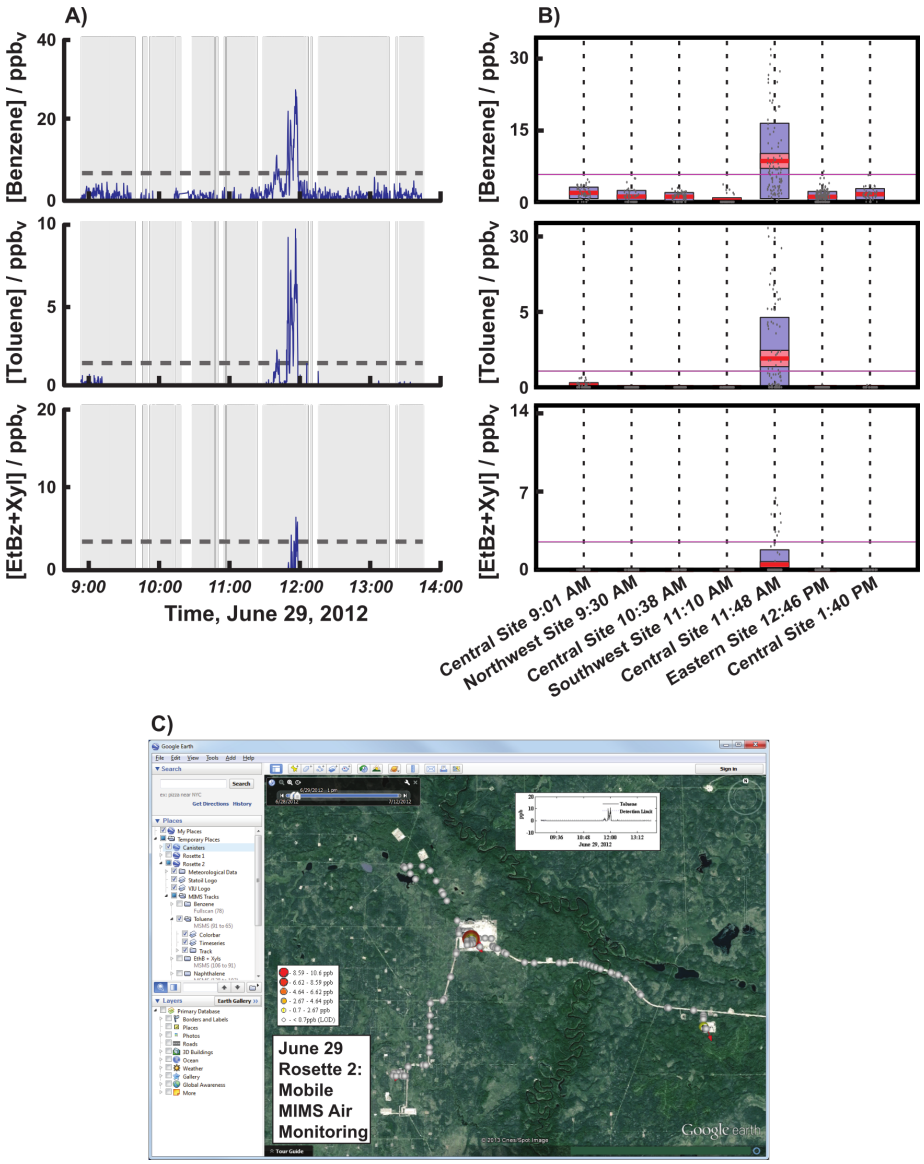


Figure 4.5: (a) Five-hour time series for atmospheric benzene, toluene, and ethylbenzene + xylenes (EtBz + Xyl) showing data collected in moving vehicle (white background) and while stationary (gray background). The horizontal dotted line represents the calculated detection limits. (b) Whisker box plots for stationary deployments only showing mean concentrations, 25-75 percentiles and data outliers. (c) Google Earth screenshot of the atmospheric toluene data collected on-site. Geospatial time series data for all analytes can be inspected in a single *.kmz file along with the relevant meta–data.

Subpanel a illustrates the data obtained for benzene, toluene, and ethylbenzene (+xylene). The shaded regions represent data collected while the vehicle was stationary (with the vehicle engine off), whereas the unshaded data was collected

while moving. Most of the time VOC concentrations are well below our observed detection limits (dashed horizontal line). The signal appearing around 12:00 h was observed while the vehicle was parked just downwind of a relatively small, lined settling pond used to hold process reuse water. Subpanel b displays a whisker plot of the stationary data only and illustrates the distribution of chemical concentrations as 25–75 percentiles as well as outliers. Subpanel c illustrates a Google Earth screenshot depicting the toluene concentration track. The navigation panel on the left sidebar of the screen allows the user to select the analyte to display. The data can be viewed in a video mode, playing back the data evolution over time. Screen overlays that include legend, data time series, and institutional logos can also be generated when desired. Importantly, each data point can be queried for its source file, scan information, raw counts, concentration, detection limit, time, latitude, and longitude. In summary, Google Earth has proven to be an extremely useful tool for data visualization and analysis due to its data structure and wide availability.

4.3.2 Field Work–Aqueous Monitoring

Water samples can be readily analyzed using the same membrane interface and ion trap mass spectrometer system by diverting the aqueous sample stream into the MIMS interface using the aqueous sampling manifold (Figure 4.1, valves A1 and A2). Continuously infused IS delivered via a syringe pump can be utilized for real-time calibrations using predetermined response factors as above. The other syringe pump (Figure 4.1) can be loaded with analyte standards and employed for periodic in-field calibrations by standard addition methods. The in-line sample heater and heat exchanger system can be used to preheat samples and improve response times, if necessary. Figure 4.6 illustrates data for the analysis of a VOC contaminated boiler feed water sample, diluted 24:1 to avoid space charge effects in the ion trap from excessively high analyte concentrations. The sample inlet line was switched from deionized water to diluted boiler feed water at 21:24. Data analysis indicated the diluted sample had a concentration of 29 ppb. At 21:39 (dashed bar A), the continuous infusion of a standard solution containing both benzene (19 ppb) and toluene-d_8 (19 ppb) was initiated. The software system allows for sample analysis by IS and/ or standard addition methods, depending on the injected solution.

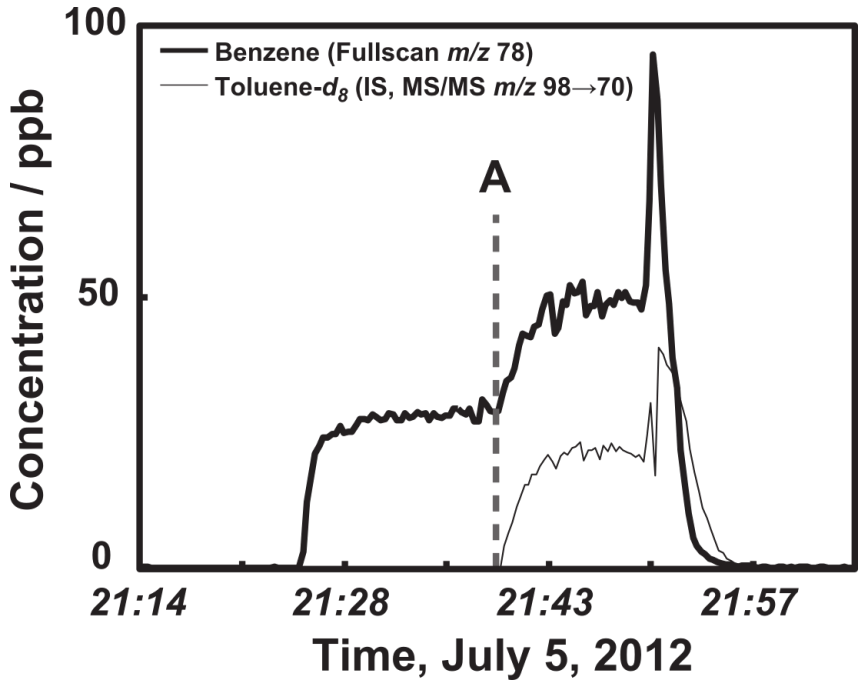


Figure 4.6: In-field analysis of a heavy oil process water sample. At 21:39 (dashed bar A), an infusion containing both benzene (19 ppb) and toluene-d_8 IS (19 ppb) commenced. Pre-analysis dilution was 24-fold.

The benzene signal was calibrated using the standard addition data, whereas the toluene-d_8 is shown as a demonstration of the use of an IS. Once again, the use of an IS relays important information to the field operator about instrument performance by comparing on-site signal intensities to those observed pre-deployment. The sudden jump in signal at 21:50 is a result of an entrained air bubble that occurred when switching the sample stream to a washout blank (DI water). The abrupt change observed for the IS signal would be a suitable trigger to suggest that this is compromised data, allowing it to be censored (if desired) from any further data analyses.

Since the instrument can be employed to report continuous, calibrated VOC concentrations in aqueous samples in realtime, it is a powerful in-field monitoring tool for dynamic chemical systems. Industrial sites such as SAGD operations have numerous operational systems to process and reuse water supplies. On-line process monitoring can provide important information to industrial operators. Furthermore, sensitive and selective on-site monitoring of contaminants in surrounding surface and ground waters aids in better environmental stewardship and protection initiatives.

4.3.3 Implications and Future Work

The combination of instrumentation, data analysis, and visualization software presented here provides a novel approach that provides quantitative, information-rich data sets that enable real-time, on-site decision making. This is especially useful for timely process control decisions, emergency response scenarios, adaptive sampling during field measurement campaigns, and long-term environmental monitoring studies. The presented system is amenable to several improvements including the inclusion of a thermally assisted membrane [19] to improve detection limits for SVOC analytes and the implementation of various chemical ionization methods to improve instrument selectivity [107, 109, 116]. Future software development will focus on cataloguing data for improved online database access, additional data input features (e.g., real-time dilution calculations), and improved data (and meta-data) presentation for real-time quality control analysis. Additional peripheral equipment development will include continuous wind vector determinations and simultaneous video monitoring capabilities. The presentation of more extensive datasets including validation studies for hydrocarbons in both air and water will follow in subsequent publications.

4.4 Conclusions

A novel field portable membrane introduction mass spectrometry (MIMS) system is presented that utilizes in-house developed real-time data analysis and visualization software for geospatial mapping of VOC/SVOCs in the environment. The system has been used for monitoring hydrocarbon contaminants in air and water samples during in-field sampling campaigns in and around oil and gas extraction facilities in Northern Alberta, including the direct, in-field measurement of process waters. Real-time detection limits are in the low ppb range. The presented system allows operators to develop intelligent, adaptive sampling strategies based on data being produced in real-time, and provides data to enable remotely located decision makers to implement corrective actions when needed. Continuous mass spectral time series datasets are obtained, processed, and visualized using in-house developed software. Data are temporally resolved and, therefore, capable of capturing transient concentration excursions. In the case of air monitoring, data capture over a wide spatial area by using the system in a moving vehicle is also possible. Although the

presented system is currently limited to electron impact ionization (EI), we are exploring the use of softer chemical ionization strategies to alleviate isobaric interferences that arise from the EI fragmentation of matrix species.

Chapter 5

Combining Portable Mass Spectrometer and Whole Air Sampling Canister Data for Atmospheric Analysis

Draft manuscript to be submitted Spring, 2016. Davey, N. G.; Bell, R. J.; Simpson, I. J.; Blake, D. R.; Gill, C. G.; Krogh, E. T. "Combining Portable Mass Spectrometer and Whole Air Sampling Canister Data for Atmospheric Analysis." Sample collection strategy and data acquisition by R. Bell, E. Krogh and N. Davey in consultation with I. Simpson. Mapping and time series data figures generated with software developed by R. Bell. Analysis of whole air sampling canisters by I. Simpson and D. Blake. MIMS data collection and treatment of the data from both sampling strategies and manuscript preparation by N.Davey. Editorial contributions to date by C. Gill and E. Krogh.

5.1 Introduction

The release of volatile organic compounds (VOCs) into the environment from both anthropogenic and natural sources can have a significant negative impact on environmental conditions and human health. There is also considerable variation in spatial and temporal VOC concentrations, depending on the number and nature of the sources. Therefore, there is a need for sensitive, selective and cost effective analytical methods for the chemical analysis of raw air samples. The conventional technique for the analysis of VOCs in air involves sampling the atmosphere with evacuated canisters, followed by chromatographic separation and characterization [87]. Although this technique has been shown to be very sensitive

and selective, it represents a single point in time and place, and may not capture concentration fluctuations in dynamic systems, such as the atmosphere. VOCs are also subject to dispersion by mixing and active removal. For example, atmospheric lifetimes for VOCs range from hours to days, depending on the various photochemical [117] and deposition [118] mechanisms at play.

A number of fence line monitoring strategies have been employed for fugitive emission monitoring and source tracking of VOCs. In particular, sorption tubes [119] and solid–phase micro extraction (SPME) [120] followed by gas chromatography (GC), flame ionisation detection (FID), electron capture detections (ECD) or mass spectrometric analysis, are sensitive and selective techniques that have been employed for on–site analysis. These adsorptive enrichment strategies are well established and effective, but represent an integrated concentration for a period of time, in a particular place. These methods are generally too slow to capture rapid changes in concentration or provide timely information in the event of an accident or emergency.

Membrane introduction mass spectrometry (MIMS) is well suited to the analysis of raw air samples because the technique provides continuous data sets for the concentration of numerous analytes [14, 23, 79, 121]. MIMS has been used for direct chemical analysis, without sample pre–treatment or chromatography, for many years and for a variety of sample types and analytes [1, 3]. The technique relies on a semi–permeable membrane which, at the same time, allows for pre–concentration of VOCs and SVOCs while the bulk of the sample matrix is excluded from the vacuum of the mass spectrometer. Tandem mass spectrometry (MS/MS) can be used to sort the mixture of analytes, based on characteristic mass to charge (m/z) ratios and fragmentation pathways, if ion–traps or triple quadrupole mass analysers are employed.

In this paper we report the results of an atmospheric monitoring campaign that focused on the industrialized region of Ft. Saskatchewan, AB. In this region there are numerous facilities, including hydrocarbon upgraders and chemical refineries associated with bitumen processing as well as a number of other heavy industries. Previous work by Simpson *et al.* [122] has indicated that elevated levels of hydrocarbons in this region may be of concern for the surrounding community. Continuous real–time datasets were produced, from a MIMS system, that provide calibrated molecular information about sample composition and concentrations in this area.

As with any unconventional analytical technique, it is desirable to have multiple

methods for quantitation so than one can compare and validate the analytical results obtained [123]. A field portable MIMS system developed by our group was used to obtain geospatial time series data, which was collected concurrently with a whole air sampling (WAS) canister strategy, employed by the Rowland–Blake research group (University of California, Irvine). This group is internationally recognized as a leader in analytical atmospheric research. The WAS methodology employed is well established and described in detail by Simpson *et al.* [87]. Due to the nature of the sampling strategies employed, there is a great deal more MIMS data than WAS canister data. Therefore, only select data sets with both types of data are presented herein.

5.2 Materials and Methods

5.2.1 Mass Spectrometer System

The mass spectrometer system used was a Griffin 400 cylindrical ion trap, which was operated using electron ionization (EI) with a base pressure of 1.0×10^4 Torr base pressure and an $\sim$1.0 mL/min helium flow. Helium carrier gas was delivered to the lumen of the membrane by a miniature 16 L compressed gas cylinder (Model 49617HE, Leland Ltd., South Plainfield, NJ, USA). The membrane inlet system, described in detail elsewhere [124], uses Dow Corning Silastic polydimethylsiloxane capillary tubing (10.0 cm x 0.94 mm OD x 0.51 mm ID) with a wall thickness of 215μm for sample introduction rather than a GC column. The membrane and the sample transfer lines were maintained at 50°C during analysis by a heated aluminum block and an insulated wire rope heater, respectively. For continuous atmospheric monitoring, a diaphragm pump (Model B–Series Dia–Vac; Air Dimensions, Deerfield Beach, FL, USA) was used to pass outside air through an internal standard chamber and over the membrane at a flow rate of 1850 mL/min. A toluene–d_8 Kin–Tek Trace Source permeation tube, with an emission rate of 625 ng/min at 50°C, was used as an internal standard for in field quantification using relative response factors (method described in Etzkorn *et al.* [23]. Two solvent cleaned microporous stainless steel inlet filters (Model SS–6 F; Swagelok, Solon, OH, USA) in series were also used as part of a heated sample transfer line (1/4" o.d. Teflon tubing) to remove particulates. The instrument was powered by a bank of four 6 V lead–acid batteries (Model T–145 Plus; Trojan Battery Company, Santa Fe Springs, CA, USA), and transported in a

mid–sized SUV. Furthermore, the instrument was encased in a mu–metal sheath to shield the ionization source from the Earth's magnetic field. The necessity of this shielding is described in detail by Bell *et al.* [125], and is reproduced in this thesis as Chapter 6 (*vide infra*). The instrument schematic is shown in Figure 5.1.

For lab based validation studies, a second MIMS system, that used a chloroform chemical ionization (CI) strategy for quantitative analysis, was connected in series to the sample stream. This system is described in detail by Davey *et al.* [126] and is reproduced in this thesis as Chapter 7 (*vida infra*).

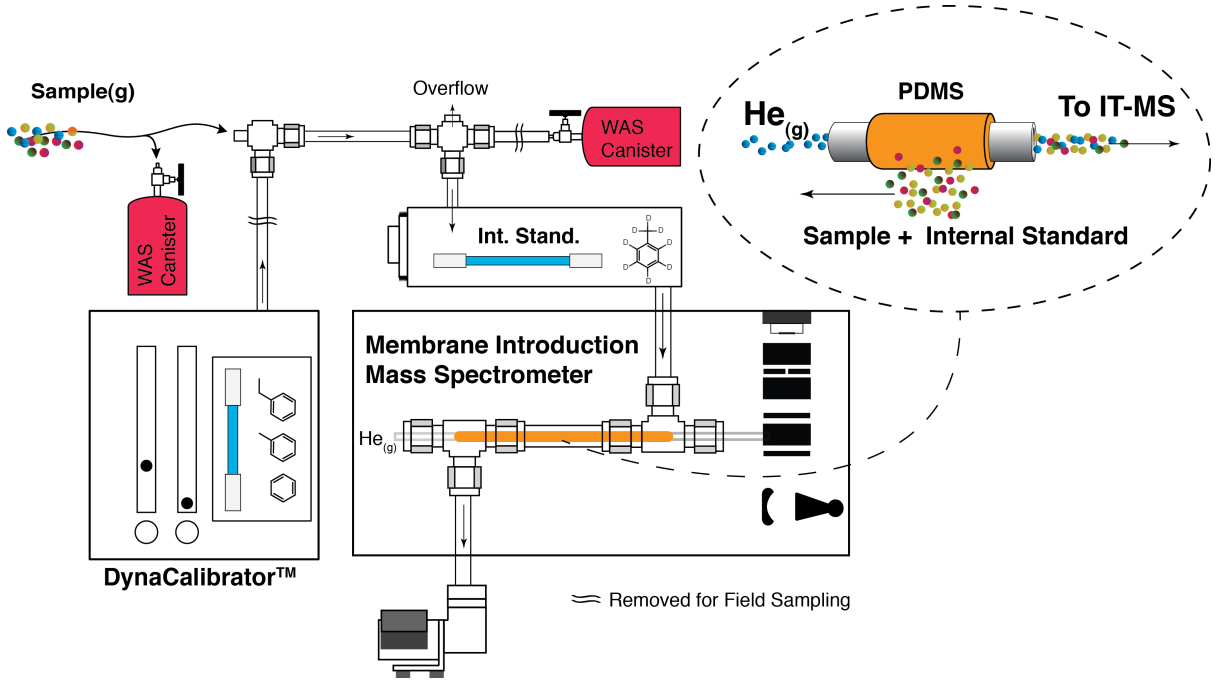


Figure 5.1: Schematic of MIMS instrumentation and WAS canister configuration for both field and lab based validation studies.

5.2.2 Dynacalibrator Gas Standard Generator

Pre–deployment calibrations and validation studies were performed using a Dynacalibrator (VICI, model 340) and certified Kin–Tek Trace Source permeation tubes to generate gaseous standards for the target analytes (benzene, toluene, ethylbenzene/xylene(s), chlorobenzene, chloroform, naphthalene, dimethyl sulfide, dimethyl disulfide and methyl iodide). The Dynacalibrator was removed for field sampling.

5.2.3 Air Sampling Canisters

Electropolished 2–L stainless steel canisters, provided by the Rowland–Blake research group, were used to collect whole air samples. For laboratory comparison studies WAS canisters were connected in–line with the MIMS system. For field studies, the WAS canisters were opened in the vicinity of the MIMS sample inlet at a distance typically < 1 meter. All cans were analyzed 2–3 months after collection. The analytical system for the WAS canisters consist of a 5 column/detector analytical system with 2 GC–FIDs, 1 GC–MS, and 2 GC–ECDs. Details of canister preparation and sample analysis can be found in Simpson *et al.* [87].

5.2.4 Lab–Based Validation Study

To determine the agreement between the MIMS system and a traditional whole air sampling (WAS) GC–FID/ECD/MS system, gaseous standards were generated with a Dynacalibrator and delivered to both sampling systems at the same time. A schematic of the experimental set up can be seen in Figure 5.1. A typical experiment would proceed as follows: (1) Gaseous standards were prepared using temperature equilibrated permeation tubes in a Dynacalibrator. (2) With the valve to the WAS canister closed, the sample was passed over the membrane interface via a second heated chamber containing an internal standard and the system was allowed to reach steady state. (3) The 2L WAS canister was then opened and allowed to fill over a period of 1–2 minutes. (4) The WAS canisters were then closed and returned to the UC–Irvine laboratory for analysis. A schematic of a representative lab–based dataset is given in Figure 5.2a. An example mobile air monitoring dataset is presented in Figure 5.2b, indicating chronogram fluctuations, resulting from atmospheric concentration changes, and the strategy employed for comparing MIMS and WAS datasets. Since WAS canister data represents an average atmospheric concentration during the fill–time of a canister ($\sim$ 2 minutes), it was necessary to average the MIMS data for the same amount of time for comparison. Furthermore, a 'time–delay' was estimated when selecting the MIMS data to account for time it takes an analyte to reach the detector. This 'time–delay' was estimated to be the sum of the time for the analyte to reach the membrane via sampling lines (4–5 seconds) plus the time for the analyte to diffuse across a 215 μm thick PDMS membrane (30–60 seconds, depending on the analyte).

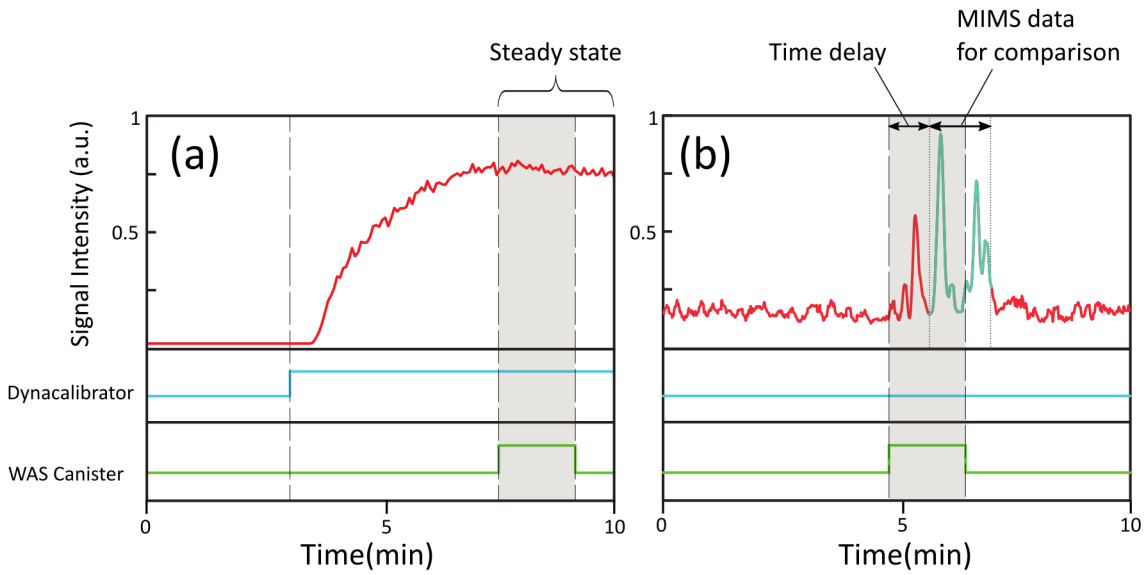


Figure 5.2: Schematic of typical sequence of events for WAS canister and MIMS comparison experiment. Signal intensity is representative chronogram for one particular MS/MS transition. (a) Lab–based sampling strategy: Gaseous standard delivered to membrane interface at ∼3 minutes. WAS canister allowed to fill at ∼7 minutes once steady state is established. (b) Field–based sampling strategy: MIMS real time data collected from a mobile platform is used to guide WAS canister fill location/time. MIMS data used for comparison is 'delayed' to account for sampling and membrane transport times.

5.2.5 Field Studies

A field portable membrane introduction mass spectrometer was developed and employed to identify nine target analytes in air. These nine compounds were chosen to represent a range of environmentally relevant compound classes and are listed, along with pertinent MS parameters, in Table 4.1 of Chapter 4. Field data was collected over multiple 8–hour runs, which included both stationary data acquisition and monitoring transects. On–board GPS and mass spectral data were correlated and processed with Labview to yield calibrated, geospatial data in real–time. After mobile data collection, the raw data was processed using MATLAB (Mathworks, Natick, MA, USA) and saved as .kmz files for visualization in Google Earth.

Processing involved background subtraction, direct calibration, internal standard response factor calibration, interference factor correction for interferences, and finally extraction for visualization. A detailed description of the data work up is presented in Chapter 4 (Subsection 4.3.1).

5.3 Results and Discussion

5.3.1 Lab Based

In an effort to better understand the field data and validate our quantitation methods, a lab–based comparative study was conducted, employing steady–state concentrations of contaminants in air samples. This strategy was employed to eliminate difficulties introduced by rapidly changing concentrations and minimize uncertainties introduced by time delays. WAS canister sampling was followed by off–line laboratory analysis, which provided data to compare with the MIMS results. Table 5.1 shows replicate measurements of a 38 ppbv gaseous toluene standard. The sample also contained benzene, however, this data is not included as a custom temperature regulator for the benzene permeation tube malfunctioned during the course of this particular experiment. In general, the data presented in Table 5.1 suggests reasonably good agreement between WAS canister and MIMS results. Percent difference, relative to the WAS canister results, is reported for three different quantitative MIMS strategies (EI–direct calibration, EI–internal standard calibration, and CI–internal standard calibration). The average percent error for the MIMS result using direct calibration was found to be -22%. The % difference was reduced with the use of an internal standard (-7%) for quantitation. This result demonstrates the effectiveness of an internal standard at correcting for variation in instrument performance (i.e. sensitivity) between the time of calibration and sampling. In other words, the internal standard is compensating for signal drift, which is important for field deployments or any circumstance when there is delay between calibration and measurement. Furthermore, since the efficiencies of ion sources and detectors are known to change over time (particularly at high pressures and in the presence of oxygen), this methodology can be used to initiate maintenance routines to prevent collection of low quality data. The average % error for the MIMS result was found to be -23% when chemical ionization with a chloroform reagent gas and a toluene–d_8 internal standard was used for

quantitation. This result is consistent with that of the EI–direct calibration results, and offers no quantitative advantage for the particular sample measured. For a detailed description of the chemical ionization strategy employed here, the reader is directed to Chapter 7 of this document.

In Table 5.2, the results for three samples of varying degrees of complexity are presented. Complexity in this context, refers to the number of chemical compounds in the sample that have the potential form isobaric species and contribute to biases (see Figure A.7 for the fragmentation pathways of select alkylbenzenes). In general, the magnitude of the difference increases with sample complexity for both EI calibration methods. The % difference for the CI calibration is, in general, less affected by sample complexity.

Sample 1 contains a mixture of toluene and ethylbenzene. In comparison with the WAS result, the EI–MIMS showed a positive bias for toluene with both direct calibration (+14%) and internal standard calibration (+34%). By comparison, the bias for toluene in Table 5.1 is reported as negative value, which suggests that, despite the application of interference correction factors, there is a positive bias in the reported toluene concentration due to ethylbenzene. Chemical ionization MIMS, on the other hand, showed a negative bias (-17%) when compared to the WAS result. The data suggests that the toluene concentration reported by CI is not positively biased by the presence of ethylbenzene. In comparison with the WAS result, the EI–MIMS showed a negative bias for ethylbenzene with both direct calibration (-10%) and internal standard calibration (-3%). Chemical ionization MIMS also showed a negative bias (-27%) when compared to the WAS result. It should be noted that the MIMS data for ethylbenzene, *m/p*–xylene and *o*–xylene is reported as a sum, since these structural isomers cannot be distinguished by the technique. For % difference calculation purposes, the WAS canister data for these isomers was also summed.

Sample 2 contains a mixture of toluene, ethylbenzene and *m/p*–xylene. In comparison with the WAS result, the EI–MIMS showed a negative bias for toluene with both direct calibration (-47%) and internal standard calibration (-33%). Chemical ionization MIMS also showed a negative bias (-18%) when compared to the WAS result. By comparison, the bias for toluene in Sample 1 is reported as a positive value, which suggests that as the number or concentration of isobaric species increases, there is a possibility of overcorrection to the toluene signal, which results in a negative bias. Chemical ionization MIMS also showed a negative bias

Table 5.1: Comparison of WAS canister and MIMS data for replicate gaseous standards.

Matrix	Analyte	Dynacal. ppbv	WAS Can ppbv	MIMS (EI) ppbv (dir.cal.)	[a]%diff	MIMS(EI) ppbv (int. stand.)	[a]%diff	MIMS (CI) ppbv(int.stand.)	[a] %diff
Air	Toluene	38	38.311	29	-28	35	-9	33	-15
	Toluene	38	35.056	29	-19	37	5	32	-9
	Toluene	38	36.503	31	-16	42	14	23	-45
		Avg. Toluene	37	30	-21	38	-8	29	-23

[a]% difference is the MIMS result relative to WAS canister concentration.

(-18%), but this result is consistent with that of Sample 1 (-17%), suggesting that *m/p*–xylene is not isobaric with toluene when CI is employed.

In comparison with the WAS result, the EI–MIMS showed a positive bias for ethylbenzene/xylene(s) with both direct calibration (40%) and internal standard calibration (48%). In contrast, chemical ionization MIMS showed a negative bias for ethylbenzene/xylene(s) (-20%) when compared to the WAS result. The CI result is consistent with that of Sample 1, suggesting that the addition of *m/p*–xylene does not affect the precision of the result.

Sample 3 contains a mixture of toluene, ethylbenzene, *m/p*–xylene and α–pinene. In general, the results are consistent with those of sample 2, which suggests that the EI correction for the pinene/toluene system is effective. The CI MIMS result has minimal % difference (-9%), which suggests that α–pinene does not affect the toluene signal.

By inspection of the EI ethylbenzene data from Samples 1, 2 and 3 it is clear that positive bias increases with sample complexity, which in turn implies that the correction factors applied require refinement. The data for CI–MIMS suggests that bias is consistently negative, regardless of sample complexity. Direct calibration EI, internal standard calibration EI and CI MIMS data all show significant negative bias for α–pinene (-125, -114, and -92 %, respectively) when compared to WAS. This data suggests a calibration error. The likely cause of this was a customized permeation tube chamber, used solely for α–pinene, that was likely hotter than predicted. This would lead to an increased emission rate (ng/min) from the permeation tube standard, which in turn would result in an under–prediction by MIMS (16 ppbv) compared to the actual concentration (43.497 ppbv) as reported by WAS.

5.3.2 Field Based

Figure 5.3 is an example Google Earth map of atmospheric ethylbenzene/xylene(s) concentration near Ft.Saskatchewan, AB. The magnitude of the concentration is proportional to the size and color of the dots, and the highest observed concentrations were between 19–24 ppbv. Point–in–time WAS canister location is indicated by blue and green canister pictograms. The MIMS data shows several low–level ethylbenzene detections, particularly at the location indicated by WAS sampling occurred. These results demonstrate the utility of real–time data collection and analysis for 'big–picture' visualization of the chemical landscape, an

Table 5.2: Comparison of WAS canister and MIMS data for isobaric gaseous standards.

Sample	Analyte	Dynacal. ppbv	WAS Can ppbv	MIMS(EI) ppbv (dir.cal.)	[a]%diff	MIMS(EI) ppbv (int. stand.)	[a]%diff	MIMS (CI) ppbv(int.stand.)	[a] %diff
1	Toluene	38	35.517	41	14	50	34	30	-17
	Ethylbenzene	16	14.400						
	m/p–xylene	0	nd	13	-10	14	-3	11	-27
	o–xylene	0	nd						
	α–pinene	0	nd	nd	-	nd	-	nd	-
2	Toluene	38	32.205	20	-47	23	-33	27	-18
	Ethylbenzene	16	13.285						
	m/p–xylene	21	17.336	46	40	50	48	25	-20
	o–xylene	0	0.045						
	α–pinene	0	nd	nd	-	nd	-	nd	-
3	Toluene	38	42.744	31	-32	35	-20	39	-9
	Ethylbenzene	16	15.973						
	m/p–xylene	21	21.56	60	46	67	56	30	-22
	o–xylene	0	0.044						
	α–pinene	16	43.497	10	-125	12	-114	16	-92

[a]% difference = (([MIMS]-[WAS])/mean) x 100 %

for directing an adaptive sampling protocol to areas of interest.

Figure 5.4 is an example Google Earth map of atmospheric benzene concentration, collected at the same time as the data for ethylbenzene, near Ft.Saskatchewan, AB. However, the magnitude of the benzene concentration is significantly higher, with observed concentrations between 105–131 ppbv. As in the previous figure, point–in–time WAS canister location is indicated by blue and green canister pictograms. Additionally, a red arrow indicated the wind speed and direction measured as the time and place of canister sampling. These results suggest that the source of benzene is upwind of the site where canisters were filled.

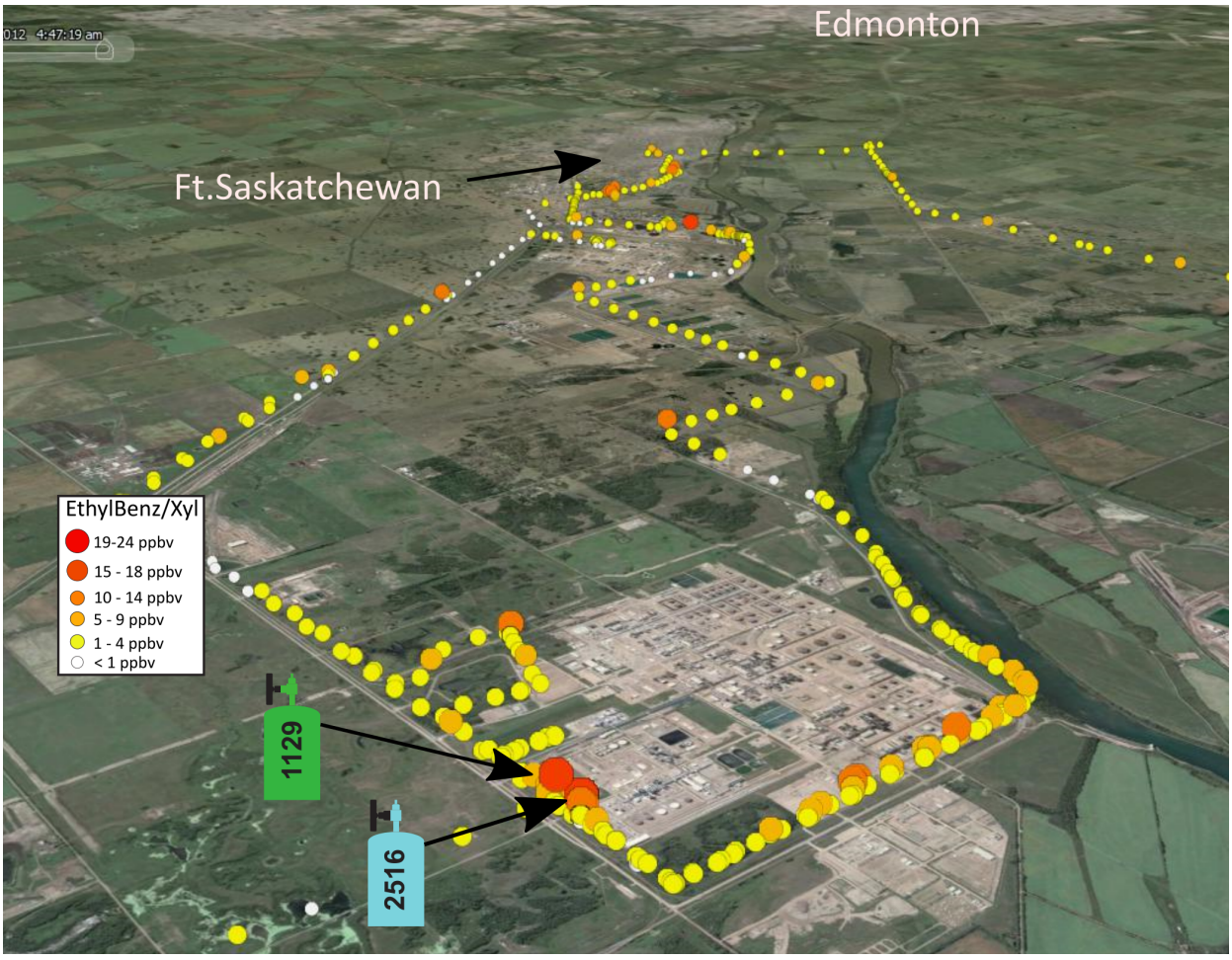


Figure 5.3: MIMS air data inter–comparison 2012. Google earth screen grab of atmospheric ethylbenzene concentration near Ft.Saskatchewan, AB. WAS canister fill location is indicated by blue (2516) and green (1129) pictograms.

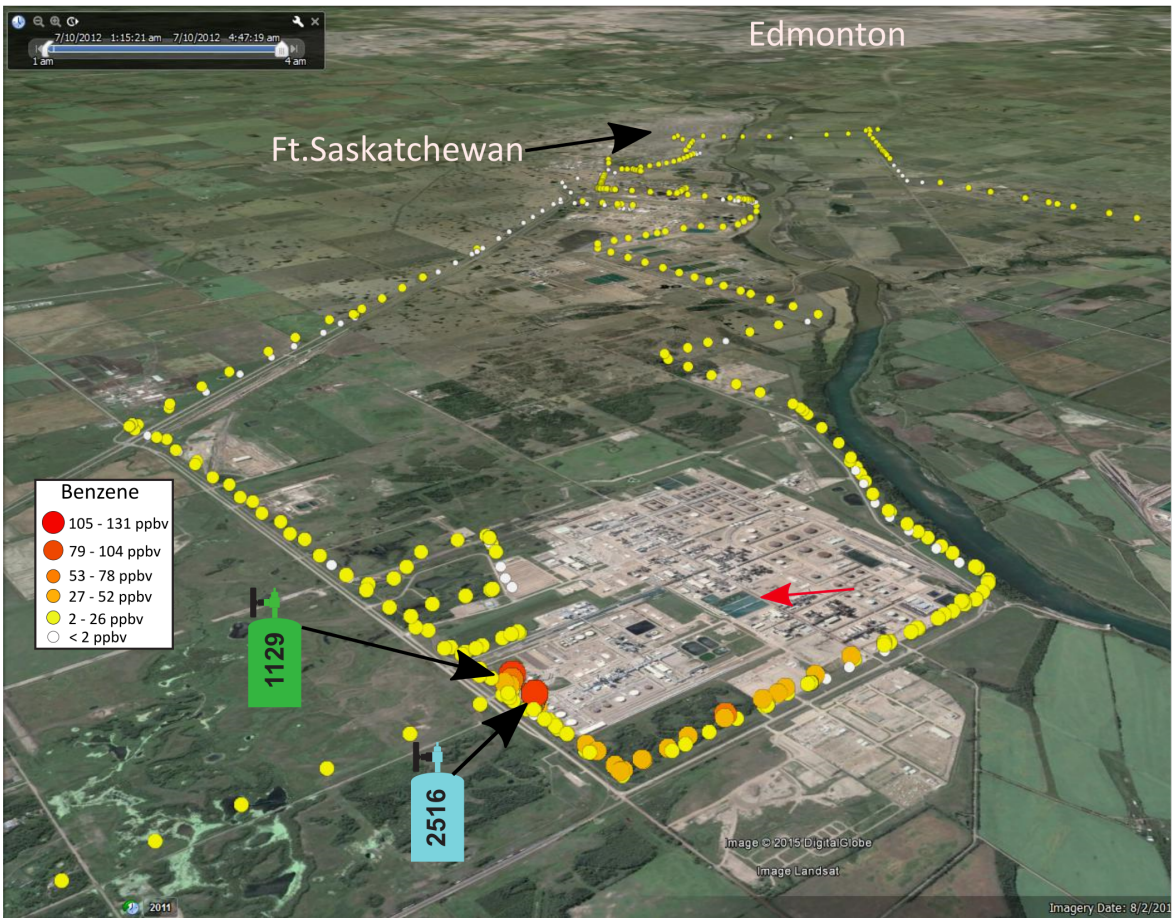


Figure 5.4: Google earth screen grab of atmospheric benzene concentration near Ft.Saskatchewan, AB. WAS canister fill location is indicated by blue (2516) and green (1129) pictograms. Wind direction and speed was measured on–site and is indicated by a red arrow (328.5° at 9.5 m/sec)

Figure 5.5 is an example time series of the same data presented in figures 5.3 and 5.4, with superimposed point–in–time air canister sampling indicated by vertical blue and green bars. The MIMS data that was averaged, for comparison to canister data, is displayed in red for each of the chronograms. Further, the detection limit for each compound is plotted as a horizontal dotted line near the baseline of each chronogram. The MIMS data for toluene is shown in Subpanel a and indicates several low–level toluene detections, particularly at approximately 10 am. The toluene result for WAS canister 1129 was 922 pptv and the MIMS result was 1400 pptv. Given the challenges associated with estimating 'delay time', canister fill time (fill rate decreases with time) and identical air masses, this result is considered a good level of

agreement. The MIMS toluene data used for comparison with canister # 2516 was below the detection limit, and the reported value for the canister was 744 pptv. In Subpanel b, high concentrations of benzene are reported by both MIMS and WAS canister. For canister sample # 1129, the canister concentration is reported to be 902 pptv, while the calculated MIMS concentration was 17 100 pptv. The results for sample # 2516 are also vastly different, with the canister concentration reported to be 156 196 pptv, and the MIMS 74 400 pptv. In Subpanel c, the concentration of ethylbenzene/xylene(s) for sample # 1129 is reported to be 10 610 pptv for the canister, and 11 400 pptv for the MIMS. These results are in good agreement but do not reflect the positive bias ($\sim$ 50%) expected from the results for samples 2 and 3 in Table 5.2.

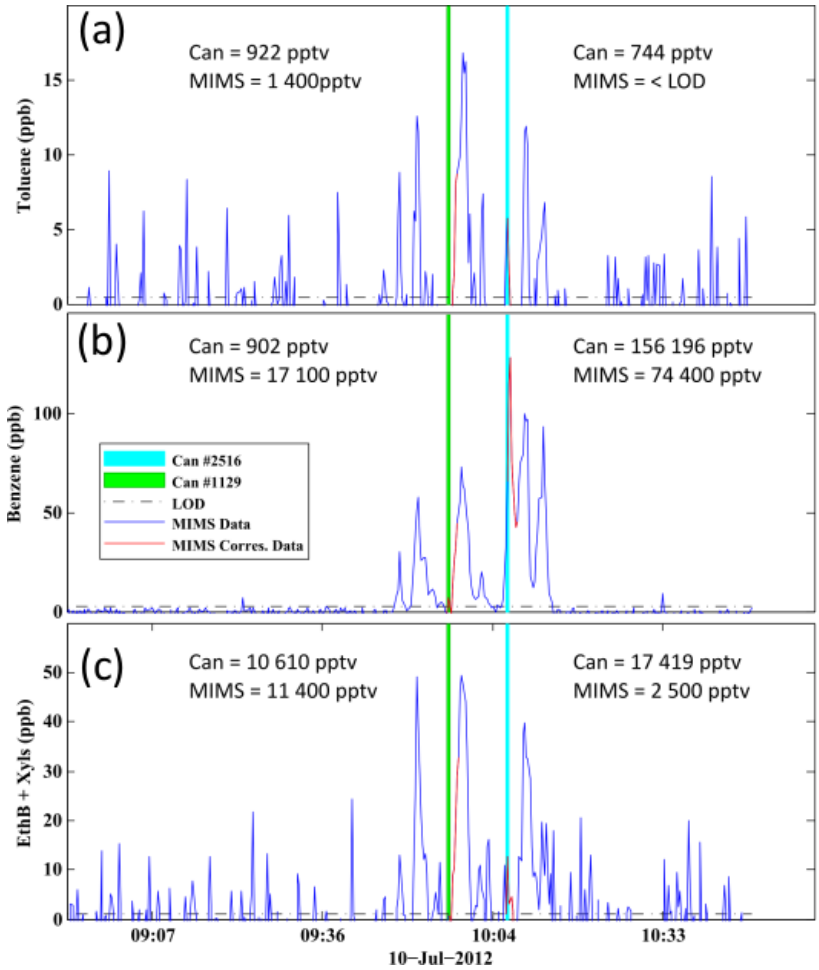


Figure 5.5: Time series data for atmospheric toluene, benzene, and ethylbenzene + xylene(s). Green and blue vertical lines indicate the time of canister sampling and approximate fill time. The corresponding MIMS data shown in red indicates the portion of the time series used for comparison purposes.

5.4 Conclusions

The data presented in Figure 5.5 illustrates the strengths and weaknesses of both WAS and MIMS as analytical strategies for atmospheric analysis. The strengths of MIMS methodology, as exemplified by this data set, are as follows: *First*, MIMS can be used to inform WAS sampling time and location. For accurate compositional information about air masses, an effective and efficient sampling strategy is required. Using mobile MS to map contaminants in space and time gives the sampler a great deal of valuable information. *Second*, considerable cost can be saved by knowing where and when to sample. Canisters # 1129 and # 2516 were filled because significant concentration excursions were observed, in real–time, by the operators of the portable MIMS. *Third*, regional scale mapping (mobile MIMS) and following change over time (stationary MIMS) provides a highly resolved picture of chemical variability in time and space.

The strengths of the WAS methodology, as exemplified by this data set, are as follows: *First*, WAS is orders of magnitude more sensitive than MIMS. For sample 2516 in Subpanel a, the analytical result from WAS is 744 pptv, while the result for MIMS is below the limit of detection. This may be due to mistimed sampling or miscalculated time delay for the comparison. Regardless, in the case of low concentrations (<ppbv), the low detection limit of the WAS methodology is advantageous. *Second*, WAS is also more selective than MIMS. The result in Subpanel c is reported as a sum of ethylbenzene and xylene(s). This is strictly because ethylbenzene and the structural isomers of xylene cannot currently be distinguished by MIMS in real-time. WAS analysis employs a sophisticated GC–MS methodology that quantifies each of these species independently. The result is presented as a summation simply so that WAS and MIMS results can be compared.

In conclusion, this study suggest that the WAS and MIMS methodologies are complementary, and when combined, present a powerful adaptive sampling platform. The MIMS/WAS concentrations reported are generally within 30–50% agreement depending on the complexity of the sample. The only exception to this is α–pinene, which is likely the result of an experimental error and therefore, requires further study. A 30–50% agreement for the MIMS data, is certainly good enough to provide useful semi–quantitative information, especially when the added advantage of real-time information and spatial variability are considered.

An important outcome of this research is an alternative to the long–standing

problem of assessing environmental impacts using a randomized set of measurements in a particular environmental compartment. In contrast to conventional field sampling designs, which often return a large number of no–detects, mobile mass spectrometry can be used to rapidly survey a site and then, make informed decisions about where and when to collect conventional grab samples for off–line, lab–based analyses. This is particularly advantageous when chromatographic methods are necessary for compositional information that includes specific isomer or congener constituents, where the cost of sampling, clean–up and analysis can be high. This approach may work both for routine monitoring of industrial sites, as well as for large scale mapping of VOC emissions. Such applications would be beneficial in critical incident scenarios, as well as for routine monitoring associated with hydrocarbon extraction and processing. Furthermore, with the number of hydraulic fracturing sites across North America increasing, real time monitoring and adaptive sampling strategies may also help identify areas of potential risk to both human and environmental health.

Chapter 6

The Effect of the Earth's and Stray Magnetic Fields on Mobile Mass Spectrometer Systems

Reproduced in part from Bell, R. J.; Davey, N. G.; Martinsen, M.; Short, R.T.; Gill, C. G.; Krogh, E. T. "The Effect of Earth's Magnetic Fields on Mobile Mass Spectrometer Systems" *J. Am. Soc. Mass Spectrom.* **26**, 201–211 (2015). This chapter is primarily the work of R. Bell with significant contributions from N. Davey. It is included in this thesis because the developments described were a crucial step in our quest for the acquisition of reliable data from a moving vehicle. Thanks to previous work by T. Short, R. Bell was able to describe, model, and prevent the effect of Earth's magnetic field on the mass spectrometer used for this study. The manuscript was prepared R. Bell. Contributions by N.Davey included involvement in establishing the orientation effect, participation in discussion regarding proposed physical explanations of the effect, and implementation of several hardware solutions to minimize the effect. The first of theses solutions was to encase the instrument in thin mu-metal foil which reduced, but did not eliminate the effect. More effective was the construction of both mu-metal and Metglas magnetic shields to fit inside the vacuum chamber of the mass spectrometer. Editorial contributions were from C. Gill, N. Davey and E. Krogh. Particularly valuable insight and discussion was provided by R.T. Short.

6.1 Introduction

The popularity of field portable mass spectrometry is growing as many of the technical hurdles of bringing laboratory equipment into the field are overcome [96, 101, 116]. On-site analysis requires that instrumentation can be transported conveniently, powered remotely, be free of self-contamination, and can

be serviced in adverse conditions. Additionally, the instrumentation should be capable of data collection while moving, and overcome any additional hurdles resulting from changing environmental and sample conditions. For example, non-steady state or transient conditions are likely to be more prevalent and may require correction [54, 56]. Additionally, varied sample conditions, such as temperature, pressure, and humidity, may alter the relative instrumental response [116, 127–129], and changing environmental conditions may adversely affect the instrument itself [130]. To our knowledge, apart from a report by Short *et al.*(2000) [130], the effect of magnetic fields, such as the Earth's, on portable mass spectrometer signal intensity has not yet been addressed by the mass spectrometry community. Electron beams that have a short path length or have sufficiently high energies are not meaningfully affected by weak magnetic fields. Additionally, weak magnetic fields are likely to have a negligible impact on the deflections of ion beams because of their significantly greater relative momentum. However, when precise, low-energy electron beams are employed, care must be taken to reduce the influence of uncontrolled magnetic fields. For example, photoelectron spectrometer components are intentionally lined with or constructed from magnetically permeable materials to limit the influence of magnetic fields [131]. Nickel-iron alloys such as mu-metal and other magnetically permeable materials have a magnetic permeability many times that of free space, and tend to absorb passing magnetic fields by providing a preferred location for field transmittance. Thus, when instrumentation is encased in mu-metal, magnetic fields inside the instrument are greatly reduced, avoiding unintended electron beam deflections. Although impractical in the context of portable mass spectrometry instrumentation, Helmholtz cages have also been employed to compensate for the effects of the Earth's magnetic field in testing facilities [132] and in high resolution cathode ray tubes [133]. In mass spectrometry, relatively low energy electron beams (e.g., 70 eV) are used in electron ionization (EI) sources. Though generally the ion source is located as close as possible to the mass analyzer, maintaining a flexible design sometimes necessitates transmission distances of several centimeters before electrons enter a small ion source electron aperture (e.g., $<$ 3 mm diameter). In these cases, ionization efficiency (and therefore the instrument's relative sensitivity) will be dependent on the electron beam flux stability. Normally, in a stationary mass spectrometer, local magnetic fields are constant, and electron beam deflections go unobserved, or are compensated for by instrumental tuning optimizations. Occasionally, these fields are

not constant; for example, we have observed that locating a solenoid pump or solenoid valve near the mass spectrometer's vacuum housing may result in a detectable effect on the signal intensity. For example, when sampling underwater vents in Yellowstone Lake in September 2003 with a portable underwater membrane introduction mass spectrometry system, an observable beat in the measured signals resulted from the operation of the solenoid sampling pump (Supplementary Figure A.6). Post-deployment, it was discovered that the beat intensity was proportional to the proximity of the solenoid pump to the instrument's vacuum chamber. Encasing the pump in magnetically permeable metal resolved the issue (data not shown). Field portable instrumentation also experiences varied magnetic fields as a result of changing its orientation with respect to the Earth's magnetic field. The resulting transient deflection of electron trajectory may generate a significant source of instrumental variability. In addition,the magnetic fields created by various mass spectrometer systems (e.g., vacuum pumps, inductors, or filament current) may also affect electron beam deflection. The summation of multiple magnetic field vectors will have an additive effect that is directionally dependent. These effects are difficult to observe when instrumentation is operated in a GC mode because of the highly variable nature of the instrumental signal during a GC scan. Further, the effects are compensated for if instrument orientation is not changed between calibration and sample analysis, as recommended by instrument manufacturers. However, when operating in a continuous measurement mode, signal variability becomes easily observed when underway. In our case, the effect was highly intensified during operation with a sub-optimum electron lens voltage. In this study, we characterize the influence of magnetic bearing on the relative instrument response of several field portable mass spectrometers, simulate the electron beam transmission efficiencies for several instrumental conditions, and demonstrate simple instrumental modifications that provide magnetic shielding, resulting in better signal stability and sensitivity gains.

6.2 Experimental

As noted above, we have experimentally observed a directional dependence of the relative instrument response for a variety of field portable mass spectrometers. To better understand this phenomenon, simulations were performed using SIMION® (v8.1, Scientific Instrument Services Inc., Ringoes, NJ, USA) software that

incorporated the influence of the Earth's magnetic field on an electron impact ion source as an instrument is rotated through 360°. Results from the rotation of a vertical electron beam were compared with that for a horizontal electron beam. Additional simulations explored the result of asymmetries generated from the use of a linear filament geometry as an electron source in an otherwise cylindrical system, and also the additive effect of local instrumental magnetic fields with the Earth's magnetic field. Simulation results were directly compared with experimental data collected in the laboratory. To reduce the influence of magnetic fields on the relative instrumental response, three methods were explored experimentally and compared with simulations. First, the ion source's electron beam focus was altered, allowing the comparison of unfocused and well-focused electron beams. Next, the entire instrument was protected from the Earth's magnetic field by a mu-metal casing, reducing the presence of directionally dependent magnetic fields. Last, Metglas (an amorphous metallic ribbon material with very high magnetic permeability) was used to line the inside the instrument's vacuum chamber surrounding the electron beam to reduce the influence of both the Earth's and the much of the instrument's magnetic field.

6.2.1 Mobile Mass Spectrometer Relative Response Versus Orientation

To demonstrate the effects of the orientation of the Earth's magnetic field on the relative instrumental response of different mobile mass spectrometers, experimental field data obtained from four different instruments were compared by analyzing a steady-state internal standard signal while the mass spectrometer's magnetic orientation (azimuth) was changed. All mass spectrometers utilized membrane sampling inlets employing polydimethylsiloxane capillary membranes maintained at constant temperatures. Membrane introduction mass spectrometry (MIMS) provides a direct analysis approach for the continuous quantitative online monitoring of specific analytes and internal standards. For additional background on MIMS, which is often employed in mobile mass spectrometry systems because of its simplicity, several reviews of the technique have been published [1, 14, 79]. The first instrument used was a field operable MIMS system made from a bench top, hyperbolic electrode quadrupole ion trap (QIT) (Model Saturn 2000; Agilent

Technologies, Santa Clara, CA, USA), employing internal ionization. In this instrument, the electrons ejected from a hot filament are accelerated to 70 eV and transmitted ∼1.7 cm before a focusing gate electrode guides the electrons through a 1 mm aperture in one of the ion trap's endcaps. The quantity of ions formed (and thus the relative signal intensity) is proportional to the number of electrons that pass through the 1 mm aperture. In addition, this instrument has the electron beam on a horizontal axis, parallel to the Earth's surface. To compare instrument response to magnetic orientation, a continuously infused 1 ppb aqueous dimethylsulfide solution was analyzed using full scan mass spectra (m/z 62) while operated onboard a moving marine research vessel (R/V Suncoaster, St Petersburg, FL, 1999) that was intentionally rotated 360°. Field orientation was determined by measuring the magnetic field perpendicular to the electron beam using a three-axis magnetometer (Model 2300; Honeywell, Morristown, NJ, USA) [54]. Data were also collected from a field portable cylindrical electrode quadrupole ion trap (CIT) (Model Griffin 400; FLIR Systems, West Lafayette, IN, USA), equipped with a custom built membrane interface. This instrument uses a 75 eV electron beam for ionization within the ion storage volume of the trap. The electron path length from the filament to the end cap aperture is approximately 4.6 cm and a simple, three electrode cylindrical Einzel lens is used to focus the electron beam through a 2.5 mm aperture in one of the trap endcap plates. In this system, the electron beam axis is perpendicular to the Earth's surface (i.e., a vertical electron beam). Toluene–d_8 (used as an internal standard) was supplied to the membrane interface in air samples using a permeation tube (Kin-Tek, La Marque, TX, USA) housed in a thermally regulated permeation chamber in line with the membrane interface. The full scan instrument response with respect to orientation was obtained by operating the mass spectrometer inside a moving vehicle while analyzing exterior air continuously infused with 75 ppbv toluene-d_8 (m/z 98). Orientation was derived from GPS data while the vehicle was traveling in a 'figure eight' pattern. The third instrument included in the study was a compact linear quadrupole mass spectrometer (Model Transpector CPM; Inficon, Syracuse, NY, USA) implemented as the mass analyzer in an underwater membrane introduction mass spectrometry system [134]. This mass spectrometer uses a closed electron ionization source, whereby 70 eV electrons produced by the filament travel about 2 mm before passing through a 5 mm × 2 mm slot. The data used here, collected from field studies made in Lake Maggoire, St Petersburg, FL, were also used in work published by Wenner

et al. (2004) [6]. In this work, orientation was also derived from GPS data while the vehicle was travelling in a 'lawn mower' pattern. Electron beam direction (vertical vs. horizontal) was not determined. The final instrument examined in this study was also a hyperbolic electrode quadrupole ion trap that utilizes an external electron ionization source (Model GCQ; Finnigan MAT, San Jose, CA, USA). This system employs an ion source in which 70 eV electrons from the filament are collimated into a spiralling beam by two permanent magnets (∼300–400 G). The focused electrons are passed through two apertures (each about 2.6 mm diameter) over 4.8 mm distance prior to entering the ion source, travelling on a vertical axis (i.e., perpendicular to the Earth's surface). Ions generated in the source are subsequently injected into the ion trap by a compact ion lens system. Full scan data (m/z 98) from a toluene–d_8 internal standard infused into ambient air at 341 ppbv were obtained in the same manner as described for the CIT (vide supra). The data used here, collected while conducting field measurements in Tacoma, WA, was analyzed as part of a study published by Davey *et al.* (2014) [101]. Orientation was derived from GPS data.

6.2.2 Electron Beam Deflection Simulations

Ten simulations conducted using SIMION® software are presented to understand the contributing factors and possible solutions to unintended electron beam deflections by magnetic fields in a mass spectrometer ion source. The electron beam was simulated as it travelled from the electrons' origin, through the focusing lens, and either passing through the end plate aperture or impacting the endplate. For these simulation studies, the ion source geometry and voltages of the CIT (*vide supra*) were used. The 2D–cylindrical model used to simulate the CIT ion source and transmission efficiency is shown in Figure 6.1. Constant values for the simulations included the electron deflector plate (-10 V), the ion trap endplates (0 V), and ring electrode (75 V), the initial electron kinetic energy (0.2 eV), mean electron source location (x = 0 mm, y = 0 mm), and filled electron axial cone angle (80°). The initial electron kinetic energy was calculated assuming a 2050°C filament [135], using a Maxwellian distribution [136, 137]. Simulations were performed using 10,000 electrons at each of eight rotational steps (45°) relative to the Earth's magnetic field, with an additional ninth condition of no magnetic field from the Earth. Set-points that were varied between simulations are summarized in Table 1.

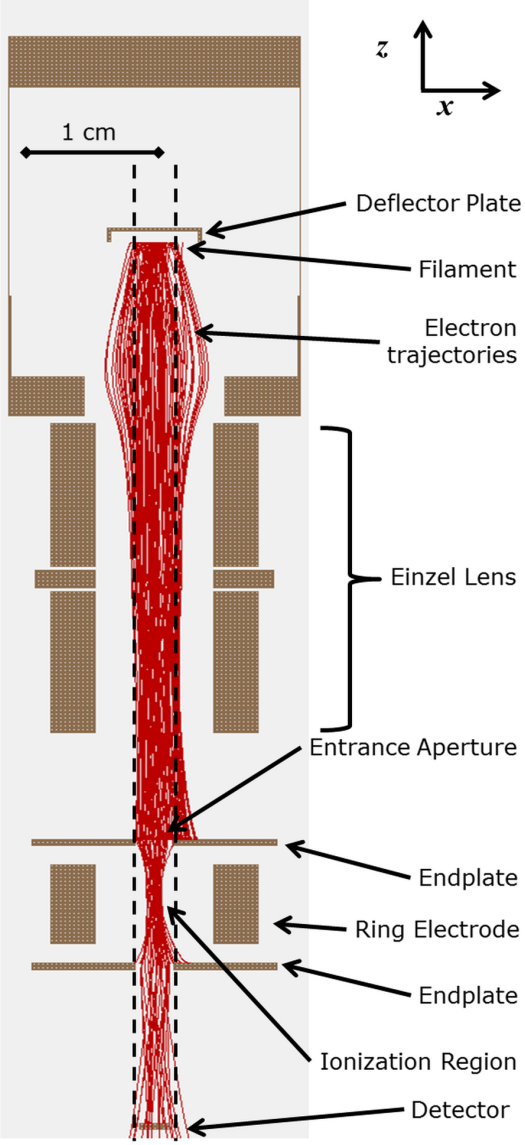


Figure 6.1: SIMION® model approximating the CIT ion source shown in a vertical orientation relative to the Earth's surface (xy plane). The electron trajectories shown in this example are influenced the Earth's magnetic field, the sum of which is out of the page (y) and, as a result, electron deflection is rightward (x). The dashed reference lines demarcate the entrance aperture's x position and are intended to help visualize electron deflection.

Intensities for the Earth's magnetic field in Nanaimo, Canada ($Bx = 0.18G$, $By = 0.054G$, and $Bz = 0.51G$) were obtained using the IGRF function from the Matlab (Mathworks, Natick, MA, USA) file exchange, and confirmed using the an Android smartphone (Model Incredible; HTC Corporation, Taoyuan City, Taiwan).

The smartphone contained a vector magnetometer that was monitored and logged using the AndroSensor (ver. 1.9.4.4a) application. Simulations 1 through 3 were conducted to test whether the cause of observed signal variations in field measurements could be due to the relative orientation of the Earth's magnetic field. The electron beam in these simulations was oriented perpendicular to the Earth's magnetic field (i.e., a vertical electron beam), as is the case for the normal operation of the CIT system. Simulation 1 (intended to be the idealized case) was conducted with all electrons originating from a point source. Simulation 2 was identical, except that the origin of the electrons approximated the linear filament found in the CIT system. Here, the electrons were sourced from a Gaussian distribution (SD = 0.3 mm) along a line in the y direction. Simulation 3 was performed using the same conditions as Simulation 2, with the exception of an additional secondary magnetic field. This secondary field was not rotated with the Earth's magnetic field, thus simulating the measured magnetic field originating within the instrument itself. The intensity of this vector ($Bx = 0.18G$, $By = 0.054G$, and $Bz = 0.51G$) was determined using a magnetometer adjacent to the instrument's vacuum housing, and subtracting the Earth's magnetic contributions. Because the magnetic field in the instrument housing varies strongly within a few centimeters, this determination is likely one of the largest sources of error for these simulations. Simulations 4 through 6 were parallel experiments to Simulations 1 through 3 except that the magnetic vectors were altered to reproduce the Earth's field rotating about the instrument's yz plane, simulating a horizontal electron beam. The horizontal beam has a distinctly different symmetry with respect to the Earth's magnetic field than the vertical electron beam. Although the CIT was not designed to be operated in this orientation, a horizontal electron beam was employed in the hyperbolic electrode quadrupole ion trap (i.e., Saturn 2000, *vide supra*).

6.2.3 Electron Beam Defocusing Studies

Together, Simulations 3, 7, and 8 were designed to determine the importance of electron trajectory deflection when the electron beam is refocused by altering the Einzel lens voltage while in the vertical electron beam configuration. Simulation 3 was used as a reference, employing the manufacturer recommended set-point of 25 V for the Einzel lens, whereas Simulation 7 and 8 used a lens voltage of 75 V and 200 V, respectively. For direct comparisons with the simulations, analogous experiments

were conducted on the CIT system. Toluene was used as a constantly infused analyte (via 70 ppbv air samples continuously infused to the membrane interface), and the instrument was located on a free moving turntable where 0° is magnetic north in Nanaimo, Canada. In this case, the instrument analyzed the toluene using an MS/MS scan (m/z 91→65, 10 μA electron current, 150 ms ionization time, 1.5 V dissociation voltage, and 20 ms dissociation time).

6.2.4 Magnetic Field Shielding Effects

Simulations 3, 9, 10, and their associated parallel experiments (again, using the CIT) were performed to determine the effectiveness of using magnetically permeable materials to reduce the intensity of the Earth's magnetic field experienced by the mass spectrometer. Simulation 3 was used as a reference point, and Simulation 9 was designed to match the conditions that were determined after paneling the entire instrument with mumetal. In this case, the instrument's outside casing was covered with about 1.6 m^2 of 0.1 mm thick nickel alloy foil, or mumetal ($\mu \approx$ 50,000) (Product Number 8912 K32; McMaster Carr, Elmhurst, IL, USA), held in place with adhesive tape. Magnetic fields inside the instrument after the mu-metal was installed were determined by locating the magnetometer next to the vacuum housing and rotating the operational instrument through 360°. The magnitude of instrument's and Earth's magnetic field vectors were resolved using custom Matlab code. It was determined that the mu-metal resulted in a 66% reduction in the intensity of the Earth's x, y, and z magnetic field vectors. The instrument's internal magnetic fields changed slightly, but this was highly dependent on the exact location of the magnetometer. Because of this, it was decided to retain the original numbers for the instrument's magnetic field for consistency with each simulation. Simulation 10 was designed to match the conditions that were determined after the interior of the vacuum chamber was lined with a 10 layer thick cylinder of 0.015 mm thick Metglas ($\mu \approx$ 290,000, Metglas 2075 M; Metglas, Conway, SC, USA) mounted on the interior wall of the CIT instrument's vacuum chamber. Several small holes were cut in the Metglas cylinder to allow the necessary electrical feed-through connections required for normal operation. The magnetic fields in the vacuum housing were characterized by locating the magnetometer within the vacuum chamber and rotating the (non-operational) instrument through 360°. It was determined that the xy components of both the Earth and instrument magnetic

Table 6.1: Parameters Varied Between Simulations of the CIT Ion Source. Electron Beam Orientation is with Respect to the Earth's Surface (i.e., the xy plane). Lens and Ion Trap Design are Depicted in Figure 6.1 and Described in Text

Sim.#	Description	Electron beam orientation	Lens (V)	SF of electron source on y (mm)	Earth's Field (G)			Instrument referenced field		
					Bx	By	Bz	Bx	By	Bz
1	Earth's field only	vertical	25	0	0.18	0.054	0.51	0	0	0
2	Earth's field + filament	vertical	25	0.3	0.18	0.054	0.51	0	0	0
3	Earth's field + filament + instrument's field	vertical	25	0.3	0.18	0.054	0.51	0.21	-0.047	-0.63
4	Earth's field only	horizontal	25	0	0.18	0.054	0.51	0	0	0
5	Earth's field + filament	horizontal	25	0.3	0.18	0.054	0.51	0	0	0
6	Earth's field + filament + instrument's field	horizontal	25	0.3	0.18	0.054	0.51	0.21	-0.047	-0.63
7	Earth's field + filament + instrument's field + altered focus	vertical	75	0.3	0.18	0.054	0.51	0.21	-0.047	-0.63
8	Earth's field + filament + instrument's field + very altered focus	vertical	200	0.3	0.18	0.054	0.51	0.21	-0.047	-0.63
9	Earth's field + filament + instrument's field + mu-metal around instrument	vertical	25	0.3	0.060	0.018	0.17	0.21	-0.047	-0.63
10	Earth's field + filament + instrument's field + Metglas in vacuum chamber	vertical	25	0.3	0	0	0.51	0	0	-0.63

fields were negligible. Because the top and bottom of the chamber were not protected by Metglas, there was a significant z field. Over the course of the study, it was also determined that the difference between the instrument's internal magnetic field was small when operating or not, suggesting the instrument's fields are primarily sourced from the permanent magnets in the turbomolecular vacuum pump (Model TC100; Pfeiffer Vacuum, Asslar, Germany). Neither the mu-metal foil nor the Metglas were annealed for this work, which would further increase their relative magnetic permeability. Figures were generated using Matlab, and the data plotted with respect to the field orientation was best fit with a line determined by a nonlinear fit to y = a + b∗sin(c + x) + d∗sin(2∗(e + x). Error bars shown in simulated data represent the SD of electron transmission through the aperture for the 10,000 simulated electrons binned into groups of 10. Error bars shown in experimental data represent the SD of the 24 steady state signal measurements.

6.3 Results

6.3.1 Mobile Mass Spectrometry Sensitivity Versus Directional Bearing

For the purpose of demonstrating the in-field response of a mobile mass spectrometer to relative to the Earth's magnetic orientation, internal standard signal intensities for the four mobile mass spectrometer systems examined are plotted in Figure 6.2. Data shown in Figure 6.2a and 6.2b were produced by quadrupole ion traps using internal ionization directly within the ion storage volume, requiring the injection of electrons through an endcap aperture. In both cases, there was an observed dependence on directional bearing in which the signal intensity displays one maxima per 360° rotation. Shown in Figure 6.2c are data obtained for a quadrupole ion trap with an external ion source that generates ions using electrons focused by a strong magnetic field. Ions produced in this system were subsequently injected into the ion trap. The data illustrate the external ion source exhibited no signal dependence with respect to magnetic orientation, suggesting the strong magnets focusing the electrons into the ion source effectively overcome any influence from stray magnetic fields. Similarly, the data collected using the single quadrupole mass spectrometer, shown in Figure 6.2d, indicated no signal dependence with respect to the directional bearing. This mass spectrometer

has a very short electron trajectory and a relatively large electron aperture slot in the ion source; as such, it is unlikely that electron beam deflections were significant under such conditions.

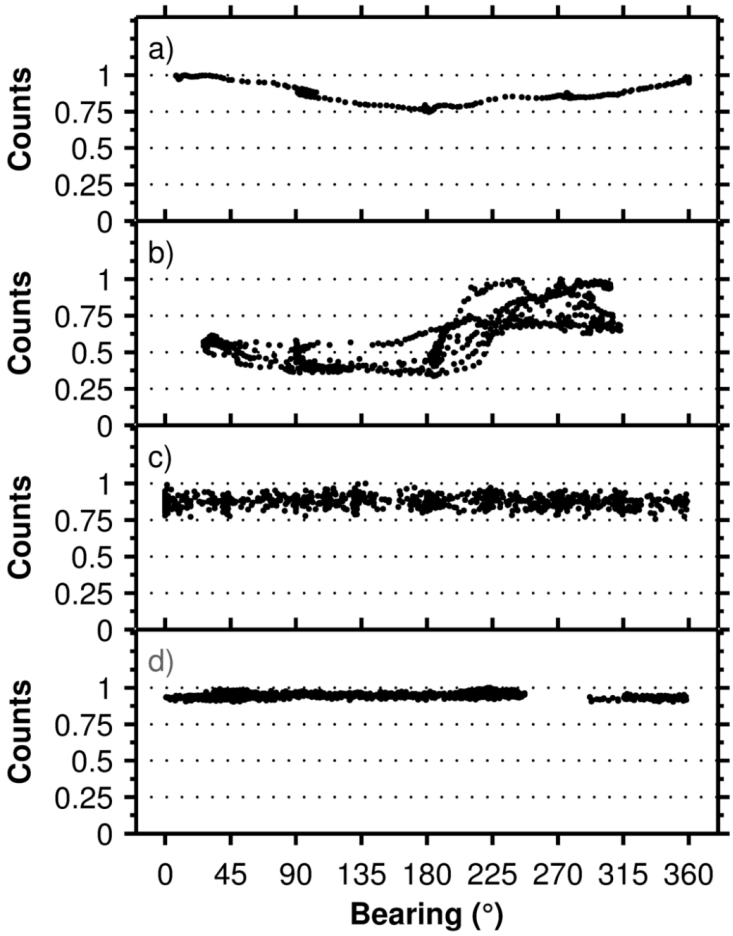


Figure 6.2: Moving mass spectrometers' response to an internal standard plotted versus directional bearing. (a) An ion trap with internal ionization (e.g., electrons are injected into the ion trap where ionization occurs) and an electron beam horizontal to the Earth's xy plane. (b) Another ion trap with internal ionization but vertical electron beam. (c) An ion trap with external ionization (e.g., ionization occurs outside the trap and ions are subsequently injected into the trap). (d) A closed source quadrupole mass spectrometer. Models and ion source designs are further described in the Experimental section. It is notable that only instruments with internal ionization exhibit a directional dependency.

On the whole, the field data indicate mass spectrometers with relatively long electron trajectories and small entrance apertures (e.g., internal ionization ion trap type systems) are strongly affected by directionality, whereas short path lengths, large

apertures, and strong collimating magnetic fields are likely to negate any directional bearing dependency. Regardless of horizontal or vertical ionizing electron beam axes relative to the earth's magnetic field, one maximum per rotation was observed in the directional dependence of the relative instrumental sensitivity of the mobile mass spectrometer systems exhibiting this effect.

6.3.2 Ion Source Simulations

Simulation 1 has an ion source that is cylindrically symmetric and has the electron beam travelling in the vertical direction. As a result, the transmission of electrons through the endplate aperture in Simulation 1, which rotates the Earth's magnetic field about the vertical axis, showed no reproducible directional dependence (Figure 6.3a). The mean transmission was 8.7%, which is almost half the 14.7% that is simulated to occur without the Earth's field present. The inclusion of the Earth's field, while reducing electron transmission by deflecting the center of the electron beam away from the aperture, had no directional dependency attributable to the cylindrical symmetry and vertical orientation.

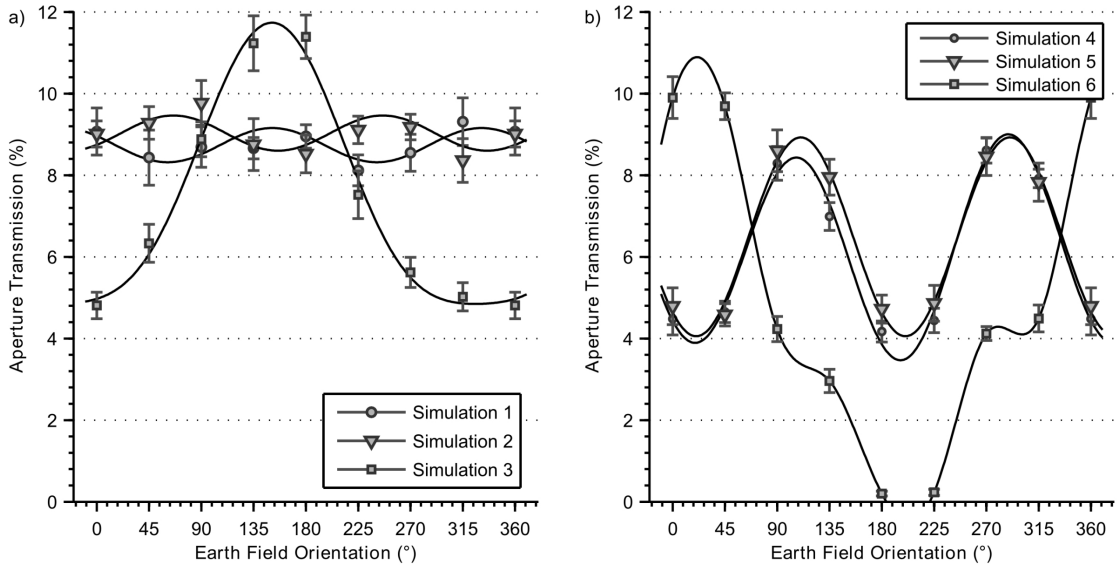


Figure 6.3: Simulation of electron transmission of a vertical (a) and a horizontal (b) electron beam through endplate aperture versus the Earth's field orientation. Simulation 1 and 4, Earth's field + point source filament; Simulation 2 and 5, Earth's field + transverse filament wire; and Simulation 3 and 6, Earth's field + transverse filament wire + instrument's field.

Simulation 2 adds an asymmetry to the system by including the length of the

filament when simulating the origin of each electron. Set-points were such that over 99.7% of electrons were sourced from the middle 1 mm section of filament wire. Figure 6.3a illustrates that there was little effect from this asymmetry. When the length of the filament was exaggerated (e.g., electrons sourced from a 5 mm long filament, data not shown) two maxima per rotation were observed. This would be the expected result from a system with bilateral symmetry. The inclusion of the asymmetry did not have a significant effect on the directional dependency, and the resulting two maxima were not observed in any of the experimental field data. Simulation 3 is the closest representation of the operating conditions of the CIT instrument. In addition to including the accurate representation of the filament and the Earth's magnetic field, it includes a static secondary field that is referenced to the instrument itself. A strong directional dependency with one maximum per rotation is illustrated in Figure 6.3a. In this simulation, the Earth's magnetic field is of similar magnitude to the static field. Therefore, when the two fields interfere destructively (e.g., at 135°–180°), the electrons were not significantly deflected and experienced a higher transmission efficiency through the aperture. However, when the two fields interfere constructively (e.g., at 315°–360°), the electrons were strongly deflected, and fewer electrons were transmitted. Figure 6.4a depicts, in greyscale, the relative likelihood of an electron's position as it reaches the ion trap's endplate. The effect of the summation of the two magnetic field vectors becomes clear, demonstrating why the constructive and destructive interference of the two magnetic fields has the strongest influence on directional dependence. It is also worth noting that under 'standard conditions' (i.e., Simulation 3), while the electron beam was unfocused, there was still a greater electron density in the center of the beam. Whether or not the central area of the electron beam passes the aperture had a significant effect on the number of electrons ultimately entering the ion trap and subsequently ionizing neutral molecules.

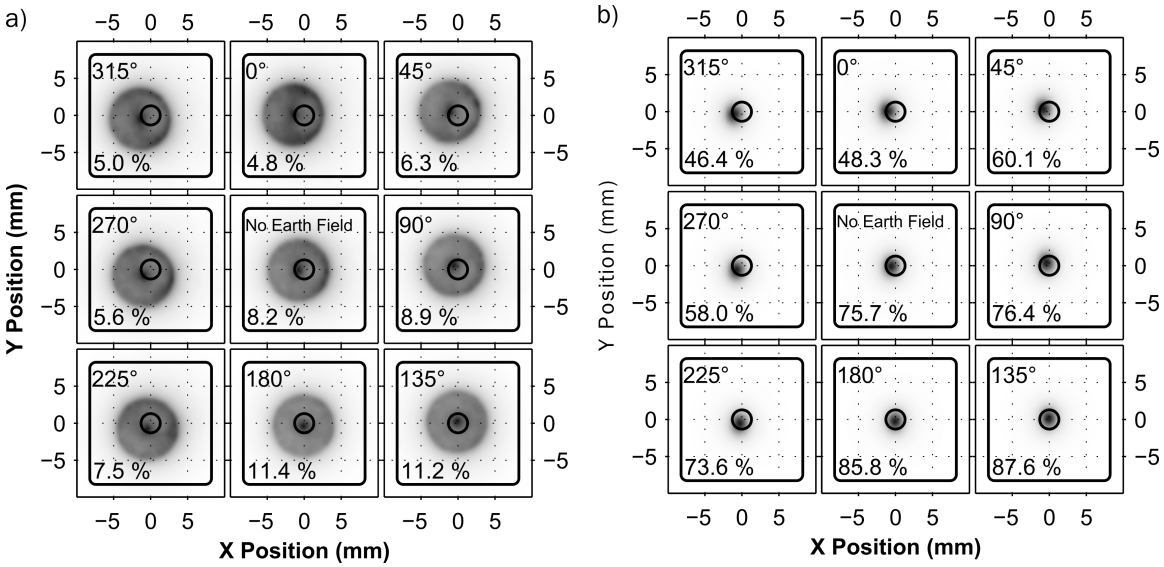


Figure 6.4: Density maps indicating the xy location of electrons as they reach the ion trap endplate for Simulations 3 [25 V lens, (a)] and 8 [200 V lens, (b)] under different magnetic bearing conditions. Each subplot is calculated from 10,000 electrons, the dark grey represents high probability of an electron at that position, and light grey represents low probability. The outside rectangle represents the outside edge of the endplate and the central circle represents the endplate aperture. Magnetic bearing and percent of electrons passing the aperture are indicated.

In the case of the vertical electron beam, Simulation 3 (Figure 6.3a) accurately predicted the one maximum per rotation signal observed in the field measurements for the mobile mass spectrometers. Given the additional asymmetry that results from a horizontal electron beam, one might expect two maxima in such a system. However, Figure 6.2a depicts a mass spectrometer in the field with a horizontal electron beam–also with one maximum per rotation. Simulation 4 (horizontal electron beam, point source electron source, Figure 6.3b) shows that the effect of the Earth's field alone does, in fact, create a two maxima directional dependency. The inclusion of the filament wire in the electron source has a rather small effect (Figure 6.3b, Simulation 5). However, Simulation 6, which included the additional instrument referenced magnetic field, shows a dramatic one maximum directional dependency (Figure 6.3b). The constructive/destructive interference of the two fields clearly had a very strong effect on the system and explains why the QIT, with a horizontal electron beam, displays a dominant one maximum direction dependency on the field. It is noteworthy that the dimensions of the QIT are different from the CIT and the magnitude of signal variation was not expected to be

in agreement between Simulation 6 (Figure 6.3b) and Figure 6.2a.

6.3.3 Reducing the Relative Response Variability

Having established a plausible mechanism for the variation in signal intensity with respect to the instrument's magnetic orientation, Simulation 3 was used as a starting point for subsequent simulations and experiments. These studies were aimed at determining an effective way to reduce the observed sensitivity dependency related to directional bearing. Simulations 3 and 7–10 were matched with a parallel experiment performed in the lab with a CIT instrument mounted on a turntable. Simulations 7 and 8 simulate the results when the electrons are not focused according to manufactures specifications by the Einzel lens prior to the aperture. Figure 6.4b shows the improved aperture transmission relative to Figure 6.4a resulting from altering the lens voltage from 25 V (Simulation 3) to 200 V (Simulation 8). Experimental data are in relatively good agreement with Simulations 3, 7, and 8 (Figure 6.5). These data suggest that a defocused electron beam (Simulation 3) does not necessarily reduce the directional dependency, but does reduce instrumental sensitivity. Not shown are simulations with an increased secondary field. In these simulations, a well-focused beam can result in an extreme directional dependency as the entire beam may be transmitted or rejected by the aperture depending on the state of interference with the Earth's magnetic field. Simulation 9 compared electron aperture clearance with Simulation 3 after a reduction in the Earth's magnetic field by adding mu-metal on the outside of the instrument, and Simulation 10 compared transmittance after a reduction in both the Earth's and instrument's fields by adding Metglas on the inside of the vacuum chamber. These simulations were directly compared with instrumental data collected under the same magnetic conditions (Figure 6.6). Simulation 3 indicates a 58.7% variation in signal intensity as a result of the additive effect of the Earth's and the instrument's fields. Simulation 9 indicates that this is reduced to a 21.7% signal variability with the addition of mu-metal on the outside of the instrument (a reduction of 62.9% in the signal variability). This result is comparable to the experimental data, which demonstrated a 47.4% reduction in actual signal variance between the standard and mu-metal conditions. Simulation 10 indicates we can expect 4.9% signal variability (a reduction of 93.2% in the signal variability) as a result of the Metglas addition. This result is comparable to the actual data from the

CIT that displayed a 92.3% reduction in signal variability between the standard and Metglas conditions. This reduction made the relative response variability due to the instrument's magnetic orientation virtually indistinguishable from other instrumental noise.

6.4 Discussion

Regardless of the specifics of the mass spectrometer instrument symmetry, the results of these studies suggest the best way to minimize directional response dependency is to shield low energy electron beams from both the Earth's and instrument's magnetic fields. In doing so, the electron beam can be properly aligned for optimum ionization, regardless of the orientation of the instrumentation during mobile measurements. Both simulation and experimental results indicate that in addition to significantly reducing the signal variability during deployment, the focusing lens may be tuned to ensure a higher electron throughput yielding significant improvements in sensitivity. Simulations indicate that a well-tuned lens can improve instrumental sensitivity nearly 10–fold. However, it should be noted that shielding of the electron beam from stray magnetic fields becomes imperative in this case, as it is possible that the tightly focused electron beam could miss the entrance aperture entirely. With increased sensitivity, the opportunity to reduce the required filament emission current arises; this may be desirable when the vacuum chamber is under relatively oxidative conditions, as is common in MIMS systems. This would yield longer filament lifetimes and lower the signals from background gases [128, 138].

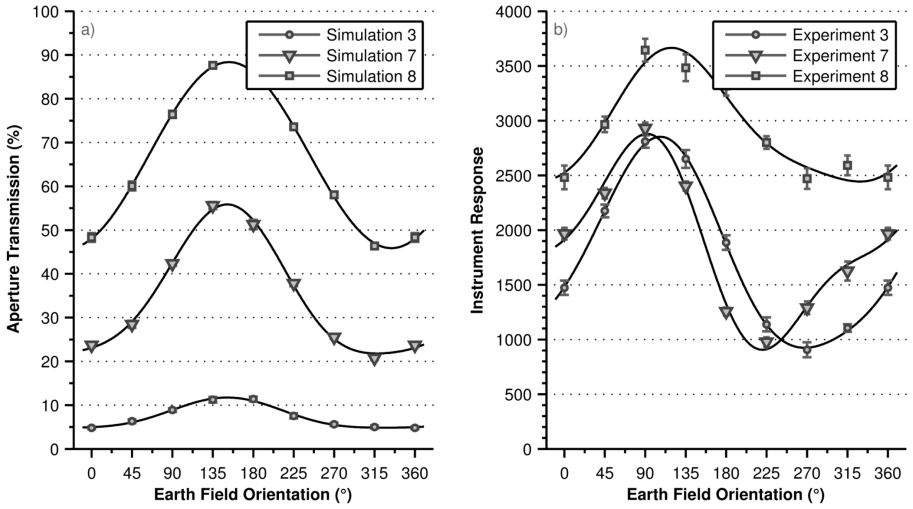


Figure 6.5: Electron transmission versus Earth's field orientation under varied lens set-points. (a) Illustration of the percentage of electrons transmitted with a lens set-point of 25 V (Simulation 3), 75 V (Simulation 7), and 200 V (Simulation 8); (b) plots the instrument response to an internal standard during a parallel experiment performed on a mass spectrometer under the same conditions as the simulation.

Another factor that should be considered is the electron current control feedback mechanism. In order to produce a constant electron ionization current, ion sources are designed to maintain a constant flow of electrons by using a feedback control system. Typically, there are two methods to monitor and control filament emission current. One is achieved by monitoring the filament emission current using the filament power supply circuitry; this methodology provides no correction for the variations in transmission through the ion trap entrance aperture. Another method is to monitor the electron current on an aperture plate in the ion optical system (e.g., the ion trap entrance aperture); use of this method assumes that the current collected on this plate is a constant fraction of the transmitted electron current. This methodology provides feedback control for emission control circuitry but unfortunately may serve to exaggerate the directional dependence. In this case, fewer electrons may be entering the ionization region because of deflection by external magnetic fields. With more electrons striking the aperture plate, this would provide erroneous feedback that acts to decrease filament current, resulting in further reduction of the transmitted electron current. Another feedback option, however, could be to measure the electron current on the ion trap exit endplate. This feedback mechanism would compensate for variations in transmitted electron

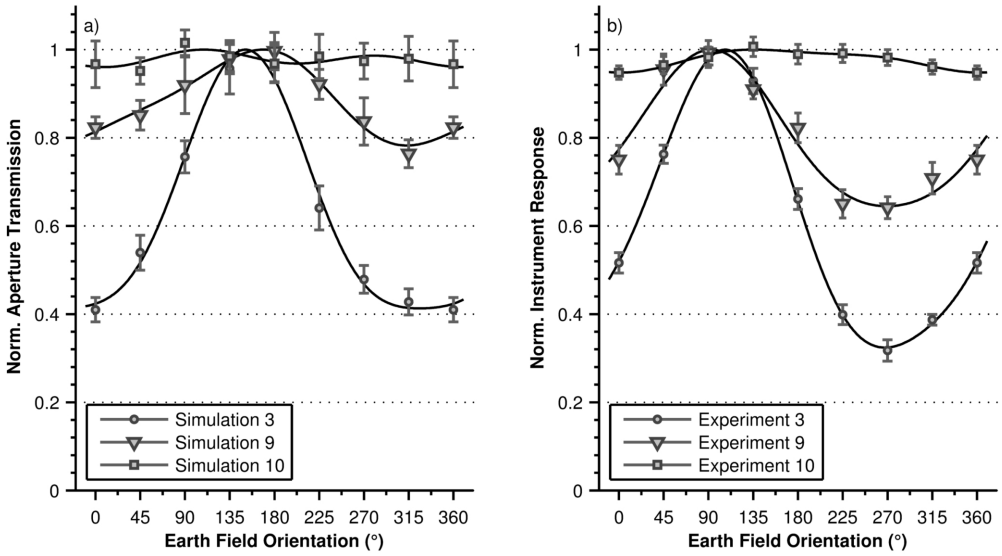


Figure 6.6: Electron transmission versus Earth's field orientation under varied magnetic field conditions. (a) The percentage of simulated electrons transmitted through the aperture with no protection from magnetic fields (Simulation 3), 66% reduction of the Earth's magnetic field by an exterior mu-metal casing (Simulation 9), and 95% reduction of both the Earth's field and instrument's field by interior Metglas (Simulation 10); (b) plots the relative instrumental response to an internal standard during a parallel experiment performed on a CIT mass spectrometer operated under the same conditions as the simulation.

current by increasing filament current when transmission is decreased. Since only the transmitted electrons contribute to the feedback, this method would compensate for deflections resulting from the Earth's magnetic field. However, it may prove impractical because of the radio frequency trapping fields of the trap, which may direct a portion of transmitted electrons into the ring electrode instead. Additionally, the use of automatic gain control may help compensate for the observed phenomena, although gain control was fixed during these studies. Since mass spectrometers can have several scan types and pre-scans, and the directional dependence of the full scan and an MS/MS scan varies slightly with the CIT (data not shown). Such variability is likely due to changes in ionization time estimated by instrumental gain control pre-scans. Investigation of this phenomenon was beyond the scope of the current study.

Solutions not explored in this work include the use of magnetically permeable paints or magnetically permeable components, especially those components closest

to the electron beam (e.g., the lenses and vacuum housing). Additionally, simulations suggest that in some situations where precision is key, it may be prudent to use a pointed filament that would give a more cylindrically symmetric electron beam than that produced by a linear filament wire perpendicular to the electron beam. Locally shielding specific instrumental components that are contributing to the instrument's magnetic field may also be beneficial, especially if it is not practical to sufficiently shield the electron beam. Some instrumental components can have very strong magnetic fields (e.g., from the filament current, turbo pump magnetic bearings, or induction coils). Further, if the component generates cyclical fields (e.g., a motor or pulsing solenoid), the field coming in and out of phase with specific mass scans may significantly affect instrument stability. Depending on aliasing and frequency reproducibly, this noise may show up as a beat (as demonstrated in Supplementary Figure A.6) or as random noise. A noteworthy source of instrumental magnetic fields may be the electric current through the filament. A filament operating at 5 amps (a high but not unusual current for an ion source), would have a field equal to the Earth's at a distance of 2 cm. While this field intensity would decrease rapidly with distance (Ampere's Law), it will be very intense in close proximity to the filament. This will cause significant deflection near the filament and be very difficult to prevent; however, the subsequent focusing via the Einzel lens dampens the effect of deflections prior to and within the lens.Magnetic fields located between the lens and ion trap entrance endplate will have the most significant impact on electron beam deflections. This effect can be observed through careful examination of electron trajectories relative to the aperture reference lines shown in Figure 6.1, and suggests this effect could be minimized by placing the Einzel lens as close as possible to the ion trap endplate. Last, as this study occurred in Nanaimo, Canada, all simulations were done assuming a field at that location (latitude, longitude, and near sea-level altitude). At higher latitudes, the Earth's magnetic z vector is rather strong and subsequently x and y vectors are rather weak. Since the z vector does not contribute to the deflection of electrons travelling in the vertical axis, the effects observed in this manuscript will be stronger at more equatorial latitudes.

6.5 Conclusions

To our knowledge, this is the first rigorous study of the influence of stray magnetic fields from the Earth and/or instrumental sources on the relative signal response and sensitivity of portable mass spectrometers. Signal variability is observed with instruments in which ionizing electrons have long path lengths and must pass through a small aperture, and are observed when the instrument is physically moved with respect to the Earth's magnetic field. It was found that the predominant source of signal variability is a result of the vector sum of the Earth's magnetic field and a secondary, instrument-referenced magnetic field. Removing either one will result in a significantly reduced directional dependence. Preferably, both fields can be shielded from the electron beam by the addition of magnetically permeable material to the vacuum chamber. In this case, directional dependence will become increasingly negligible as the deflection of the electron beam is eliminated. Subsequently, the optimum alignment of electron ionization beams may allow for improved electron beam focusing and significant gains in instrument sensitivity.

Chapter 7

Ion–Molecule Reactions for the Reduction of Isobaric Interferences in Ion Trap Mass Spectrometers

Reproduced from Davey, N. G.; Bell, R. J.; Krogh, E. T.; Gill, C. G. "A Membrane Introduction Mass Spectrometer Utilizing Ion–Molecule Reactions for the On–line Speciation and Quantitation of Volatile Organic Molecules" *Rapid Commun. Mass Spectrom.* **29**, 2187–2194 (2015). This chapter is primarily the work of N. Davey with contributions from R. Bell. Method for reagent delivery conceived by N. Davey. Implementation of CI delivery system, MS method development, data collection, data analysis, methodology to account for reagent depletion and manuscript preparation by N. Davey. Editorial contributions were from R. Bell, E. Krogh and G. Gill.

7.1 Introduction

Field–portable mass spectrometry is becoming much more practical as smaller and more robust instrumentation becomes commercially available. Membrane introduction mass spectrometry (MIMS) has benefited greatly from this miniaturization movement because instruments may now be deployed in the field, with relative ease, as a result of reduced size, electrical power consumption and cost [5]. Such developments have given researchers an unprecedented ability to monitor chemical concentrations in both time and space domains [24, 79]. Providing chemical data when and where it is needed yields information that can inform infield decision making, such as adaptive sampling strategies, the mitigation of exposure risks and identification of discrete sources [139]. Portable MIMS systems have been used for the detection of dissolved gases and VOCs in aqueous

samples [6, 52, 60, 127], VOCs and semi–volatile organic compounds (SVOCs) in atmospheric samples [43, 80, 81, 101, 124, 140, 141],and SVOCs in contaminated sand [24, 31]. MIMS has been the subject of numerous reviews, [1, 3, 14, 79] and will only be briefly described here. With MIMS, a semi–permeable membrane is used to separate gaseous or aqueous samples from the vacuum of a mass spectrometer. Analytes that permeate the membrane are transported to the mass spectrometers ion source either by an acceptor phase (i.e. a sweep gas or liquid carrier) or directly into the high vacuum of the mass spectrometer itself. In this manner, the bulk of the sample matrix is rejected, reducing or eliminating matrix effects that can occur with other direct sample introduction strategies.

One of the strengths of the MIMS technique is that it can be used to continuously monitor trace level contaminants in complex samples in real–time, over long periods (hours to days) without the use of chromatographic separations. Despite these advantages, there are still challenges in acquiring reliable quantitative data in complex matrices. Specifically, since all analytes that permeate the membrane are admitted to the mass spectrometer ion source simultaneously, MIMS can be prone to isobaric interferences when measuring low molecular weight molecules with related structures and common ion fragments (e.g. alkyl aromatics, such as the benzene/toluene/ethylbenzene/xylene 'BTEX' suite). This is especially true when operated in electron ionization (EI) mode, which generates numerous fragment ions. As an example, a number of alkyl benzenes permeate polydimethylsiloxane (PDMS) membranes, and readily fragment under EI conditions (via benzylic bond cleavage and/or rearrangement) to form the thermodynamically stable tropylium ion $[C_7H_7]^+$ at m/z 91, which is also the base peak in the toluene mass spectrum [142]. Furthermore, several biogenic terpenes (i.e.α–pinene) also fragment to yield m/z 91, resulting in a positive bias in measured toluene concentrations (Supplementary Information Figure A.7. Interference factors can be derived from experimental data to numerically correct for such interferences, but only for those analytes with molecular ions that also remain partially intact [116, 124]. Also, it is only possible to correct for those analytes that are targets for a particular deployment and have had interference factors determined a priori.

Chemical ionization (CI) was first used in combination with MIMS by Brodbelt and Cooks to monitor the progress of a chemical reaction in a complex mixture [143] using isobutane to generate reagent ions for the analysis of the methylation products

of cyclohexanone. In the analysis of solutions, Lauritsen *et al.* used components of the analyte–containing matrix as the CI reagent for the analysis of polar compounds in water [144] and VOCs in organic solvent [145]. Cisper *et al.* used atmospheric oxygen as a charge exchange reagent for the analysis of polar VOCs and SVOCs in air [146]. Following this, MIMS utilizing CI has been used for the analysis of biogenic alkenes [147] and alkyl aromatics [47, 48, 148] with a variety of reagent ions. More recently, a high resolution system employing H_3O^+ as reagent ions was used to analyze VOCs in aqueous solutions [149]. The principal advantage of CI is that analyte ions are generated with a minimum of excess internal energy, which results in little or no fragmentation of molecular ions. A variety of reagent ions have been used with CI for the identification of hydrocarbons, epoxide functionalities, and has even been employed for the differentiation of isomers [150, 151].

The aim of this work was to develop a novel MIMS system that utilizes chemical ionization (CI) for real–time analysis of volatile aromatic molecules such as the BTEX suite and alkyl aromatic species. We present the use of a cylindrical ion trap mass spectrometer, utilizing EI directly within the ion storage volume to generate and isolate a population of reagent ions for subsequent reaction with neutral analytes. As a novel approach, we use a second membrane interface to add reagent ion precursors directly into the (helium) sweep gas used to transport analyte from the sampling membrane to the mass spectrometer (i.e. they are not added or extracted from the sample matrix). This simplifies the experimental conditions and does not require reagent additions to the sample, while also eliminating the extra complexity of variable leak valves and extra hardware often customary for CI experiments. Mechanisms for analyte ionization can include electron transfer, charge transfer, proton transfer, hydride abstraction or other reactions such as addition/elimination, depending upon the reagent ion(s) employed. For successful CI, there must be a sufficient number of ion–molecule collisions during the residence time of the reagents in the ionization region. Ion traps offer two distinct advantages over high pressure CI using 'tight' EI ion volumes [152]: reagent ion populations can be readily varied by adjusting accumulation time; ion molecule reactions can be optimized by adjusting the CI reaction time [153].

In this study, we describe a novel CI reagent delivery system for liquid precursors, evaluate a suite of CI reagent ions for their reactivity with target VOCs, and demonstrate a strategy for quantitative analysis employing an on–line internal standard to correct for reagent ion depletion from competing analyte species or high

concentrations.

7.2 Experimental

A modified cylindrical electrode quadrupole ion trap (CIT) mass spectrometer (Griffin^{TM} 300, FLIR Systems, Inc., West Lafayette, IN, USA) was used for all of the experiments. Instrument modifications were made in–house and included replacement of the GC inlet with a flow cell membrane interface, similar to that described in other work [124]. Briefly, the MIMS interface consists of a capillary hollow fiber membrane (HFM, 10.0 cm x 0.94 mm OD x 0.51 mm ID) made of polydimethylsiloxane (PDMS) (Silastic^{TM} Silicone Tubing, Dow Corning, Midland, MI, USA) mounted in the flow cell on 22 gauge hypodermic tubing supports. Within the flow cell, sample is passed over the outside of the membrane, and helium sweep gas (acceptor phase) is flowed through the lumen of the HFM at ca 1.0 mL/min. Molecules that are soluble in PDMS diffuse through the membrane, and are subsequently transported to the mass spectrometer by the helium acceptor phase. EI and CI were directly compared for the analysis of gaseous samples ranging in concentration from 15–210 ppbv of benzene, toluene, toluene–d_8, ethylbenzene, xylene and –pinene. For EI, the standard mode of operation for this system, a 75 eV electron beam passes through the ion storage volume (termed internal EI) to ionize neutral analytes (50–150 msec ionization time) directly within the trap storage volume.

High purity chemicals were used without dilution or purification for CI reagents. Chloroform, chloroform–*d*, chlorobenzene, methyl iodide and dichloroethene were obtained from Sigma–Aldrich Canada Co. (Oakville, ON, CAN). For CI, reagent ion precursors were continuously infused into the (He) acceptor phase upstream of the sampling HFM via a smaller membrane inlet, constructed from a 0.25 OD stainless steel compression fitting tee (Swagelok, Solon, OH, USA) and a 1 cm length of PDMS HFM (0.94 mm OD x 0.51 mm ID) mounted in an analogous manner to the flow cell membrane interface described above. One side of the membrane was exposed to helium flow, via a small hole (∼0.5 mm diameter) drilled in the hypodermic tubing, while the other side was exposed to the headspace vapors of a liquid CI reagent. This configuration allowed switching of liquid reagent precursors by simply changing the precursor liquid reservoir, without breaking vacuum or adjusting any flow rates. A schematic diagram of the experimental

apparatus used to add CI reagent ion precursors to the helium acceptor phase is given in Figure 7.1a. To our knowledge, this is the first demonstration of the addition of CI reagent precursors in this manner for a MIMS experiment. Although the presented system has not been field deployed for this work, the described research could readily be implemented for in–field measurements on instrumentation designed for that purpose.

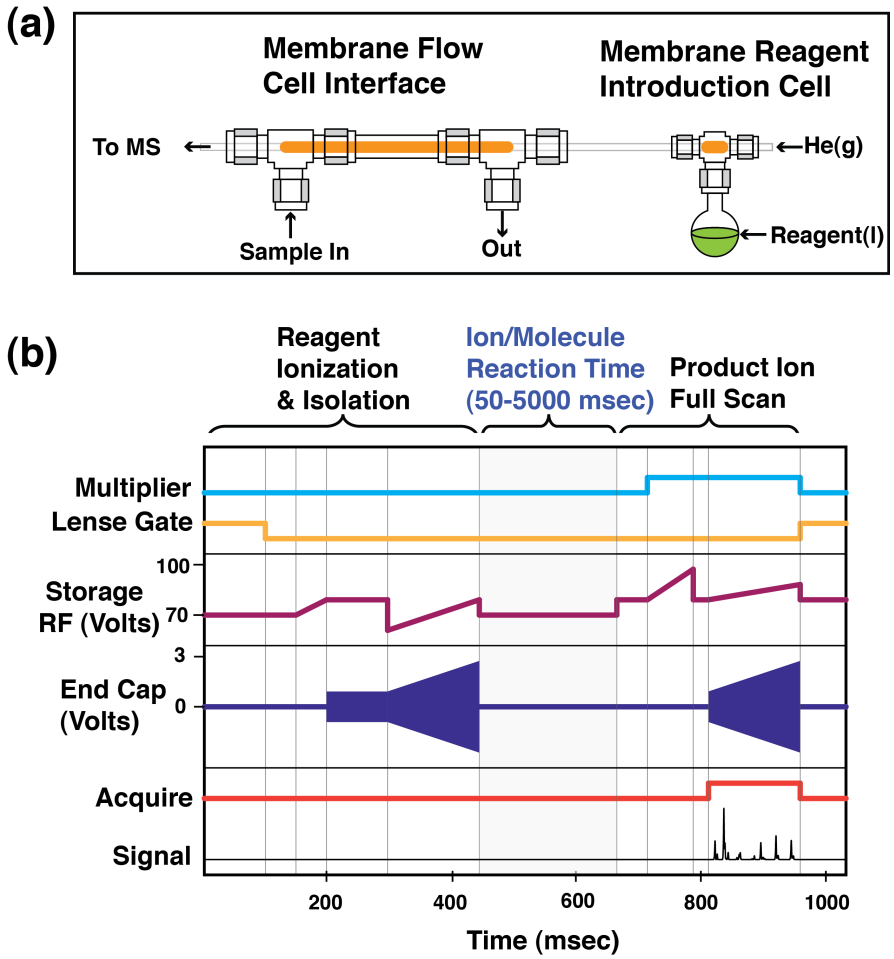


Figure 7.1: (a) Schematic diagram of apparatus used to add reagent ion precursors to the MIMS acceptor phase. Precursors are continuously infused into the helium acceptor phase via a small membrane flow cell upstream of the MIMS sampling interface. Test samples are delivered to the MIMS from a Dynacalibrator gas dilution apparatus. (b) Instrument timing diagram for a typical scan for chemical ionization of neutral VOCs via ion–molecule reaction(s), followed by a full scan mass analysis.

For CI experiments, reagent ions were generated by EI, isolated in the ion trap, and then allowed to react with neutral analyte molecules for a desired period of

time. Following this, analyte product ions were either detected in full scan mode, or isolated and analyzed by tandem mass spectrometry (MS/MS) for further confirmation of molecular structure. Analyte ions were typically isolated using a 2–3 m/z wide storage range at a q–value of 0.4 using resonant ejection with variable frequencies and amplitudes for 15 msec. The instrumental timing diagram for a typical chemical ionization experiment is presented in Figure 7.1b. The timing diagram can be subdivided approximately into three stages. First, reagent gas is ionized by EI, and the desired reagent ion isolated in the ion trap using a supplementary AC potential applied to the end caps and ring electrode to eject any ions produced by direct EI of the target analytes. Second, the reagent ions are allowed to react with neutral target analytes (reaction times 50–5000 msec) without applying a dissociation voltage (amplitude = 0V). Finally, the reagent and product ions are either ejected from the ion trap for full scan mass analysis, or isolated and fragmented further by collision induced dissociation (CID) to provide structural information for the adducts or molecular ions. For all experiments, the temperature of the membrane interface and acceptor phase transfer lines was maintained at 50°C, the manifold base pressure was $5x10^{-5}$ Torr and the ion source temperature was 150 °C.

Gas phase benzene, benzene–d_6, toluene, toluene–d_8, ethylbenzene, xylene, α–pinene, dimethylsufide (DMS), dimethyldisulfide (DMDS) and methane thiol standards were prepared using a Dynacalibrator gas dilution system, (Model 340, VICI Metronics, Huston, TX, USA) equipped with certified permeation tubes (Kin–Tek Trace Source^{TM}, La Marque, TX, USA). An internal standard (toluene–d_8) was delivered continuously into the sample stream via a certified permeation tube (Kin–Tek) housed in a temperature controlled permeation chamber, which has been previously described [124]. Detection limits were calculated for each analyte based upon three times the signal–to–noise ratio.

7.3 Results and Discussion

To examine whether a continuously infused mixture of internal standard (toluene–d_8) and chemical ionization reagent could be used for the real–time analysis of trace level VOC mixtures, several reagent ions were tested for reactivity towards a suite of environmental pollutants. Structurally diagnostic product ions are summarized in Table 1. The majority of reagent ions studied exhibited simple

charge exchange ionization when producing positive ions for the target analytes. However, reaction of $CHCl_2^+$ (the chloroform reagent ion) with aromatic hydrocarbons yielded positively charged adduct species $[M+CHCl_2\text{-}HCl]^+$. The observed mass spectral data are consistent with an addition/elimination reaction involving neutral HCl loss for the mechanism of ionization (Supplementary Information Figure S2a). Adduct formation with this reagent ion was not limited to aromatic hydrocarbons, as methanethiol also yielded positive ion adduct species (*m/z* 95) when reacted with $CHCl_2^+$. The major products for α–pinene and dimethyl disulfide (DMDS) were their intact molecular ions (*m/z* 136) and (*m/z* 96), respectively.

The reaction of $CHCl_2^+$ with dimethyl sulfide (DMS) was found to produce ions at *m/z* 61, which corresponds to a hydride transfer product $[M\text{-}H]^+$. The chlorobenzene reagent ion ($C_6H_5Cl^+$) was found to react effectively with toluene (*m/z* 92) and ethylbenzene (*m/z* 106) to yield intact molecular ions. Benzene on the other hand, did not react efficiently with the chlorobenzene reagent ion, reflected by its relatively poor detection limit of 320 ppbv (Table 1). Since benzene has a relatively high ionization energy (9.24 eV) [155] compared with chlorobenzene (9.08 eV) [156], the thermodynamics of charge transfer for this reaction are not favorable, explaining the poor detection limits. Both methyl iodide (CH_3I^+) and trichloroethylene ($C_2Cl_3^+$) reagent ions yielded positively charged molecular ions with comparable detection limits.

Table 7.1: Major product ions and detection limits for a suite of volatile target analytes using different reagent gas ions. EI detection limits from a previous study [124] are also reported for direct comparison with CI detection limits.

Reagent Gas [ion] Ionization Energy (eV)[a]	Target Analyte(MW)	Ionization Energy (eV)[a]	CI Product Ions (m/z)	CI Detection Limit[b] (ppbv)	EI Detection Limit[c] (ppbv)
Chloroform[$CHCl_2^+$]	Benzene (78)	9.2	[M+$CHCl_2$-HCl]$^+$ (125,127)	7	0.5
(11.4)	Benzene–d_6 (84)	9.3	[M+$CHCl_2$-HCl]$^+$ (130,132)	3	*
	Toluene (92)	8.8	[M+$CHCl_2$-HCl]+(139,141)	2	0.5
	Toluene–d_8 (100)	*	[M+$CHCl_2$-HCl]+(146,148)	2	*
	Ethylbenzene (106)	8.8	[M+$CHCl_2$-HCl]+(153,155)	3	2
	Chlorobenzene (112)	9.1	[M+$CHCl_2$-HCl]+(159,161)	2	2
	Naphthalene (128)	8.1	[M+$CHCl_2$-HCl]+(175,177)	3	10
	α–Pinene(136)	8.0	$M^{+\cdot}$ (136)	1	20
	Dimethylsulfide (62)	8.7	[M-H]$^+$ (61)	6	20
	Dimethyldisulfide(94)	7.4	$M^{+\cdot}$ (94)	1	*
Chlorobenzene [$C_6H_5Cl^{+\cdot}$]	Benzene (78)	9.2	$M^{+\cdot}$ (78)	320	0.5
(9.1)	Toluene (92)	8.8	$M^{+\cdot}$ (92)	15	0.5
	Ethylbenzene (106)	8.8	$M^{+\cdot}$ (106)	10	2
Methyl Iodide [$CH_3I^{+\cdot}$]	Benzene (78)	9.2	$M^{+\cdot}$ (78)	12	0.5
(9.5)	Toluene (92)	8.8	$M^{+\cdot}$ (92)	3	0.5
	Toluene–d_8 (100)	*	$M^{+\cdot}$ (100)	9	*
	Ethylbenzene (106)	8.8	$M^{+\cdot}$ (106)	12	2
Trichloroethylene	Benzene (78)	9.2	$M^{+\cdot}$ (78)	12	0.5
[$C_2Cl_3^+$]	Toluene (92)	8.8	$M^{+\cdot}$ (92)	4	0.5
(9.5)	Ethylbenzene (106)	8.8	$M^{+\cdot}$ (106)	8	2

[a]Ionization energies from NIST Chemistry WebBook [154]
[b]S/N = 3
[c]EI detection limits from Bell *et al.* [124]
* Indicates no data available from cited source.

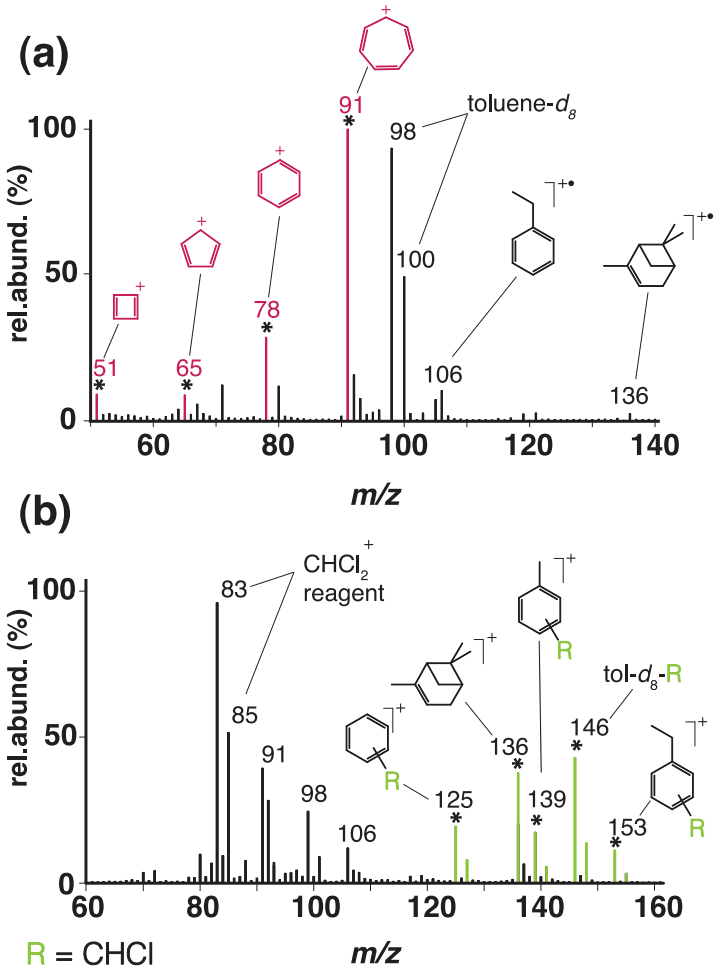


Figure 7.2: Comparison of EI and ion–molecule reaction spectra (CI) for mixture of benzene, toluene, toluened_8, ethylbenzene and pinene. (a) EI spectrum with isobaric species shown in red and marked with an asterisk. (b) Chloroform reagent ion $[CHCl_2]^+$ CI spectrum with charge transfer products as well as adduct species shown in green and marked with an asterisk.

This work is consistent with the related (GC/MS) results obtained by Wang *et al.* [157], who used tetrachloromethane as a reagent gas to effect the chemical ionization of VOCs that were first separated by gas chromatography. To further verify the nature of the ion–molecule chemistry we observe, an isotopically labeled reagent ion ($CDCl_2^+$) was used to confirm that the hydrogen is abstracted from the phenyl ring during the neutral HCl loss (Supplementary Information Figure A.8). Figure 7.2a presents an EI mass spectrum of benzene (73 ppbv), toluene (37 ppbv), ethylbenzene (16 ppbv), toluene–d_8 (155 ppbv) and –pinene (15 ppbv), while Figure 7.2b presents a chloroform CI mass spectrum of the same mixture. The EI spectrum in Figure

7.2a lacks an abundant molecular ion for ethylbenzene and –pinene because these molecules undergo extensive EI fragmentation. The typical common ions produced by aromatic molecules (m/z 51, 65, 78, 91) are also evident in the EI mass spectrum. In contrast, the ion–molecule reaction mass spectrum in Figure 7.2b exhibits greatly reduced fragmentation. Along with adduct ion formation (m/z 125,127; 139,141; 146,148 and 153,155), there are also molecular ions produced from charge transfer reactions (m/z 91, 98, 106 and 136). Further, the mono chlorine isotopic signature is clearly observed for the adduct species.

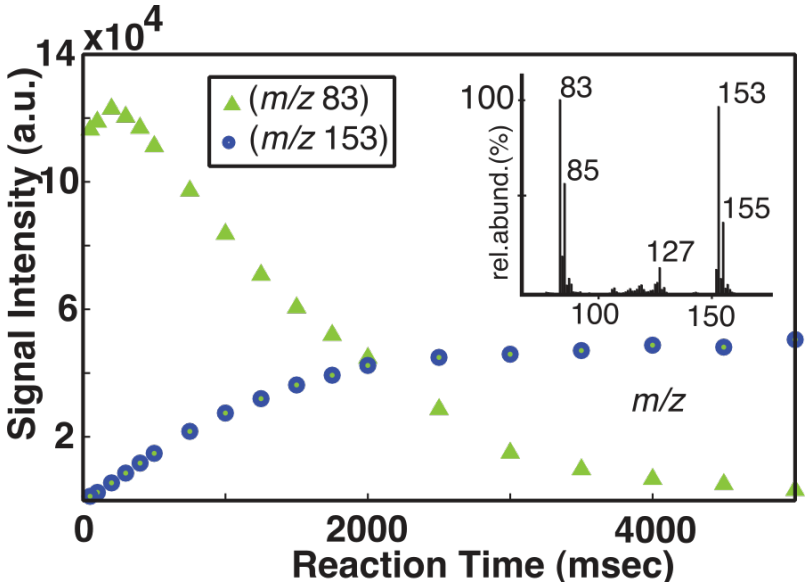


Figure 7.3: Effect of reaction time on both chloroform reagent ion (m/z 83) and ethylbenzene adduct ion (m/z 153) abundance. Inset mass spectrum of 50 ppbv ethylbenzene in air using 1500 msec reaction time.

The mass spectrum obtained for the analysis of a 50 ppbv ethylbenzene sample, using $CHCl_2^+$ reagent ion (from chloroform) at various reaction times in the ion trap is presented in Figure 7.3. To verify that this approach reduces isobaric interferences over those encountered when using EI, for comparison, the ethylbenzene EI mass spectrum obtained for a 50 ppbv sample (Supplementary Information Figure A.9) demonstrates profound isobaric interferences at m/z 77 and 91 (e.g. benzene and toluene ions), whereas the chloroform CI spectrum (Figure 7.3 inset) demonstrates virtually no interference for the toluene adduct (m/z 139, 141) and minor interference for the benzene adduct (m/z 125, 127). Figure 7.3 also illustrates that as the ion molecule reaction time increases, the abundance of the ethylbenzene adduct $[M+CHCl_2\text{-}HCl]^+$ increases linearly between 50 and 500 msec,

then gradually reaches steady state levels at approximately 3000 msec. As anticipated, the reagent ion population is depleted at longer reaction times. Reagent ion loss is also observed for long reaction times when no analyte is present (Supplementary Information Figure A.10), and when analyte concentration is increased at a fixed reaction time (Supplementary Information Figure A.11.

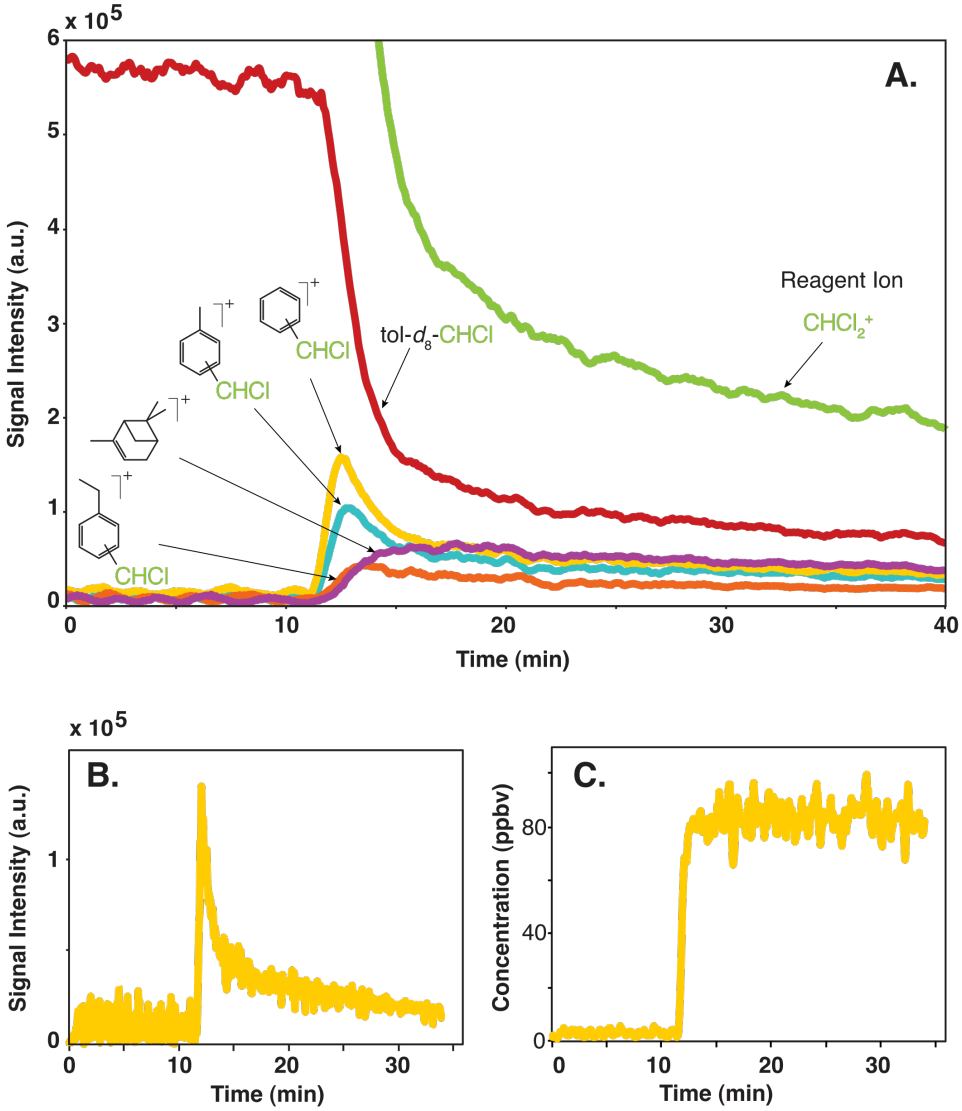


Figure 7.4: (a) Chloroform CI of benzene (73 ppbv), toluene (37 ppbv), ethylbenzene (16 ppbv) and –pinene (15 ppbv) mixture. At time = 0, the chloroform reagent ion and toluene–d_8 adduct (155 ppbv) are at steady state. At time 11min, the sample mixture is exposed to the membrane interface. (b) Ion chronogram for uncorrected benzene adduct $[M+CHCl_2\text{-}HCl]^+$. (c) Corrected benzene adduct chronogram obtained using toluene–d_8 internal standard to account for the depletion of CI reagent ions.

The ion loss process for ion traps has been well studied [158–160] because the rate of ion loss in the period of time between ionization and detection determines the overall instrument sensitivity [161]. In real world applications, the reaction time can be fixed, which renders losses due to unstable trajectories or nonlinear resonances constant, and therefore less significant. However, when measuring real samples, the concentration of analytes/chemical species in contaminant plumes can vary spatially and/or temporally by orders of magnitude, which may lead to collision (ion/neutral or ion/ion) or self–emptying (space charging) losses [161]. To compensate for the loss of reagent ion during (high) concentration excursions, an internal standard (toluene–d_8) was used to recreate the rise to steady state in the ion chronogram (Figure 7.4). As can be seen in Figure 7.4b, the uncorrected signal for benzene is observed to decrease following an initial rise as the reagent ion population is reduced by co–permeating analytes in the mixture. This effect is similar for other target analytes. By applying relative (to toluene–d_8) response factors, the concentrations observed for the analyte are corrected (Figure 7.4c).

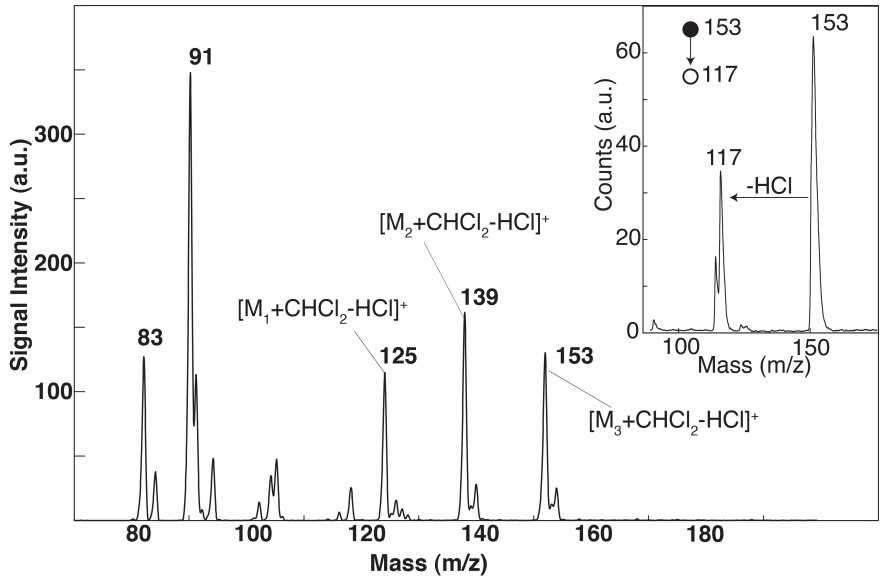


Figure 7.5: Mixture analysis of 500 ppbv benzene (M1), 276 ppbv toluene (M2) and 280 ppbv ethylbenzene (M3) in air using chloroform as a chemical ionization reagent. Inset shows CID of ethylbenzene precursor ion (m/z 153) and its product ion (m/z 117) formed via loss of HCl.

For mixture analysis, MS/MS was used to further study the diagnostic product/adduct ions. In these experiments, analytes of interests were ionized by chloroform CI, and then individual adduct species isolated and fragmented by

collision induced dissociation (CID) (Figure 7.5). The inset mass spectrum in Figure 7.5 shows the isolated adduct of ethylbenzene, m/z 153, and its characteristic CID product ion at m/z 117 produced via loss of HCl. The ability to perform tandem mass spectrometry experiments upon CI adduct ions increases the selectivity of the instrument for the quantitation of target analytes, and also provides valuable structural information.

7.4 Conclusions

The continuous infusion of internal standard (toluene–d_8) into the sample introduction system and the novel direct infusion of reagent ion precursors (e.g. chloroform) into the helium acceptor phase of a portable MIMS system, via a secondary membrane interface, is presented. This system has allowed improved selectivity for targeted VOC compounds in air by significantly reducing isobaric interferences observed in EI, without sacrificing sensitivity. The detection limits obtained with this approach are comparable to those obtained using EI (see Table 1). Ethylbenzene and xylene isomers cannot be resolved with this particular strategy, and are therefore reported as an aggregate measure. Increased selectivity for the majority of ion/molecule reactions studied was achieved with the exception of the energetically unfavourable charge transfer reaction between the chlorobenzene reagent ($C_6H_5Cl^+$) and neutral benzene (C_6H_6). To account for reagent ion depletion during mixture analysis, the use of continuously infused internal standard (toluene–d_8) in the sample can be used to correct the data and improve quantitation. MS/MS analysis was used to characterize the ion molecule adduct species and also to demonstrate additional selectivity. Future directions include improvement of detection limits at both membrane and mass spectrometer level, and evaluating the system for the in–field monitoring of target compounds in complex aqueous samples such as industrial process waters.

Chapter 8

Current status of portable MIMS and directions for future development

Mass spectrometry has a long history that begins at the turn of the 20th century with experiments by J.J. Thompson [162], F.W Aston [163] and at mid century, by W.Johnson and A.O. Nier [164]. The scientific development in this field since, has been tremendous and consists primarily if incremental change punctuated by revolutionary developments by E.O. Lawrence [165], Munson and Field [152], M.Dole [166], Comisarow and Marshall [167], J.Fenn [168], W.Paul [9], A.Makarov [169] and R.G.Cooks [170]. Since this thesis consists of a time–series of journal articles, it does not fully cover the recent advances and understanding of ion trap performance [5, 13, 171,172], that have been foundational to the development of a practical device for field deployment. The scientific developments presented in this thesis have contributed to the forward movement of this discipline, and are a result of the hard work and dedication of many members in our and other groups. In this final chapter, the challenges and results we have found in developing a mobile MIMS for real–time chemical analysis are summarized.

8.1 Portability

The first experimental chapter (3) of this thesis describes an in–house developed, mobile MIMS system that was deployed for real–time, in–field use to provide fine–scale temporally and spatially resolved quantitative measurements of hazardous air pollutants. For the traffic sites in this study, it was shown that fixed–site

monitoring stations report different concentrations than those observed by mobile MS at other sites. The main result of this study is a clear demonstration that a mobile, real–time sensor offers much more information that the traditional, fixed–point data collected. In addition, the concentrations reported by MIMS are comparable with traditional methods, but at the same time a significant amount of value–added information is collected as the instrument is mobilised from site to site. Despite the successful acquisition of spatial data, it became clear at the conclusion of the project that bench top GC–MS instrumentation would not be suitable for the development of a reliable, small footprint mobile MIMS system. Transient signal drops were observed when the instrument was operated on rough road services, likely caused by temporary vacuum breaches when stresses were experience by the delicate union between the GC oven (which housed the membrane interface) and the mass spectrometer. Further, a diesel generator was required to provide the clean and stable power required for this type of mass spectrometer. These issues were solved in part, quite simply, by the acquisition of a newly developed ruggedized portable GC–MS (Griffin 400). This can be powered with batteries (24 volts DC) or line power (110 volts AC) and does not require power down when swapping from one to the other. The major development on my part, was to integrate a robust thermally regulated membrane interface, internal standard chamber, and gas/liquid sample handling system. This system, described in Chapter 3.4, was easily transportable and operable from a moving vehicle. From a portability standpoint, this instrument design is effective and reliable. From a mass spectrometry perspective, further development is required to address the compromises associated with miniaturized mass analyzers. In this particular case (i.e. the CIT), these include limited linear dynamic range, space charging effects, and reduced sensitivity, all of which are associated small trapping volume.

8.2 Data management

We have successfully employed mobile MIMS to provide continuous geospatially resolved quantitative data using in–house developed data management software to process and visualize the data. Real time determination of detection limits was demonstrated Chapter 4, and allows the field operator to be alerted to decreased sensitivity, which prevents collection of meaningless data. However, it is clear that at this time that no single portable instrument is capable of providing a complete

picture of environmental chemical condition. As researchers become more proficient at real time data handling, it makes good sense to incorporate numerous sensors that can be easily supplanted as new technologies emerge or current technologies improve. With that in mind, more versatile mobile monitoring platforms will undoubtedly play an important role in the future of environmental chemical sensing, and will require further software development so that a multitude of sensors can be chosen for one's particular requirements.

8.3 Isobaric interferences

Since volatile and semivolatile analytes pervaporate through the membrane interface at the same time (without chromatographic separation), full resolution of isobaric isomers may not be possible.The majority of phenylalkane ions generated by electron ionization(EI) are vibrationally excited and well above the dissociation energy level. Unfortunately, phenylalkanes and biogenic terpenes have a number energetically favorable fragments in common, which complicates mass spectral interpretation and quantification, which can confound the distinction between anthropogenic and biogenic hydrocarbons. Ethylbenzene readily fragments in EI to yield m/z 91 ($C_7H_7^+$, tropylium ion), which can lead to positive bias in toluene concentration (m/z 91$\rightarrow$65). To some extent, we have been able to account for this problem by the application of interference factors. However, there are limitations to this strategy. For example, IFFs cannot be used to account for isobaric unknowns or isobaric VOCs that that have low ionization energies and appearance energies. α–pinene, produced from coniferous trees, is such an interferent and cannot be effectively corrected for. It's molecular ion (m/z 139) dissociates almost entirely under EI conditions to m/z 91, 92 and 93. The problem was solved in principal as outlined in Chapter 7. Presented is a low energy, chemical ionization strategy that effectively eliminated isobaric interferences for a suite of environmentally relevant target analytes. Although this strategy has been effective in the laboratory, it has not yet been tested in a field deployment.

Other techniques involving chromatographic separations or softer ionization strategies may be more appropriate if distinguishing these species is critical to a particular study. Additionally, high sensitivity for analytes in gaseous samples can be achieved via methods such as proton transfer reaction mass spectrometry (PRTMS) [102, 107] and selected ion flow tube mass spectrometry

(SIFT–MS) [108, 109]. Of course, for these techniques the challenges of field deployment and isobaric interference must also be considered, and therefore, still require further evaluation at this time.

8.4 Controlling environmental variables

Chapter 6 investigates unexpected signal variability that has been observed in portable ion traps with internal electron ionization. The orientation dependent variability was most pronounced in instruments where ionizing electrons have long path lengths and must pass through a small aperture. It was found that the predominant source of signal variability is a result of the Earth's magnetic field in combination with a secondary magnetic field from within the instrument. By developing an effective shielding strategy for the electron beam of affected instruments, significant improvements in ionization efficiency, and therefore sensitivity, are demonstrated. For effective field deployment, shielding the inside of the vacuum chamber is the best approach to reduce both instrumental and Earth's magnetic field. Further development is required in this area, and could include development of vacuum chambers with magnetically permeable coatings.

However, we have assumed that the effect of atmospheric pressure is negligible for field deployments. A particular data–set from a deployment in the Canadian Cascades, suggests that this assumption if false and the altitude does, in some way, affect the mass spectrometer signal we observe. In particular, we have observed fluctuations in the internal standard signal with changes in altitude (Figure 8.1).

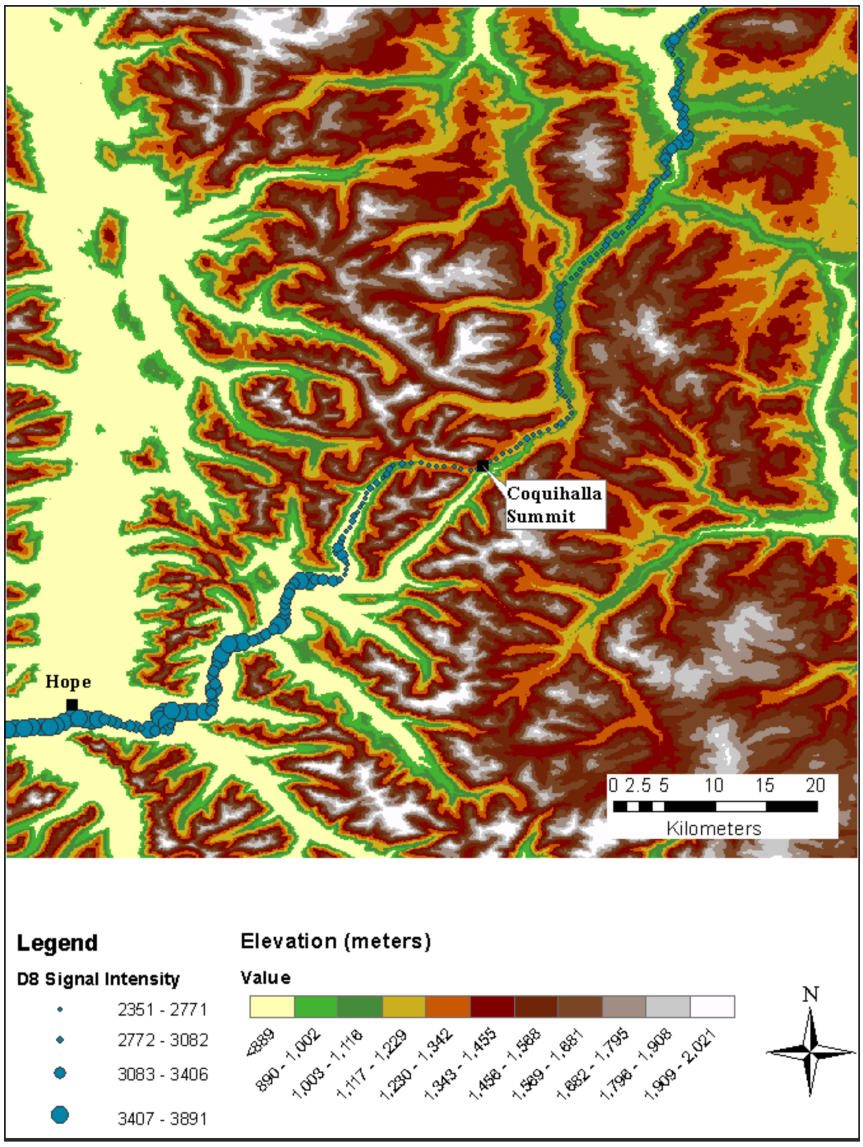


Figure 8.1: Digital Elevation Model (DEM) of toluene–d_8 signal intensity variation with respect to elevation.

Regardless of the precise nature of the actual effect, as long as the change in toluene–d_8 signal intensity is due to a change in d_8 concentration, the internal standard calculations are valid and the instrument can be considered to be functioning properly (albeit with higher detection limits). This is, of course, the primary advantage of using an internal standard. There is, however, a scenario where this would not be the case. If the effect is the result of decreased emission rate of the internal standard permeation tube, due to change in temperature of the outside air, the concentration of all analytes in the sample would be significantly overestimated. To determine

whether this is the result of a change in mass spectrometer or sample introduction performance, an internal standard, such as benzene–d_6 could be infused in the He acceptor phase. This would quickly, in all likelihood, eliminate the mass spectrometer as a cause for this effect. If the phenomenon is simply related to altitude effects on sample air pumps, a mass flow controller will solve this problem.

These preliminary results further illustrate some of the challenges that are associated with taking typically lab–based instrumentation into the field. Effects that would not normally be observed in the laboratory–where temperatures, pressures, and electric or magnetic fields are constant–must be studied and understood to ensure reliable results are obtained in the field.

8.5 Validation and expanding range of analytes

Comparisons of MIMS and a traditional high quality WAS canister analysis strategy were made both in lab and in field. Combining WAS with mobile MIMS monitoring provides complimentary data sets that, when combined, present a powerful adaptive sampling platform that can provide meaningful chemical information about geospatial distributions, temporal changes and dynamic mixing. However, further study is required to understand and control the effects of mixed matrices on the quantitative precision of EI–MIMS. Other strategies developed specifically for the analysis of VOCs in air include the following: Proton transfer reaction mass spectrometry (PTR–MS) is a sensitive technique (detection limits for VOCs in the pptr range [102]) that works by pumping ambient air through a drift tube, where hydronium ions (H_3O^+) are used as soft chemical ionization reagents. The duty cycle of this technique permits detection of concentration fluctuations, but sensitivity can be compromised by variations in atmospheric humidity [173]. Furthermore, the method does not distinguish between isobaric compounds and a number of clustering and secondary ion–molecule reactions in the drift tube can create interferences for some compounds [174]. Tandem mass spectrometry (MS/MS) is not currently available with PTR–MS as a potential option to solve this problem. Another system, developed by the Ontario Ministry of the Environment, allows direct sampling of the atmosphere using atmospheric pressure chemical ionization (APCI) combined with a triple quadrupole mass spectrometer (TQMS) [139]. This system is capable of MS/MS and has been operated from a mobile platform, but it's size and power demands make it better suited for urban

environments where good roads and line power are available. The range of analytes currently amenable to portable MIMS is limited, practically, to small ($m/z < 250$) non–polar VOCs and SVOCs. This is a limitation of the current technology and improvements are needed to extend the range of suitable analytes to include larger, more polar molecules. With the recent development of field portable atmospheric pressure mass spectrometers, a logical next step in this area of research would be the development of a field portable atmospheric pressure MIMS system for the analysis of aqueous contaminants such as naphthenic acids.

The future directions for real–time MIMS include, but are not limited to, the following: *First*, the sensitivity of the system must be improved, which could be accomplished by optimizations at the membrane, ion source and mass spectrometer levels. For example, a mass spectrometer with a bigger trapping capacity, soft ionization, and a high surface area membrane inlet, would tick all of these boxes. *Second*, fence line monitoring strategies combined with real–time multivariate statistics, could facilitate the identification of precise chemical sources and exposures. Finally, it is clear that with the advent of field portable mass spectrometers, a new paradigm for environmental monitoring is taking place. The lab is now often times being taken to the sample, rather than taking the sample to the lab. The clear benefits of this research are an improved understanding of environmental chemical fluctuations and both spatial and temporal domains. Ultimately, with this timely information readily available, sampling decisions could be adapted and corrective measures could be simplified and accelerated.

Appendix A

Supplementary Material

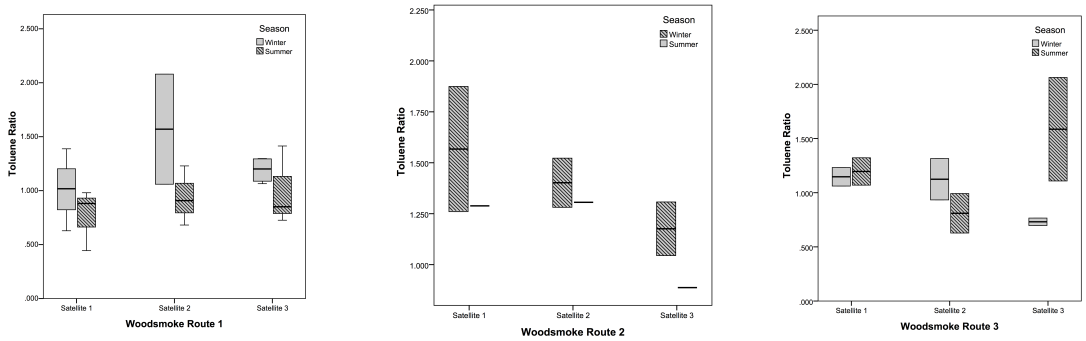


Figure A.1: Toluene concentrations at satellite sites, relative to the respective central site for each route.

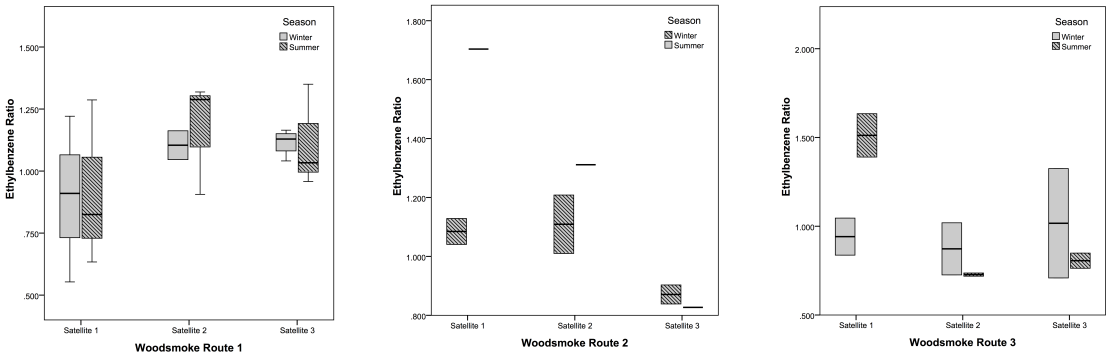


Figure A.2: Ethylbenzene concentrations at satellite sites, relative to the respective central site for each route.

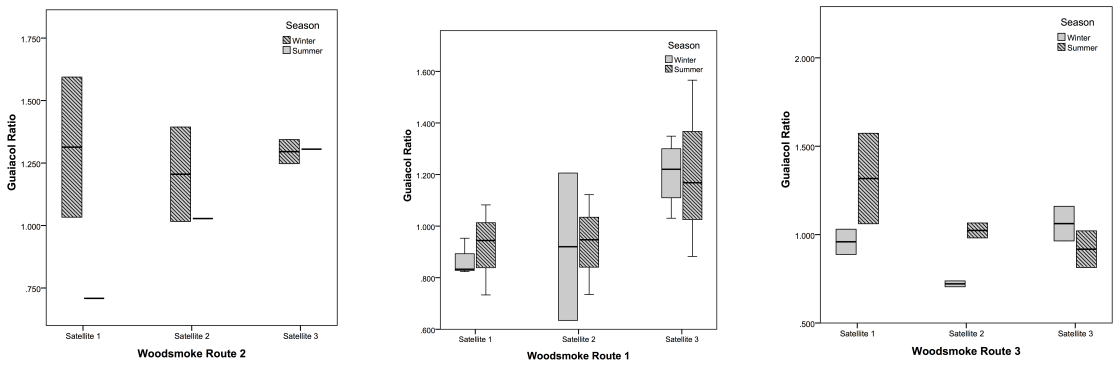


Figure A.3: Guaiacol concentrations at satellite sites, relative to the respective central site for each route.

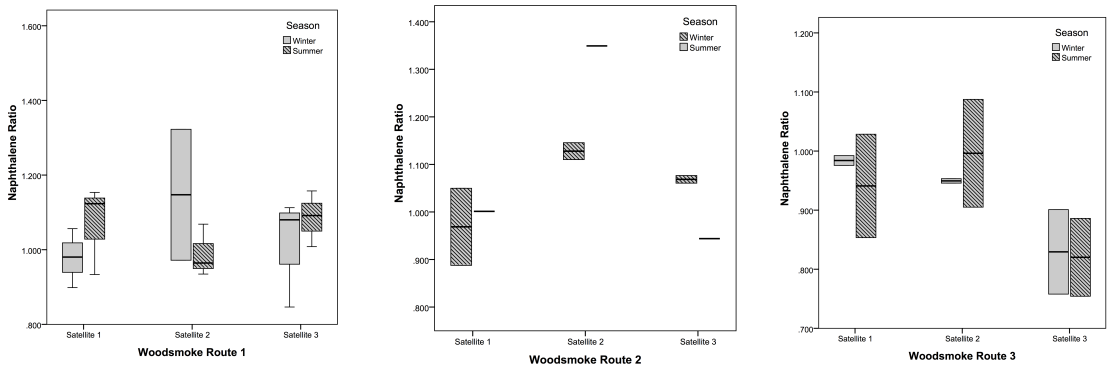


Figure A.4: Naphthalene concentrations at satellite sites, relative to the respective central site for each route.

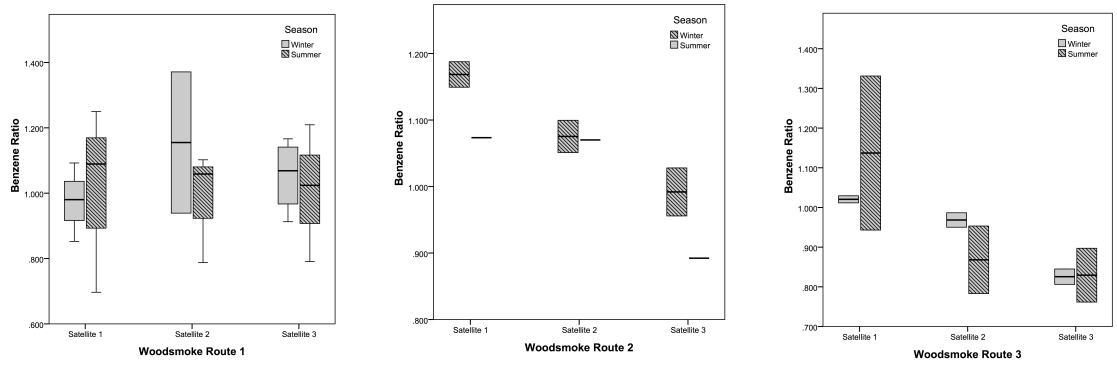


Figure A.5: Benzene concentrations at satellite sites, relative to the respective central site for each route.

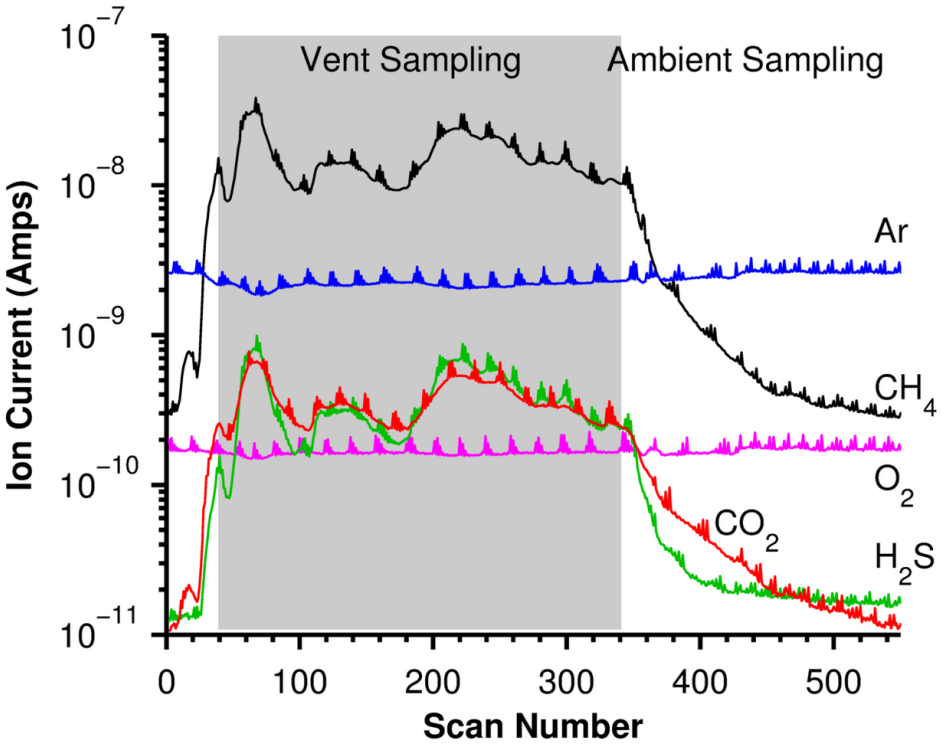


Figure A.6: Instrument response from an underwater mass spectrometer sampling ambient and hydrothermal vent water in Yellowstone Lake in 2002. The beating noise is a result of magnetic fields produced from a pulsing solenoid water sampling pump.

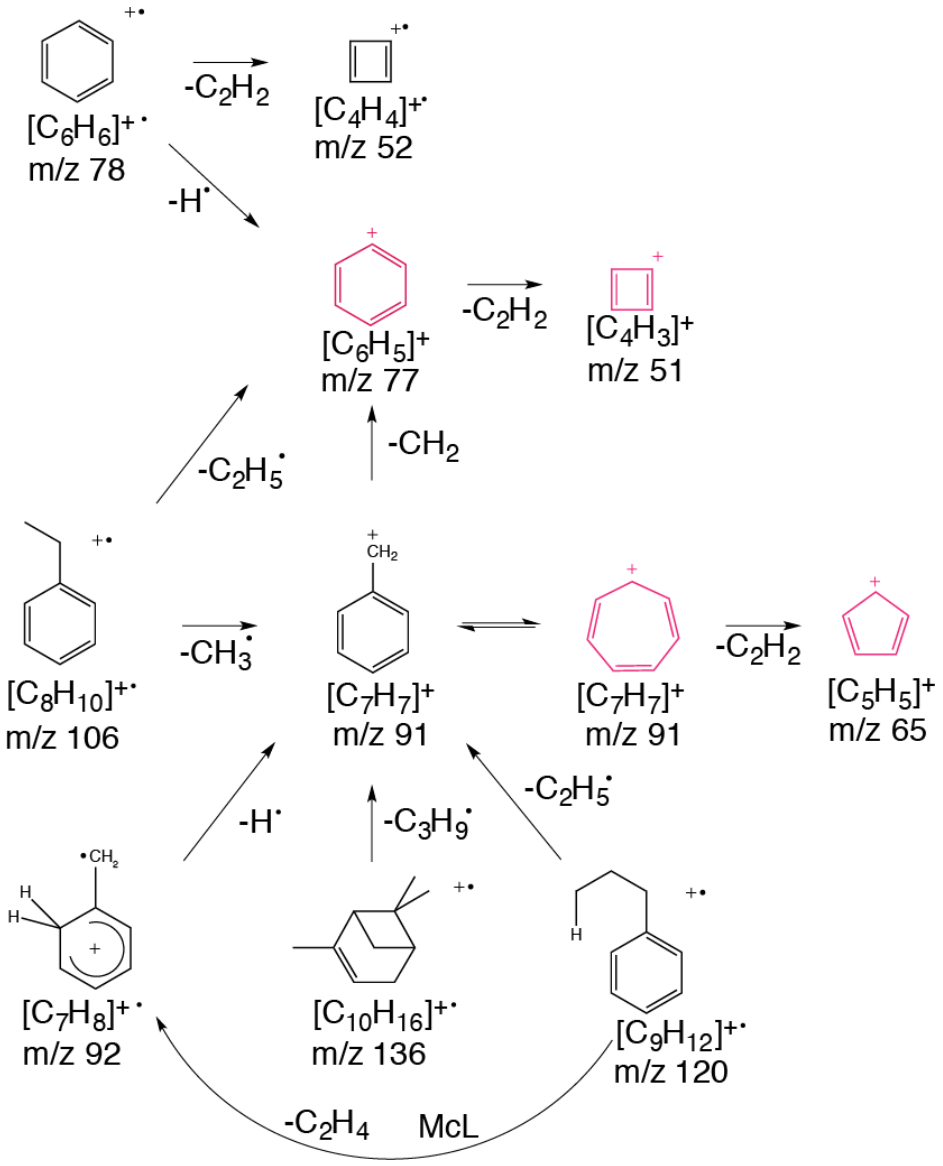


Figure A.7: Pathways for common positive ion formation from different precursors in EI.

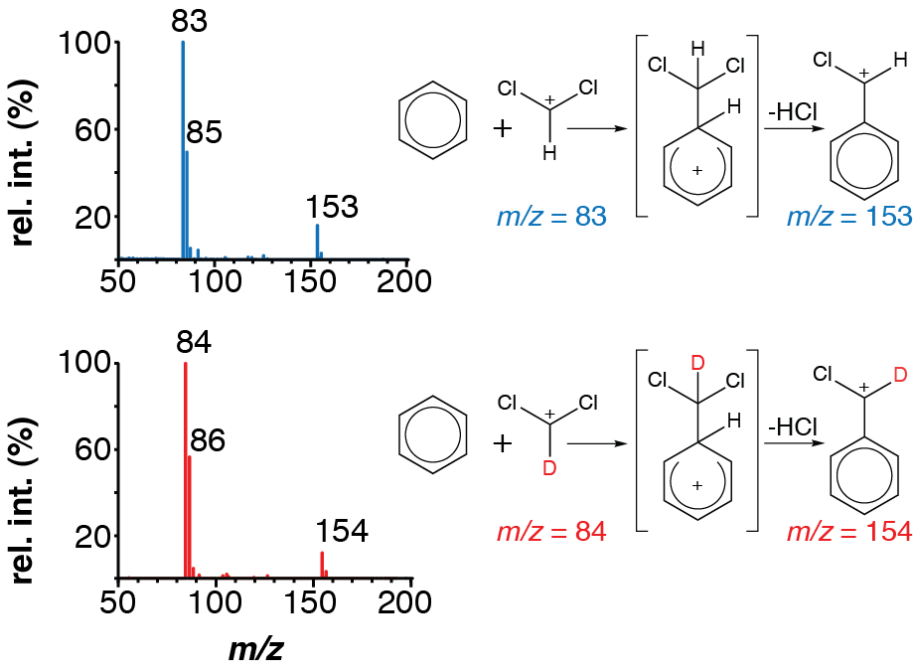


Figure A.8: (a) Chloroform CI mass spectrum of benzene and proposed reaction pathway for adduct ion formation with $CHCl_2^+$. (b) Chloroform-*d* CI mass spectrum of benzene and proposed reaction pathway for isotopically labelled product ion.

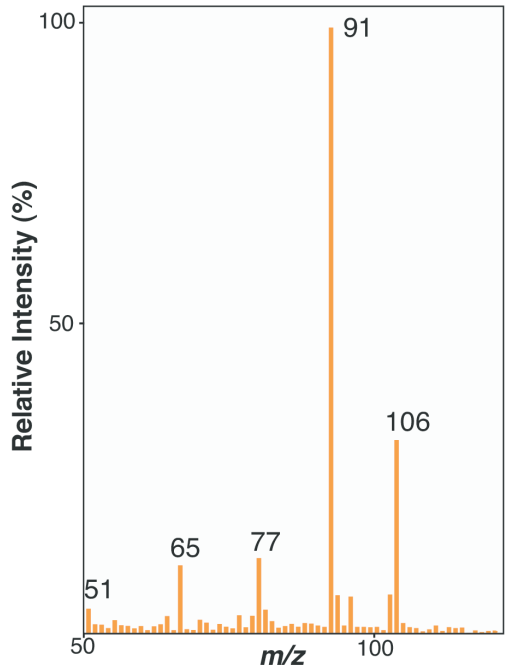


Figure A.9: EI mass spectrum for ethylbenzene (50 ppbv).

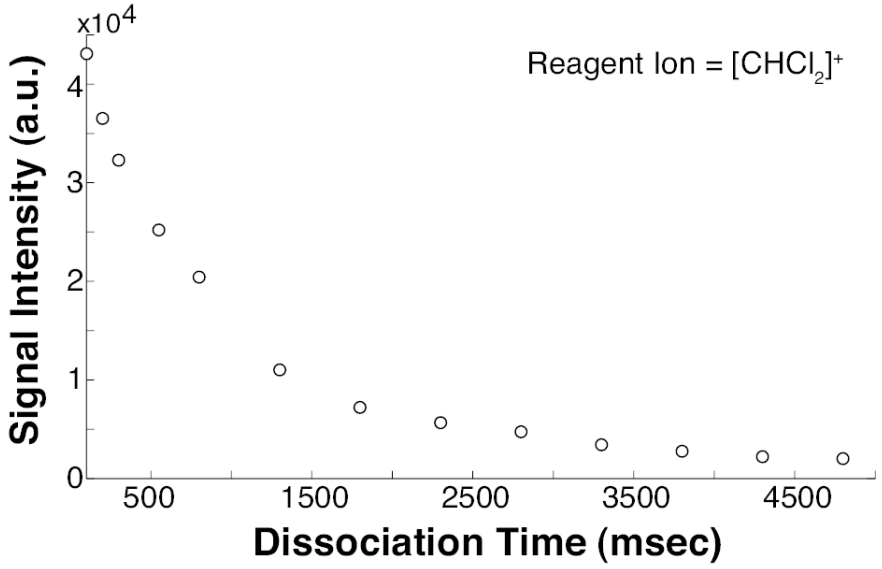


Figure A.10: Chloroform reagent ion ($CHCl_2^+$) population as a function of reaction time with no analytes added to the system.

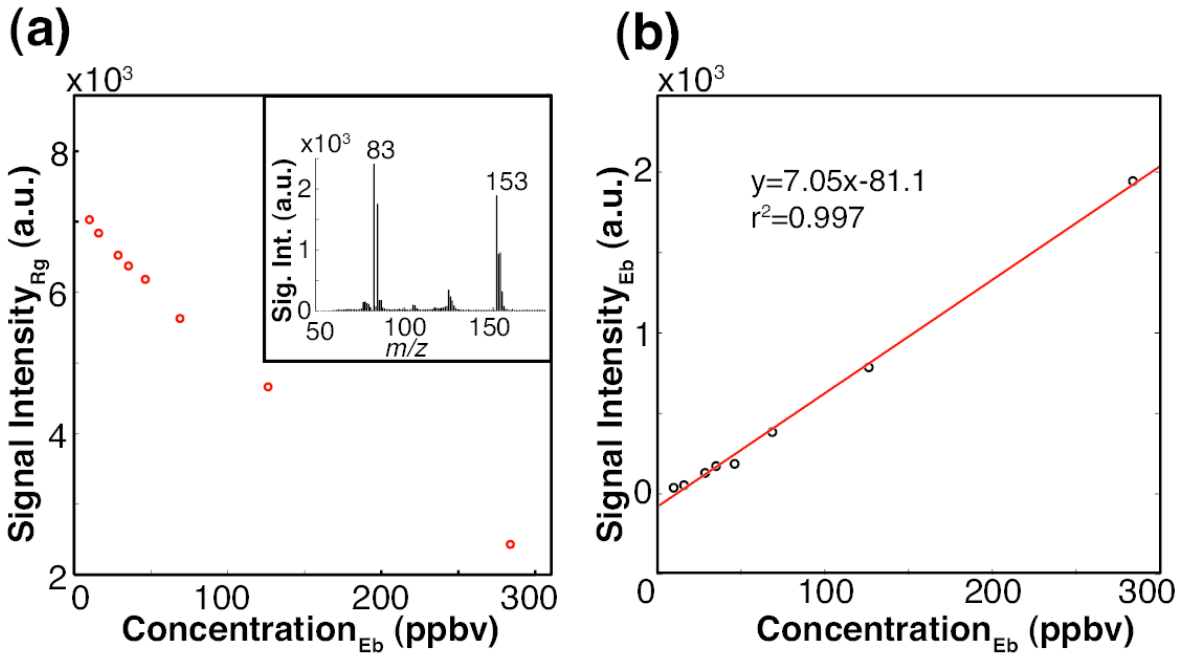


Figure A.11: (a) Chloroform reagent ion (Rg) signal intensity depletion with increased concentration of ethylbenzene (Eb) analyte at constant reaction time (2 seconds). Inset mass spectrum taken at 284 ppbv ethylbenzene. (b) Direct calibration of ethylbenzene using chloroform as CI reagent ion precursor and the resulting adduct ion (m/z 153) for quantitation.

Appendix B

Field portable membrane introduction mass spectrometer–early developments

B.1 Design of membrane based sampling interface

The instrumentation described in Chapter 3 was a modified lab based GC-MS system (Thermo GCQ). Despite the successful acquisition of spatial MS data, the system had several shortcomings. These included high power consumption, mechanical weaknesses, large physical size of the instrumentation, and the inability to calibrate and manage data in real-time. With funding from Statoil, a ruggedized field portable GC-MS (Griffin 400) was acquired which immediately addressed several of the aforementioned shortcomings; power consumption was reduced to ∼150 Watts, the physical size of the instrumentation was significantly reduced, and the instrument was designed for field portability and therefore mechanically robust. To address the remaining challenges, a number of in–house custom modifications were required. Each of these modifications required design, construction, integration, and testing. These modifications are described below and were foundational for enabling the studies presented in Chapters 4–7.

An aluminum platform was custom made to support a membrane interface, an internal standard permeation chamber, an air sampling pump, microprocessors, temperature controllers and 3–way valves for sample handling. To make use of shock mountings included with the Griffin 400 (Figure B.1a), the instrument was almost entirely disassembled to gain access to the frame, so that any modifications would rest on the shock absorbing platform. The disassembled instrument is shown

in Figure B.1b.

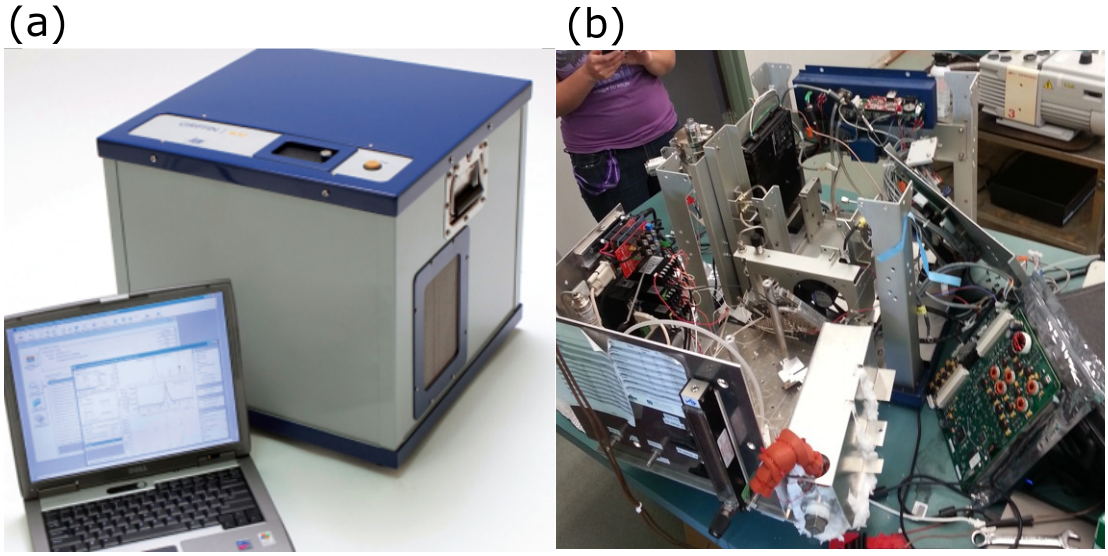


Figure B.1: (a) Commercially available portable GC-MS. (b) Disassembled instrument to allow construction of shock mounted membrane introduction interface.

The major components that constitute a modified mass spectrometer for membrane introduction are presented in Figure B.2. The aluminum platform (16"×11"×1/4") was supported by aluminum angle stock that was fastened to the shock mounting system of the Griffin 400. Threaded holes drilled and tapped in a 1 1/2" grid pattern to allow for numerous points of attachment for the components of the membrane inlet system. The internal standard chamber was machined from a solid cylinder of aluminum (2"d ×10"l). A 1 1/4"× 6" hole was drilled in one end of the cylinder to house the internal standard permeation tube. The temperature of the chamber was maintained with 50 Watt heater cartridge and temperature sensor that was re-purposed from the GC injector of the Griffin 400. Two other holes were drilled and tapped for 1/4" Swagelok to allow the sample to pass through the chamber, mix with the internal standard and be delivered to the membrane interface via a Teflon transfer line. To ensure ample heating of the sample, 7' of 1/4" stainless steel tubing was coiled around the heated internal standard permeation chamber. The sample inlet tubing was passively heated from the internal standard chamber and was typically maintained at 50°C. The membrane interface was supported by two 6 1/4"aluminum rods, which aligned the membrane interface transfer line with the inlet of the ion trap.

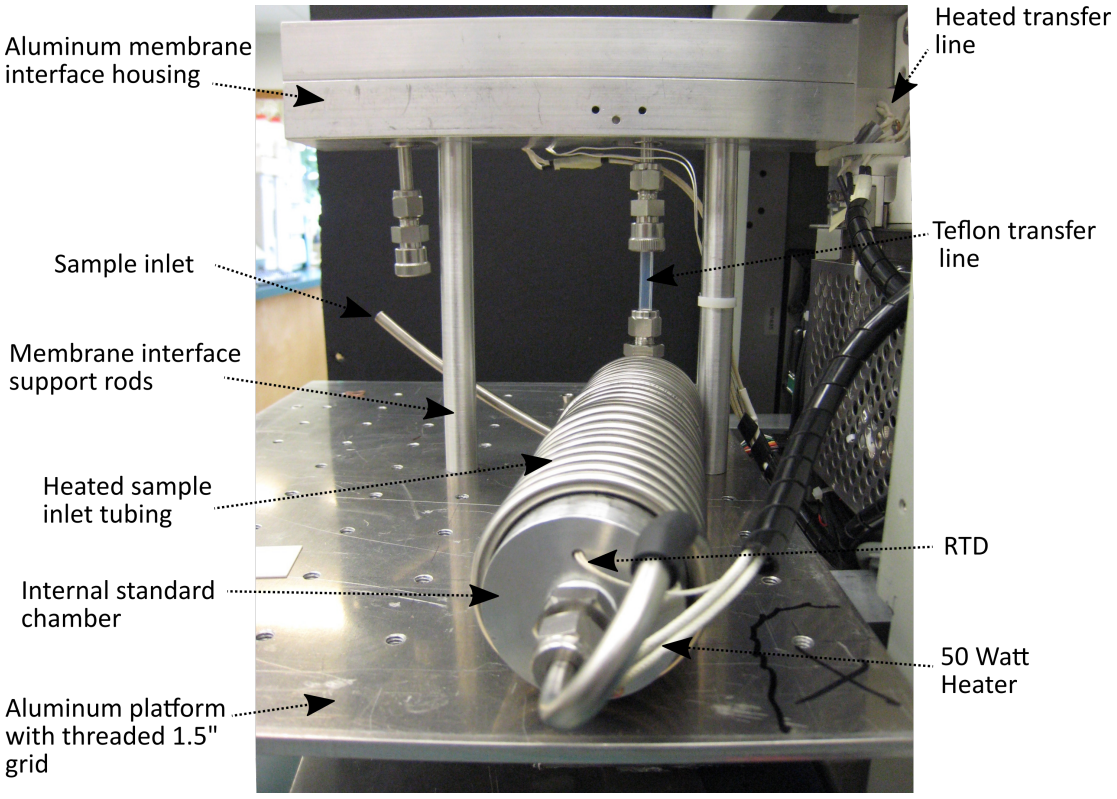


Figure B.2: Major components of customized mass spectrometer for membrane introduction.

To control the temperature of the membrane, an aluminum housing was machined from two pieces of aluminum bar stock (10"×2"×1"). Heaters and RTDs were re-purposed from the GC system to heat the membrane interface. A detailed view of the housing and membrane interface is presented in Figure B.3. The exit of the membrane interface was fed to the vacuum of the ion trap with a short heated transfer line. All the components described that came into contact with the sample were encased in fibre insulation to ensure even heating and thus prevention of cold spots. The sample inlet shown in Figure B.2 was extended to the roof of the vehicle with a 1/4" o.d. Teflon sample line (Cole Parmer). This line was wrapped in heat rope, insulation and shrink wrap. To prevent particulates from entering the system, sample was drawn into the MIMS system via two solvent cleaned microporous stainless steel inlet filters in series (15 and 5μm) (Model SS-6 F; Swagelok, Solon, OH, USA). The sample line and inlet filters were maintained at 50°C with SOLO temperature controllers (Model 4824, Automation Direct, Cumming, GA) which were mounted on the side of the instrument front panel.

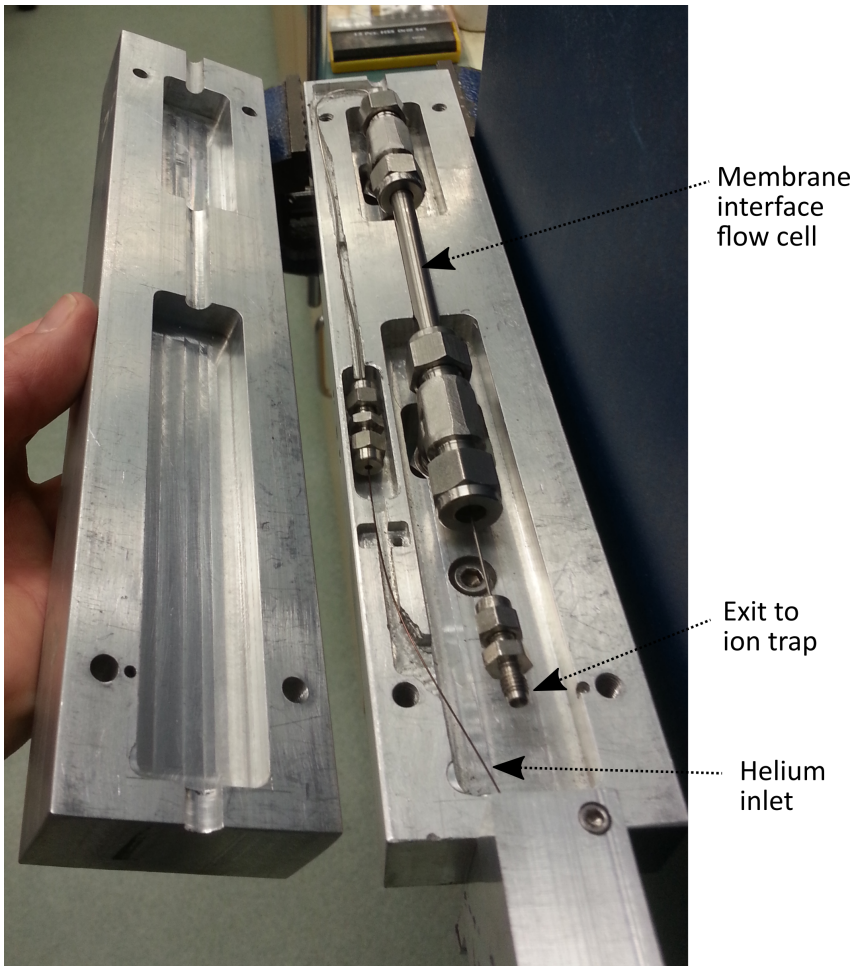


Figure B.3: Membrane interface housing.

Although the majority of this thesis focuses on gaseous sampling, the instrument was designed to be capable of aqueous sampling as as well. To achieve this, two three-way valves were incorporated that allowed for aqueous sampling without flowing liquid through the internal standard chamber. Valves were incorporated on the front panel of the customized interface (see Figure B.4) so that the user could easily switch between air/water sampling. Before and after the analysis of aqueous samples, zero air was flushed through the system to clean and dry the lines. Also on the front panel is a control for the air sampling pump and a 10–turn needle valve gas flow meter (Model FM 4312) used to fine tune the air sample flow rate. In later iterations of the instrument development, both sample pump switching and voltage regulation were controlled programmatically as described in Appendix C.



Figure B.4: Instrument front panel with two three way valves to allow switching between aqueous and gas sampling.

B.2 Calibration

B.2.1 Direct calibration and MS/MS

Reliable quantitation is a primary objective for any analytical technique. Since MIMS does not employ chromatography, calculating peak area from a chromatogram and calculating concentration from a calibration curve is not possible. However, in MIMS the mass spectrometer is scanning continuously, which allows for plots of ion current as a function of time (chronograms). Chronogram signal intensity can be plotted as a function of concentration to yield calibration curves for analytes of interest. In our group we refer to this method of calibration as direct external calibration. For effective quantitative analysis of complex mixtures with MIMS, tandem mass spectrometry (MS/MS) can be employed for additional specificity. In this thesis, a major transition took place between Chapters 3 and 4. At that time a new portable cylindrical ion trap (CIT) was acquired to replace a cumbersome and delicate bench top quadrupole ion trap with hyperbolic electrodes. The first MIMS calibration curve acquired from this instrument, with all of the aforementioned modifications, is presented in Figure B.5.

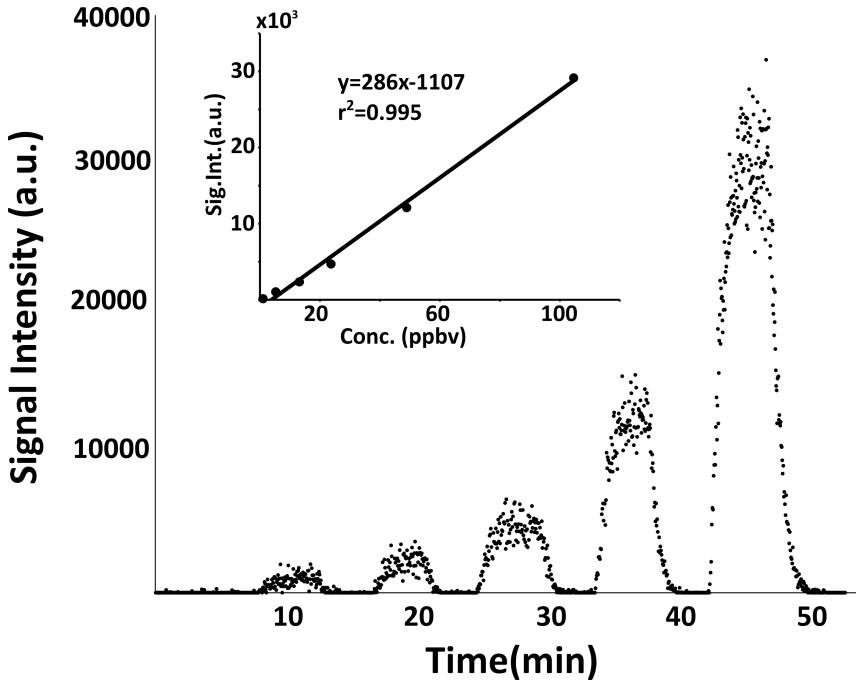


Figure B.5: First chronogram and resulting calibration curve (inset) acquired on the Griffin 400 MIMS system for a gaseous toluene standard (SIM for m/z 91).

All MS/MS methods that had been previously developed would not be useful for the CIT due to its smaller internal volume and consequently vastly different storage, dissociation, and scanning voltages. During the course of characterization, several insights were gained. First, it became clear that some analytes could not be fragmented reliably with the CIT that had worked very well in the hyperbolic QIT. For example, benzene, which has a well described fragmentation pathway (78→51), showed highly variable day to day MS/MS results. Redundant benzene scans (SIM and reconstructed SIM) were therefore included in the field deployment method in case the MS/MS scan for benzene failed. Although the analytes included in the field methods may have changed slightly from deployment to deployment, the most common targets and the performance characteristics are listed in Table 4.1.

Second, mass shifting, presumably due to space charging effects were observed at high concentrations during calibration studies. Figure B.6 shows mass shifting of a toluene-d_8 calibration chronogram. The product ion at approximately 50 minutes is shown being detected at m/z 71 rather than 70. Although the concentration is higher (>600 ppbv) than would be generally expected for a single analyte in the field, this data does demonstrate the need for better understanding of space charge effects in MIMS for complex mixture analysis.

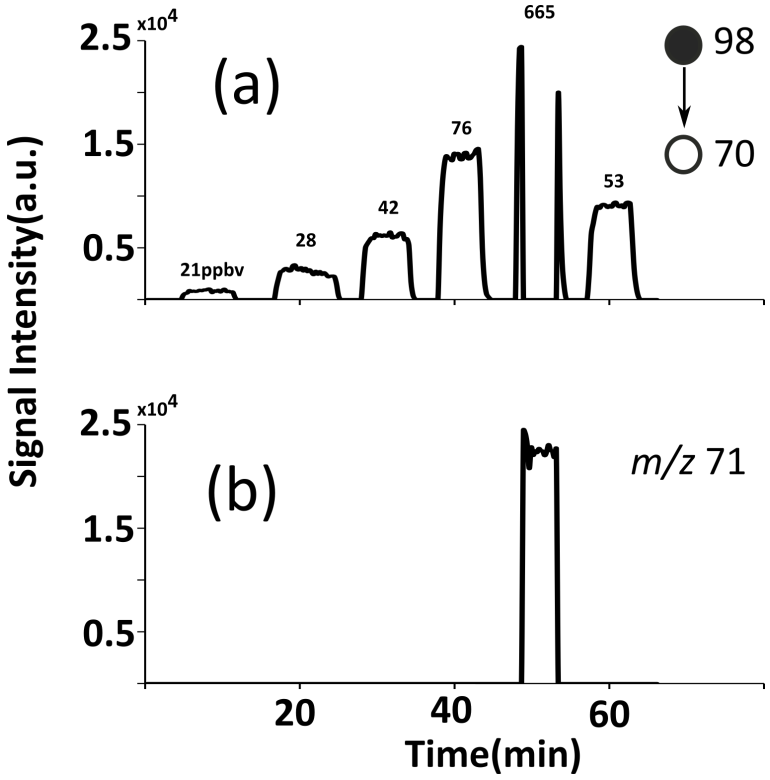


Figure B.6: Calibration chronogram for toluene-d_8 with mass shifting at high concentration. (a) MS/MS transition 98→70 showing loss of signal for m/z 70 at approximately 50 minutes. (b) Reconstructed chronogram for m/z 71 from the same data set used in (a).

Third, during calibration studies it was observed that ion-molecule chemistry in cylindrical ion traps (CITs) occurred readily under standard membrane introduction, tandem mass spectrometry (MS/MS) conditions. For example, the MS/MS spectrum for chlorobenzene showed an abundant peak at m/z 95 (Figure B.7). Due to the nature of the MS/MS experiment, this peak is most probably the result of an ion/molecule reaction between the phenyl ion ($C_7H_7^+$) and neutral water that has permeated through the membrane. As a result of this observation, a detailed study of ion/molecule chemistry in CITs was undertaken, the results of which are presented in Chapter 7.

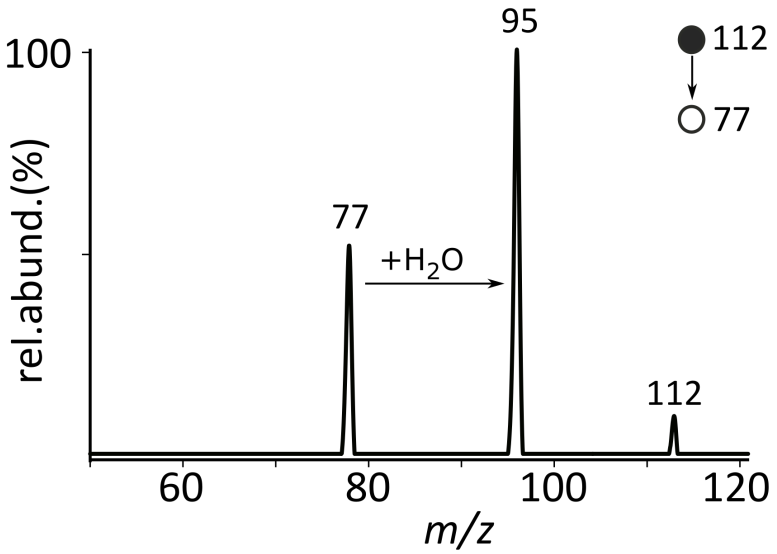


Figure B.7: Chlorobenzene MS/MS with abundant water adduct at m/z 95.

B.2.2 Internal standard calibration

The utility of a continuously infused internal standard for real-time MIMS cannot be overstated. As stated in Chapter 4.3, an internal standard is primarily used for quantitation, but just as importantly, provide the analyst with valuable feedback with respect to degradation in instrument performance due to contamination or filament wear, for example. For this work a certified toluene-d_8 permeation tube (Kin-Tek, La Marque, TX, USA) was housed in a custom made chamber (Figure B.8). The key features of this chamber are that the internal standard could be easily accessed from the chamber opening without altering sample plumbing, the relatively large thermal mass of the aluminum cylinder helped maintain a constant temperature, the sample line could be heated by the cylinder before entering the chamber, and that the entire assembly could be temperature regulated with hardware repurposed from the Griffin 400 heating system. As a final step, the entire assembly was wrapped in high temperature Fiberfrax® insulation. The performance of the custom permeation tube chamber was comparable to that of a commercially available gas standard generator (Figure 4.2), and was therefore deemed suitable for field deployment.

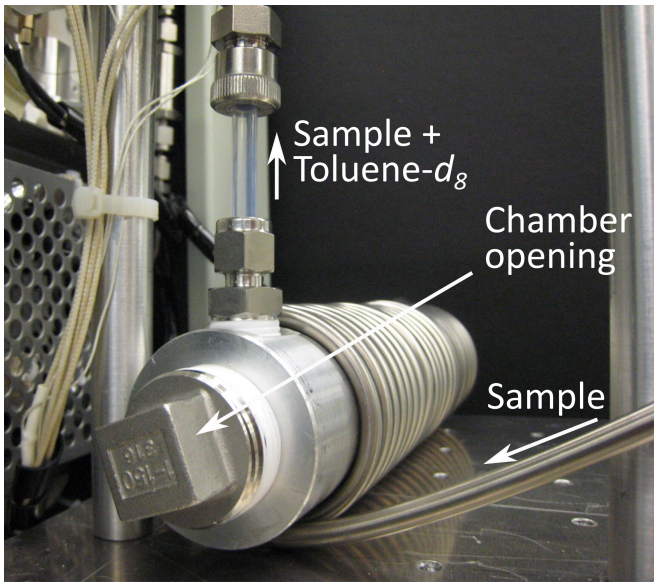


Figure B.8: Permeation tube chamber for continuous infusion of an isotopically labelled internal standard.

B.3 Improved sensitivity and response time

Two strategies were investigated, before deployment of the portable system described in Chapter 4, that would increase the sensitivity and response time of the instrument described in Chapter 3. Although a lack of thorough testing prevented implementation of these strategies for the field campaigns described in this thesis, it is likely that they will be used in the future to tune instrument performance for particular applications. The first strategy investigated was based on the findings of Thompson *et al.* [19], which showed an improvement in signal response time for SVOCs in aqueous samples when a resistively heated wire was incorporated in a HFM. The physical mechanism by which this heat improves response has not been entirely described, but the authors proposed that faster diffusion and improved desorption from the inner surface of the membrane was responsible. Although effective, the wire tended to sag when electrical current was flowing, which lead to fears of local hot spots and uneven heating in the membrane. To overcome this shortcoming, a membrane with a coiled nichrome wire was constructed (Figure B.9).

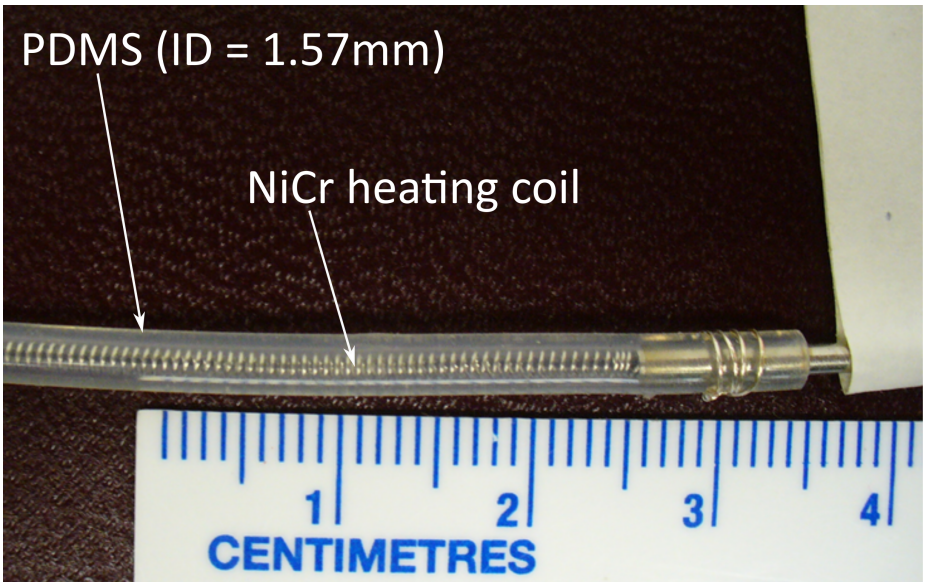


Figure B.9: PDMS membrane with coiled NiCr heating element.

Preliminary results for the analysis of a 160 ppb naphthalene solution demonstrate significantly reduced signal rise time (t_{10-90}) with increasing electrical current (Figure B.10). These results have potential implications for decreasing detection limits and rise times in both aqueous and atmospheric samples for SVOCs.

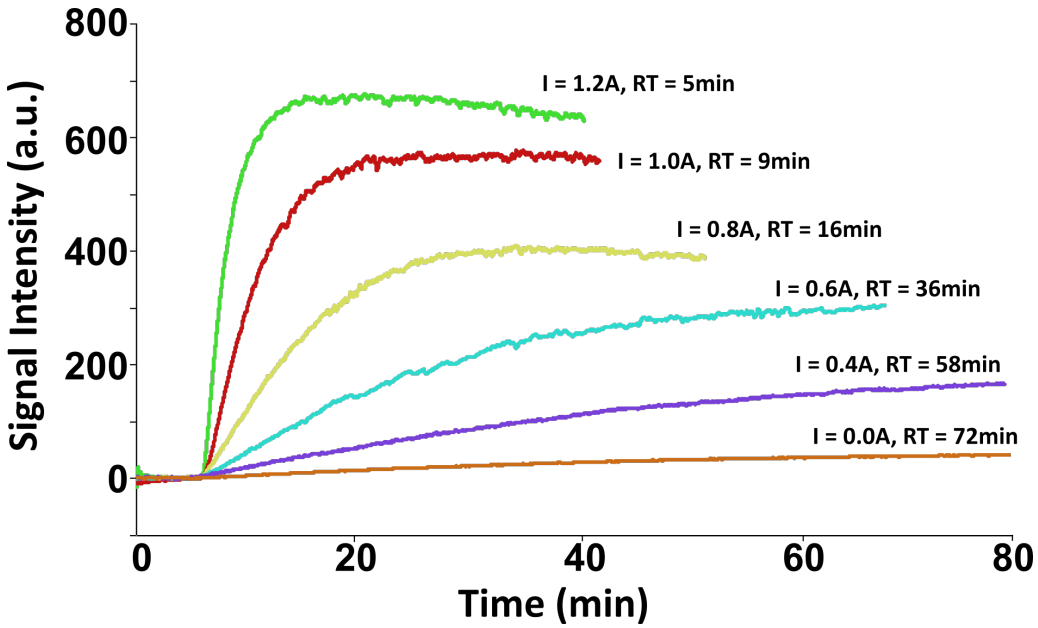


Figure B.10: The effect of electrical current on t_{10-90} for the analysis of a 160 ppb naphthalene solution.

Since the steady state flux of analyte across a hollow fibre membrane (Eq.B.1) [15] is related to the sensitivity of MIMS, it is possible to make alterations to the membrane geometry to increase performance. In Eq.B.1, F is the analyte flux (cm^3/s), L is the length of the membrane (cm), P is analyte permeability ($cm^2/s{\cdot}ppm$), C is concentration (ppm), and R_i/R_o is the ratio of inner/outer radii for the capillary hollow fibre membrane. Since the construction of a long membrane interface is not pragmatic, three shorter membranes were housed together in one interface to increase the effective length of polymer exposed to sample (Figure B.11). In Figure B.11a, three 10 cm long PDMS membranes are shown housed in a standard membrane interface with a quartz casing for observational purposes. In Figure B.11b, the inlet of the membrane interface is shown with three hypodermic tubes potted in epoxy to seal the flow cell. Although untested at present, theory predicts that this strategy should reduce detection limits roughly 3–fold for any MIMS application.

$$F = \frac{2\pi LPC}{ln(R_i/R_o)} \tag{B.1}$$

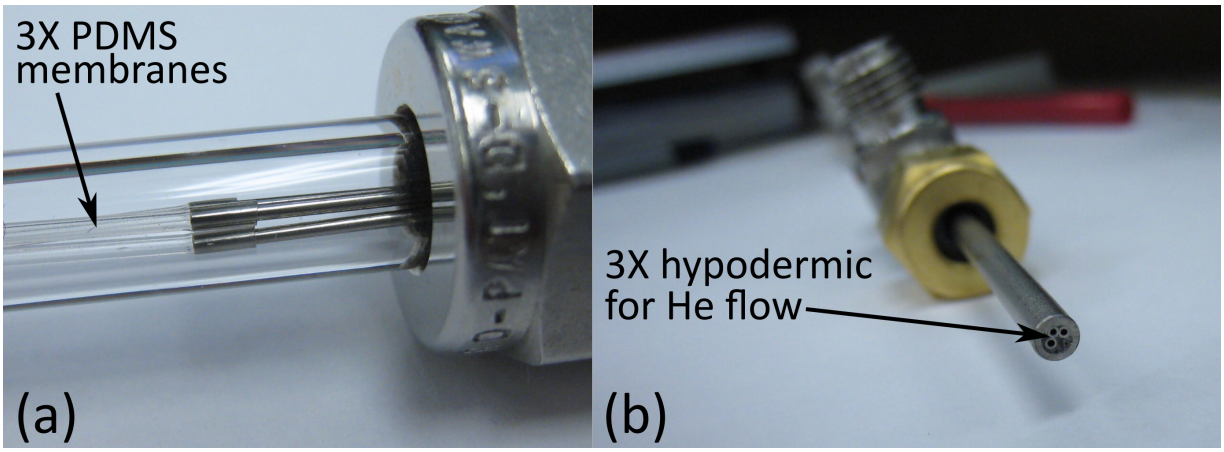


Figure B.11: Triple membrane interface design to increase sensitivity for trace level organics in air.

Appendix C

Standard Operating Procedures: Field Portable Membrane Introduction Tandem Mass Spectrometer

C.1 Description of Application

The following methodologies describe a procedure for the quantitative determination of volatile organic compound (VOC) concentrations in air and water with a portable membrane introduction mass spectrometer (MIMS). The method is suitable for both stationary and mobile analysis of a continuously infused air sample, with detection limits for most VOCs in the low parts-per-billion ($<$ 20ppb) range. The instrument discussed was modified in-house and, therefore, has a unique procedure for operation that is described herein.

C.2 Instrument Calibration

Prior to MIMS calibration and deployment, the cylindrical ion trap MS system (Griffin ICX model 400 GC-MS/MS) must be mass calibrated using the Griffin System Software (GSS) according to the instrument manufacturer's guidelines (Griffin System Software Suite, Level 1 Manual).

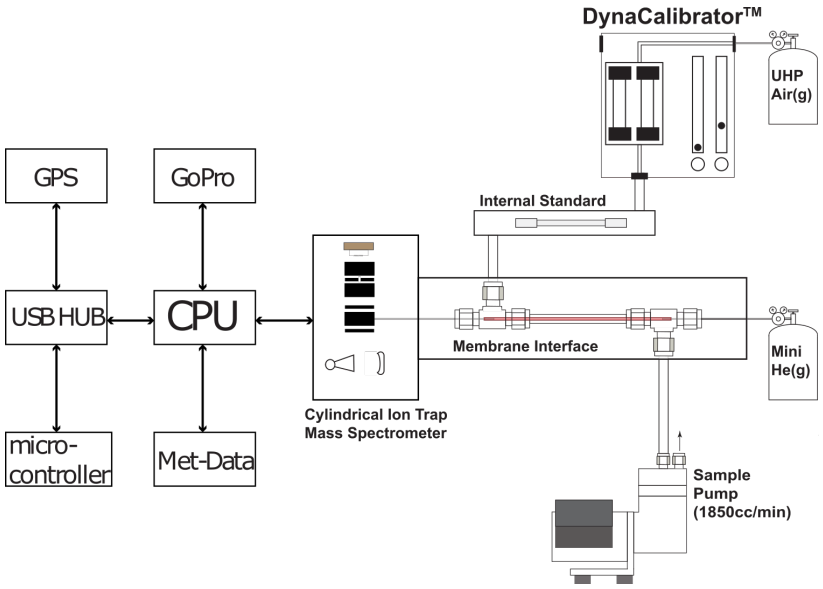


Figure C.1: Schematic of instrument calibration strategy for online analysis of VOCs in air.

C.3 Pre-Deployment Direct Calibration

The instrument is operated in electron ionization (EI) mode at about 5 x 10^{-5} torr base pressure and equipped with an in-house constructed temperature controlled membrane interface and in-line permeation chamber. Calibrations for analytes of interest are performed in the lab prior to deployment using a Dynacalibrator (Model 340, VICI Metronics Inc.) gas standard generator and certified Kin-Tek Trace Source^{TM} permeation tubes. Procedures can be further optimized for time efficiency and data quality, but typical calibration procedure is as follows:

- Select a Kin-Tek permeation tube to use for calibrating a specific analyte, and turn on Dynacalibrator using the temperature set point at which the permeation tube was calibrated. Place Kin-Tek permeation tube into the permeation chamber of the Dynacalibrator at the required calibration temperature and allow thermal equilibration for (>3 hours).

- Place an isotopically labelled internal standard such as d_8 toluene in the MIMS system permeation chamber and allow for thermal equilibration (>3 hours).

- Start Griffin System Software (GSS) and load the method that will be used in the field. This method should contain scans for the analyte, and the internal

standard. Generally MS/MS methods are preferred to allow for the isolation and fragmentation of specific analyte ions. This will increase instrument selectivity and reduce background noise.

- Connect via USB to the microcontroller using a terminal program. Windows XP and versions prior come with the Hyperterminal terminal program preinstalled. An alternative terminal program is Realterm. Turn on MIMS sample pump with the AP command, for example AP 120enter.

- Adjust the air sampling pump flow rate and the Griffin Rotameter until the sample flow rate is at a value that gives good signal intensity for the internal standard (toluene-d_8) on the mass spectrometer. We found that a sample flow rate of 1850 cc/min, allows the permeation tube to infuse 75 ppb toluene-d_8 in to the sample which gives a signal response of 6000 to 8000 counts.

Table C.1: Griffin 400 operational settings for field deployment.

Carrier Gas	UHP Helium
Carrier Gas Pressure	8 psi
Membrane Interface Temp	50°C
Heated Air Sampling Line Temp	50°C
Permeation Chamber	50°C
Trap Temperatrue	150°C
Lens Gate Open	-125 Volts
Lense Gate Closed	+80 V

- Calibrate the instrument by adjusting the flow rate of the Dynacalibrator to several different flows, ensuring the flow rate always exceeds that of the MIMS sample pump. In this way, binary mixtures with a constant concentration of isotopically labelled internal standard with different analyte concentrations are analyzed. Using data obtained in this manner, calibration curves can be obtained for each analyte.

- Plot the data and calculate analyte sensitivity and detection limits. PortableMSCalibration.exe software (currently under development outside the scope of this project using LabVIEW^{TM}) was used to plot and analyze the calibration data.

C.4 In-Field Direct Calibration

In-Field calibrations are typically employed when significant changes in instrument performance are suspected; for example, following required instrument maintenance, including filament changes, cleaning, or tuning. To perform a field calibration, select permeation tubes (e.g. benzene, toluene and toluene-d_8) are placed into the in-line permeation chamber and allowed to equilibrate overnight at the specified temperature (e.g. 50°C) with a very low flow of air (e.g. 50 mL/min). The low air flow is required to keep the permeation tubes flushed during their emission equilibration at this temperature. Following equilibration, calibrations are performed as follows:

- Start GSS, load the field method and run the instrument until the signal stabilizes (allow the instrument to fully warm up). This can take about 30 minutes.
- Start recording MS data using GSS.
- Flow Ultra High Purity (UHP) zero air over the interface in reverse direction to achieve a zero analyte present baseline (i.e. instrumental background). This can be done by directing the output three-way valve way from the air sampling pump to a supply of UHP air.
- Connect to the microcontroller using a terminal window and adjust the sample flow rate through the AP command and adjustment of the rotameter to the same approximate flow rate used during calibrations. Make note of the flow rate, as this will be need to calculate the internal standard concentration during the data work up. Using the air sampling pump and on-board airflow rotameter, calibrate using the steps specified in Table C.2.
- When calibration is complete, instrument performance is assessed using PortableMSCalibration.exe as described above, and air monitoring can begin.

C.5 Field Sampling

At least 6 hours before sampling/deployment begins, ensure the internal standard permeation tube (e.g. toluene-d_8) is present in the in-line permeation chamber, all heated zones are at stable temperatures and that a low flow of air ($\sim$ 250mL/min) is maintained throughout the sampling system (Figure C.2) until deployment. Following equilibration, a typical field sampling deployment is carried out as follows:

Table C.2: Typical set points for in-field calibration.

Step	Time	Setting	Float	Flow Rate
n/a	minutes	n/a	Black Ball	ml/min
1	0	zero air	n/a	>150
2	20	perm tubes	100	3651
3	40	perm tubes	50	1850
4	60	perm tubes	30	898
5	80	Remove perm tubes except d_8	50	1850
6	100	End	n/a	>150

- Attach heated air sampling inlet (1/4 inch Teflon tubing with 5μm particulate filter.)
- Start GSS and load the field method used for all calibrations and begin recording in a new data file.
- Allow the toluene-d_8 signal to stabilize before any changes are made.
- Connect to the microcontroller using a terminal window and adjust the sample flow rate through the "AP" command, adjusting the rotameter to the same flow rate used during calibration. For example, to set an air sampling flow rate of ~1850 cc/min, use a rotameter black ball setting of 50.
- Connect to the GPS, and ensure it is recording. This step will be dependent on the specific GPS device used.
- Connect a video recording device, if available. This step is currently under development and may be subject to site rules and regulations. The user is encouraged to include this step, as it provides visual data of events occurring in the proximity of the instrumentation during monitoring. Please follow local regulations.
- Connect to real-time data logging software. We are currently adopting existing software produced for other research partners as a plugin for real-time data visualization. This plugin allows the real-time software to calibrate the MIMS data, and then plot the data in a 3D mapping interface. The plugin for this project was developed to interface the Griffin instrumentation to the real-time software package and was test run in 2012. Please contact the corresponding

authors about the availability of this software. At this time, it is being actively developed outside of the scope of this project.

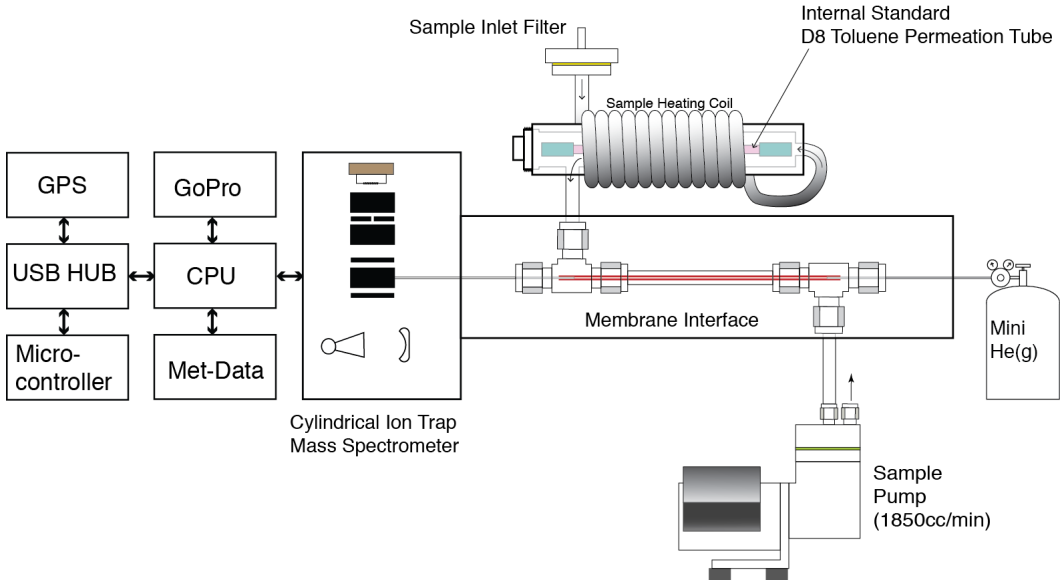


Figure C.2: Schematic diagram of the instrumentation used for online analysis of VOCs in air.

C.6 Data Analysis Progression

Raw data from the mass spectrometer must be processed to convert raw signal (counts) into concentration units (e.g., reported in parts-per-billion volume (ppbv) for atmospheric samples)). This process is illustrated in Figure C.3. Raw counts are baseline subtracted, corrected for interferences and converted to concentration using the pre-deployment direct calibrations (Figure C.3 A-C). Firstly, all raw counts must be baseline subtracted to account for the instrumental baseline:

$$Counts_{analyte} = RawCounts_{analyte} - BaselineCounts_{analyte} \tag{C.1}$$

For those analytes with known isobaric interferences, interference factors (IF) are calculated as follows:

$$IF = \frac{Counts_{analyte}}{Counts_{interferent}} \tag{C.2}$$

$$Example: IF = \frac{Counts_{toluene}}{Counts_{ethylbenzene}} = \frac{10000}{7700} = 1.3 \tag{C.3}$$

Example: When ethylbenzene (∼20 ppb) is in the system at steady state, there are 7700 counts for m/z 91 from the MS/MS transition 106→91. Also, there are 10000 counts in the toluene scan: m/z 65 from 91→65. The response factor is calculated to be 1.3. To apply the correction factor to field data for toluene:

$$CountsCorr_{analyte} = Counts_{Interferent} \times IF \tag{C.4}$$

$$CountsCorr_{toluene} = 2500 \times 1.3 = 3250 \tag{C.5}$$

$$FinalCounts_{toluene} = Counts_{toluene} - CountsCorrection_{toluene} \tag{C.6}$$

$$FinalCounts_{toluene} = 6253 - 3250 = 3003 \tag{C.7}$$

In Figure C.3 C, pre-deployment calibration data for sensitivity (counts/ppb) is used to calculate direct calibration concentration (ppb):

$$DirectCal(ppb) = \frac{FinalCounts_{analyte}}{Sensitivity} \tag{C.8}$$

As with all mass spectrometers the Griffin 400 is subject to sensitivity drifts over extended operation periods. As such, the results from the direct calibration can deviate substantially if calibrations have not been run recently. To account for this, an internal standard is used. If the counts from the internal standard deviate significantly from the time of calibration, this serves as a warning to the user that instrumental sensitivity has changed, and should be addressed. To compensate for sensitivity drift, we use the internal standard to correct the analyte signal using analyte response factors calculated during calibration. Relative (to the internal standard) response factors (RF) are calculated for each analyte using the pre-deployment calibration as follows:

$$RF = \frac{Concentration_{InternalStandard}}{FinalCounts_{InternalStandard}} \times \frac{FinalCounts_{analyte}}{Concentrationanalyte} \tag{C.9}$$

With this information, the concentration of analyte in the field sample can be calculated as follow and displayed (Figure C.3 E).

$$Concentration_{analyte} = \frac{Concentration_{InternalStandard}}{FinalCounts_{InternalStandard}} \times \frac{FinalCounts_{analyte}}{RF} \quad \text{(C.10)}$$

As a final step, the calibrated data is smoothed (e.g., boxcar 10), so that maps generated in Google Earth are more easily interpreted. This step is shown in (Figure C.3 F).

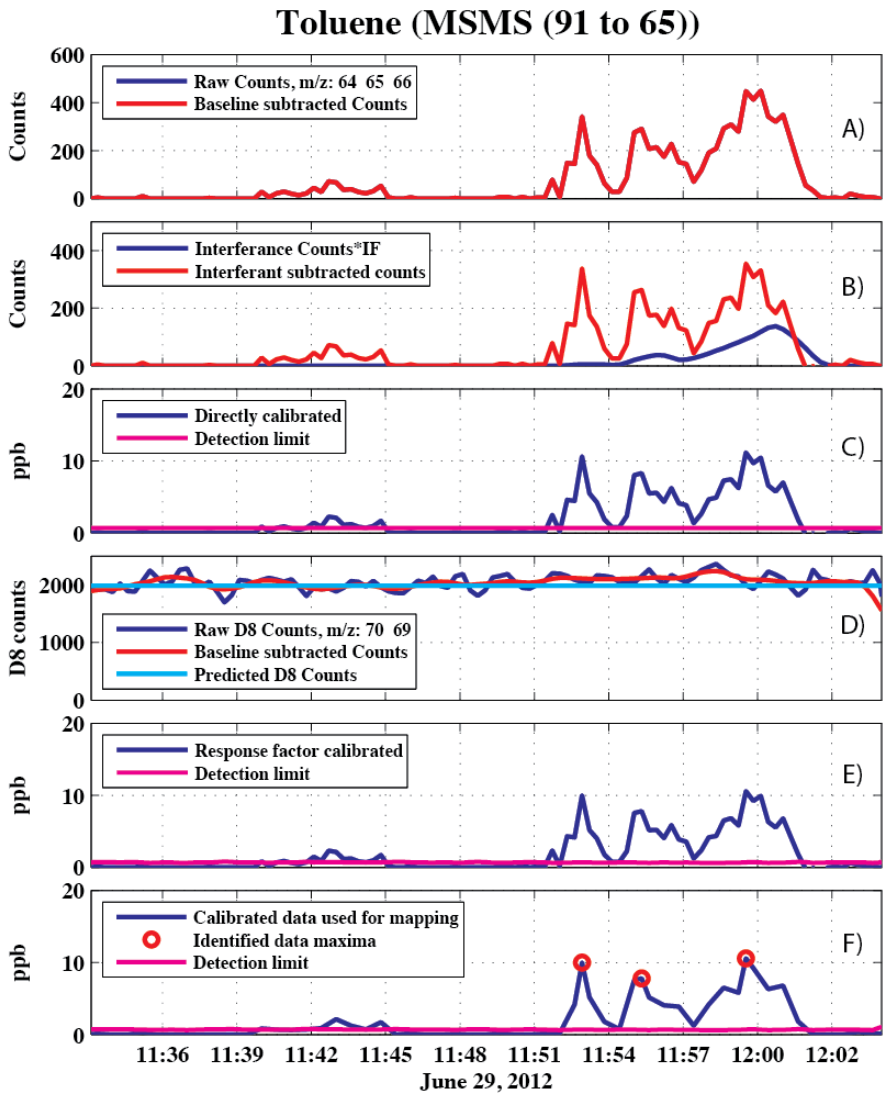


Figure C.3: Sample time series showing conversion of raw counts to calibrated concentration for a toluene MS/MS scan. (a) Raw counts and baseline subtracted counts for a toluene MS/MS scan (91→65). (b) Interference factor corrected counts for MS/MS scan (91→65). (c) Concentration and detection limit for toluene calculated from pre-deployment direct calibrations. (d) Toluene-d_8 internal standard (98→70) counts and predicted counts. (e) Concentration and detection limit for toluene calculated using relative response factors. (f) Calibrated and smoothed data with identified concentration maxima used for mapping.

Bibliography

[1] R. A. Ketola, T. Kotiaho, M. E. Cisper, and T. M. Allen, "Environmental applications of membrane introduction mass spectrometry," *Journal of Mass Spectrometry*, vol. 37, no. 5, pp. 457–476, 2002.

[2] V. Y. Cherebillo, A. Y. Elizarov, and A. V. Polegaev, "Membrane-introduction mass spectrometry analysis of desflurane, propofol and fentanyl in plasma and cerebrospinal fluid for estimation BBB properties," *Experimental Neurobiology*, vol. 24, no. 3, pp. 206–210, 2015.

[3] E. T. Krogh and C. G. Gill, "Membrane introduction mass spectrometry (MIMS): a versatile tool for direct, real-time chemical measurements," *Journal of Mass Spectrometry*, vol. 49, no. 12, pp. 1205–1213, 2014.

[4] G. Hoch and B. Kok, "A mass spectrometer inlet system for sampling gases dissolved in liquid phases," *Arch Biochem Biophys*, vol. 101, pp. 160–70, 1963.

[5] Z. Ouyang and R. G. Cooks, "Miniature mass spectrometers," *Annual Review of Analytical Chemistry*, vol. 2, pp. 187–214, 2009. Ouyang, Zheng Cooks, R. Graham 117.

[6] P. G. Wenner, R. J. Bell, F. H. W. van Amerom, S. K. Toler, J. E. Edkins, M. L. Hall, K. Koehn, R. T. Short, and R. H. Byrne, "Environmental chemical mapping using an underwater mass spectrometer," *Trac-Trends in Analytical Chemistry*, vol. 23, no. 4, pp. 288–295, 2004.

[7] F. McLafferty, "Tandem Mass Spectrometry," *Science*, vol. 214, no. 4518, pp. 280–287, 1981.

[8] G. C. Stafford, "Ion trap mass spectrometry: a personal perspective," *Journal of the American Society for Mass Spectrometry*, vol. 13, no. 6, pp. 589 – 596, 2002.

[9] W. Paul and H. Steinwedel, "A new mass spectrometer without a magnetic field," *Z. Naturforsch*, vol. 8a, pp. 448–450, 1953.

[10] R. E. March, A. W. McMahon, F. a. Londry, R. L. Alfred, J. F. J. Todd, and F. Vedel, "Resonance excitation of ions stored in a quadrupole ion trap. Part 1. A simulation study," *International Journal of Mass Spectrometry and Ion Processes*, vol. 95, no. 2, pp. 119–156, 1989.

[11] R. E. March, A. W. McMahon, E. T. Allinson, F. a. Londry, R. L. Alfred, J. F. J. Todd, and F. Vedel, "Resonance excitation of ions stored in a quadrupole ion trap Part II. Further simulation studies," *International Journal of Mass Spectrometry and Ion Processes*, vol. 99, no. 12, pp. 109–124, 1990.

[12] R. E. March, F. a. Londry, R. L. Alfred, J. F. J. Todd, A. D. Penman, F. Vedel, and M. Vedel, "Resonance excitation of ions stored in a quadrupole ion trap Part III. Introduction to the field interpolation simulation method," *International Journal of Mass Spectrometry and Ion Processes*, vol. 110, no. 3, pp. 159–178, 1991.

[13] D. T. Snyder, C. J. Pulliam, Z. Ouyang, and R. G. Cooks, "Miniature and Fieldable Mass Spectrometers: Recent Advances," *Analytical Chemistry*, vol. 88, pp. 2–29, 2016.

[14] R. C. Johnson, R. G. Cooks, T. M. Allen, M. E. Cisper, and P. H. Hemberger, "Membrane introduction mass spectrometry: trends and applications," *Mass Spectrom Rev*, vol. 19, no. 1, pp. 1–37, 2000.

[15] M. A. LaPack, *The theory and practice of membrane extractions*. PhD thesis, Michigan State University, 1994.

[16] F. R. Lauritsen, M. A. Mendes, and T. Aggerholm, "Direct detection of large fat-soluble biomolecules in solution using membrane inlet mass spectrometry and desorption chemical ionization," *Analyst*, vol. 125, no. 1, pp. 211–215, 1999.

[17] T. M. Allen, T. M. Falconer, M. E. Cisper, A. J. Borgerding, and C. W. Wilkerson, "Real-time analysis of methanol in air and water by membrane introduction mass spectrometry," *Analytical Chemistry*, vol. 73, no. 20, pp. 4830–4835, 2001.

[18] T. A. Blake, X. Zheng, T. Aggerholm, F. R. Lauritsen, and R. G. Cooks, "Determination of pentachlorophenol by negative ion chemical ionization with membrane introduction mass spectrometry," *Analyst*, vol. 127, no. 11, pp. 1463–6, 2002.

[19] A. J. Thompson, A. S. Creba, R. M. Ferguson, E. T. Krogh, and C. G. Gill, "A coaxially heated membrane introduction mass spectrometry interface for the rapid and sensitive on-line measurement of volatile and semi-volatile organic contaminants in air and water at parts-per-trillion levels," *Rapid Communications in Mass Spectrometry*, vol. 20, no. 13, pp. 2000–2008, 2006.

[20] E. VanHassel and M. E. Bier, "An electrospray membrane probe for the analysis of volatile and semi-volatile organic compounds in water," *Rapid Communications in Mass Spectrometry*, vol. 21, no. 3, pp. 413–420, 2007.

[21] E. Sokol, K. E. Edwards, K. Qian, and R. G. Cooks, "Rapid hydrocarbon analysis using a miniature rectilinear ion trap mass spectrometer," *Analyst*, vol. 133, no. 8, pp. 1064–1071, 2008.

[22] C. Janfelt, R. Graesboll, and F. R. Lauritsen, "Characterization and optimization of membrane inlets for a miniature ion trap mass spectrometer operating at a high background pressure of humid air," *International Journal of Mass Spectrometry*, vol. 276, no. 1, pp. 17–23, 2008.

[23] J. M. Etzkorn, N. G. Davey, A. J. Thompson, A. S. Creba, C. W. Leblanc, C. D. Simpson, E. T. Krogh, and C. G. Gill, "The use of MIMS-MS-MS in field locations as an on-line quantitative environmental monitoring technique for trace contaminants in air and water," *J Chromatogr Sci*, vol. 47, no. 1, pp. 57–66, 2009.

[24] N. L. Sanders, E. Sokol, R. H. Perry, G. M. Huang, R. J. Noll, J. S. Duncan, and R. G. Cooks, "Hand-held mass spectrometer for environmentally relevant analytes using a variety of sampling and ionization methods," *European Journal of Mass Spectrometry*, vol. 16, no. 1, pp. 11–20, 2010.

[25] K. D. Duncan, E. P. B. McCauley, E. T. Krogh, and C. G. Gill, "Characterization of a condensed-phase membrane introduction mass spectrometry

(CP-MIMS) interface using a methanol acceptor phase coupled with electrospray ionization for the continuous on-line quantitation of polar, low-volatility analytes at trace levels in complex aqueous samples," *Rapid Communications in Mass Spectrometry*, vol. 25, no. 9, pp. 1141–1151, 2011.

[26] R. Sparrapan, M. N. Eberlin, and R. M. Alberici, "Quantitation of trace phenolic compounds in water by trap-and-release membrane introduction mass spectrometry after acetylation," *Rapid Communications in Mass Spectrometry*, vol. 22, no. 24, pp. 4105–4108, 2008.

[27] C. D. F. Milagre, H. M. S. Milagre, J. A. R. Rodrigues, L. L. Rocha, L. S. Santos, and M. N. Eberlin, "On-line monitoring of bioreductions via membrane introduction mass spectrometry," *Biotechnology and Bioengineering*, vol. 90, no. 7, pp. 888–892, 2005.

[28] R. Clinton, C. S. Creaser, and D. Bryant, "Real-time monitoring of a pharmaceutical process reaction using a membrane interface combined with atmospheric pressure chemical ionisation mass spectrometry," *Analytica Chimica Acta*, vol. 539, no. 1-2, pp. 133–140, 2005.

[29] F. R. Lauritsen, A. Jensen, and C. H. Nielsen, "Fast and direct screening of solid materials for their potential liberation of hydrophobic organic compounds using hot cell membrane inlet mass spectrometry," *Rapid Communications in Mass Spectrometry*, vol. 22, no. 14, pp. 2234–2240, 2008.

[30] R. Haddad, R. Sparrapan, T. Kotiaho, and M. N. Eberlin, "Easy ambient sonic-spray ionization-membrane interface mass spectrometry for direct analysis of solution constituents," *Analytical Chemistry*, vol. 80, no. 3, pp. 898–903, 2008.

[31] H. Chen, Z. N. Xia, S. Pedersen-Bjergaard, B. Svensmark, and F. R. Lauritsen, "Analysis of semivolatile pharmaceuticals and pollutants in organic micro extracts using hot cell membrane inlet mass spectrometry," *Analytical Chemistry*, vol. 81, no. 10, pp. 4010–4014, 2009.

[32] F. R. Lauritsen and K. Nielsen, "Fast and direct recognition of the active ingredients in tablets using hot cell membrane inlet mass spectrometry," *International Journal of Mass Spectrometry*, vol. 295, no. 3, pp. 119–123, 2010.

[33] M. A. Mendes and M. N. Eberlin, "Trace level analysis of VOCs and semi-VOCs in aqueous solution using a direct insertion membrane probe and trap and release membrane introduction mass spectrometry," *Analyst*, vol. 125, no. 1, pp. 21–24, 1999.

[34] F. R. Lauritsen and J. Rose, "Determination of steroid hormones by membrane inlet mass spectrometry and desorption chemical ionization," *Analyst*, vol. 125, no. 9, pp. 1577–1581, 2000.

[35] L. S. Riter, L. Charles, M. Turowski, and R. G. Cooks, "External interface for trap-and-release membrane introduction mass spectrometry applied to the detection of inorganic chloramines and chlorobenzenes in water," *Rapid Communications in Mass Spectrometry*, vol. 15, no. 23, pp. 2290–2295, 2001.

[36] T. Aggerholm and F. R. Lauritsen, "Direct detection of polyaromatic hydrocarbons, estrogenic compounds and pesticides in water using desorption chemical ionisation membrane inlet mass spectrometry," *Rapid Communications in Mass Spectrometry*, vol. 15, no. 19, pp. 1826–1831, 2001.

[37] C. S. Creaser, D. G. Lamarca, L. M. dos Santos, A. P. New, and P. A. James, "A universal temperature controlled membrane interface for the analysis of volatile and semi-volatile organic compounds," *Analyst*, vol. 128, no. 9, pp. 1150–6, 2003.

[38] A. S. Creba, A. N. E. Weissfloch, E. T. Krogh, and C. G. Gill, "An enzyme derivatized polydimethylsiloxane (PDMS) membrane for use in membrane introduction mass spectrometry (MIMS)," *Journal of the American Society for Mass Spectrometry*, vol. 18, no. 6, pp. 973–979, 2007.

[39] C. S. Creaser, D. G. Lamarca, J. Brum, C. Werner, A. P. New, and L. M. F. dos Santos, "Reversed-phase membrane inlet mass spectrometry applied to the real-time monitoring of low molecular weight alcohols in chloroform," *Analytical Chemistry*, vol. 74, no. 1, pp. 300–304, 2002.

[40] M. Gernatova, P. Janderka, A. Marcinkova, and P. Ostrizek, "Use of nafion as a membrane separator in membrane introduction mass spectrometry," *European Journal of Mass Spectrometry*, vol. 15, no. 5, pp. 571–577, 2009.

[41] C. Janfelt, H. Frandsen, and F. R. Lauritsen, "Characterization of a mini membrane inlet mass spectrometer for on-site detection of contaminants in both aqueous and liquid organic samples," *Rapid Communications in Mass Spectrometry*, vol. 20, no. 9, pp. 1441–1446, 2006.

[42] L. D. Miranda, R. T. Short, F. H. W. van Amerom, R. J. Bell, and R. H. Byrne, "Direct coupling of a carbon nanotube membrane to a mass spectrometer: Contrasting nanotube and capillary tube introduction systems," *Journal of Membrane Science*, vol. 344, no. 1-2, pp. 26–31, 2009.

[43] K. Y. Hou, J. D. Wang, and H. Y. Li, "A new membrane inlet interface of a vacuum ultraviolet lamp ionization miniature mass spectrometer for on-line rapid measurement of volatile organic compounds in air," *Rapid Communications in Mass Spectrometry*, vol. 21, no. 22, pp. 3554–3560, 2007.

[44] H. Oser, M. J. Coggiola, S. E. Young, D. R. Crosley, V. Hafer, and G. Grist, "Membrane introduction/laser photoionization time-of-flight mass spectrometry," *Chemosphere*, vol. 67, no. 9, pp. 1701–1708, 2007.

[45] T. M. Allen, M. E. Cisper, P. H. Hemberger, and C. W. Wilkerson, "Simultaneous detection of volatile, semivolatile organic compounds, and organometallic compounds in both air and water matrices by using membrane introduction mass spectrometry," *International Journal of Mass Spectrometry*, vol. 212, no. 1-3, pp. 197–204, 2001.

[46] M. Alexander, E. Boscaini, W. Lindinger, and T. D. Mark, "Membrane introduction proton-transfer reaction mass spectrometry," *International Journal of Mass Spectrometry*, vol. 223, no. 1-3, pp. 763–770, 2003.

[47] F. Wedian and D. B. Atkinson, "Membrane introduction mass spectrometry of nonpolar hydrocarbons using nitric oxide chemical ionization," *Environmental Science & Technology*, vol. 37, no. 19, pp. 4425–4428, 2003.

[48] F. Alwedian and K. Abu-Shandi, "Improving the selectivity of non-polar alkanes, alkenes, and aromatic hydrocarbon compounds by the application of acetonitrile as a CI reagent," *Central European Journal of Chemistry*, vol. 7, no. 3, pp. 312–316, 2009.

[49] L. Gao, Q. Y. Song, G. E. Patterson, R. G. Cooks, and Z. Ouyang, "Handheld rectilinear ion trap mass spectrometer," *Analytical Chemistry*, vol. 78, no. 17, pp. 5994–6002, 2006.

[50] L. S. Riter, E. C. Meurer, E. S. Handberg, B. C. Laughlin, H. Chen, G. E. Patterson, M. N. Eberlin, and R. G. Cooks, "Ion/molecule reactions performed in a miniature cylindrical ion trap mass spectrometer," *Analyst*, vol. 128, no. 9, pp. 1112–1118, 2003.

[51] P. D. Tortell, "Dissolved gas measurements in oceanic waters made by membrane inlet mass spectrometry," *Limnology and Oceanography-Methods*, vol. 3, pp. 24–37, 2005.

[52] G. H. Kristensen, M. M. Klausen, V. A. Hansen, and F. R. Lauritsen, "On-line monitoring of the dynamics of trihalomethane concentrations in a warm public swimming pool using an unsupervised membrane inlet mass spectrometry system with off-site real-time surveillance," *Rapid Communications in Mass Spectrometry*, vol. 24, no. 1, pp. 30–34, 2010.

[53] G. P. G. Kibelka, R. T. Short, S. K. Toler, J. E. Edkins, and R. H. Byrne, "Field-deployed underwater mass spectrometers for investigations of transient chemical systems," *Talanta*, vol. 64, no. 4, pp. 961–969, 2004.

[54] R. T. Short, S. K. Toler, G. P. G. Kibelka, D. T. R. Roa, R. J. Bell, and R. H. Byrne, "Detection and quantification of chemical plumes using a portable underwater membrane introduction mass spectrometer," *Trac-Trends in Analytical Chemistry*, vol. 25, no. 7, pp. 637–646, 2006.

[55] R. Camilli and H. F. Hemond, "Nereus/kemonaut, a mobile autonomous underwater mass spectrometer," *Trac-Trends in Analytical Chemistry*, vol. 23, no. 4, pp. 307–313, 2004.

[56] C. Janfelt, F. R. Lauritsen, S. K. Toler, R. J. Bell, and R. T. Short, "Method for quantification of chemicals in a pollution plume using a moving membrane-based sensor exemplified by mass spectrometry," *Analytical Chemistry*, vol. 79, no. 14, pp. 5336–5342, 2007.

[57] H. E. Hartnett and S. P. Seitzinger, "High-resolution nitrogen gas profiles in sediment porewaters using a new membrane probe for membrane-inlet mass spectrometry," *Marine Chemistry*, vol. 83, no. 1-2, pp. 23–30, 2003.

[58] L. Askaer, B. Elberling, R. N. Glud, M. Kuhl, F. R. Lauritsen, and H. R. Joensen, "Soil heterogeneity effects on O_2 distribution and ch_4 emissions from wetlands: In situ and mesocosm studies with planar O_2 optodes and membrane inlet mass spectrometry," *Soil Biology & Biochemistry*, vol. 42, no. 12, pp. 2254–2265, 2010.

[59] H. Frandsen, C. Janfelt, and F. R. Lauritsen, "Fast and direct screening of polyaromatic hydrocarbon (PAH)-contaminated sand using a miniaturized membrane inlet mass spectrometer (mini-MIMS)," *Rapid Communications in Mass Spectrometry*, vol. 21, no. 10, pp. 1574–1578, 2007.

[60] M. Schluter and T. Gentz, "Application of membrane inlet mass spectrometry for online and in situ analysis of methane in aquatic environments," *Journal of the American Society for Mass Spectrometry*, vol. 19, no. 10, pp. 1395–1402, 2008.

[61] C. G. Laing, T. G. Shreeve, and D. M. E. Pearce, "Methane bubbles in surface peat cores: in situ measurements," *Global Change Biology*, vol. 14, no. 4, pp. 916–924, 2008.

[62] L. S. Riter, B. C. Laughlin, E. Nikolaev, and R. G. Cooks, "Direct analysis of volatile organic compounds in human breath using a miniaturized cylindrical ion trap mass spectrometer with a membrane inlet," *Rapid Communications in Mass Spectrometry*, vol. 16, no. 24, pp. 2370–2373, 2002.

[63] R. Haddad, M. A. Mendes, N. F. Hoehr, and M. N. Eberlin, "Amino acid quantitation in aqueous matrices via trap and release membrane introduction mass spectrometry: homocysteine in human plasma," *Analyst*, vol. 126, no. 8, pp. 1212–1215, 2001.

[64] C. Gabel-Jensen, S. A. Bak, F. R. Lauritsen, H. R. Hansen, L. Badolo, and B. Gammelgaard, "In situ identification of dimethyl diselenide in hepatocytes treated with methylseleninic acid by membrane inlet mass spectrometry," *Journal of Analytical Atomic Spectrometry*, vol. 24, no. 7, pp. 949–952, 2009.

[65] K. Beckmann, J. Messinger, M. R. Badger, T. Wydrzynski, and W. Hillier, "On-line mass spectrometry: membrane inlet sampling," *Photosynthesis Research*, vol. 102, no. 2-3, pp. 511–522, 2009.

[66] A. J. Thompson, J. M. Etzkorn, D. M. van Pel, E. T. Krogh, D. R. Drakeford, and C. G. Gill, "Membrane introduction tandem mass spectrometry (MIMS-MS/MS) as a real-time monitor for biogenic volatile organic compound (bvoc) emissions from plants," *Canadian Journal of Analytical Sciences and Spectroscopy*, vol. 53, no. 2, pp. 75–81, 2008.

[67] B. Dunges, J. Karmrodt, J. E. Baumgardner, and K. Markstaller, "Ventilation-perfusion distributions in the lungs. a novel technique for rapid measurement," *Anaesthesist*, vol. 56, no. 6, pp. 612–616, 2007.

[68] C. I. Davidson, R. F. Phalen, and P. A. Solomon, "Airborne particulate matter and human health: A review," *Aerosol Sci. Technol.*, vol. 39, pp. 737–749, 2005.

[69] L. P. Naeher, M. Brauer, M. Lipsett, J. T. Zelikoff, C. D. Simpson, J. Q. Koenig, and K. R. Smith, "Woodsmoke health effects: A review," *Inhalation Toxicology*, vol. 19, no. 1, pp. 67–106, 2007.

[70] USEPA, "National-scale air toxics assessment for 1996," Available at http://nepis.epa.gov/Exe/ZyPURL.cgi?Dockey=2000NQFK.txt (accessed April 2012).

[71] V. C. Van Hee, S. D. Adar, A. A. Szpiro, R. G. Barr, D. A. Bluemke, A. V. Diez Roux, E. A. Gill, L. Sheppard, and J. D. Kaufman, "Exposure to traffic and left ventricular mass and function: The multi-ethnic study of atherosclerosis," *American Journal of Respiratory and Critical Care Medicine*, vol. 179, no. 9, pp. 827–834, 2009.

[72] R. Dales, A. Wheeler, M. Mahmud, A. Frescura, M. Smith-Doiron, E. Nethery, and L. Liu, "The influence of living near roadways on spirometry and exhaled nitric oxide in elementary schoolchildren," *Environ Health Perspectives*, vol. 116, no. 10, pp. 1423–1427, 2008.

[73] B. Brunekreef, N. Janssen, J. de Hartog, H. Harssema, M. Knape, and P. van Vliet, "Air pollution from truck traffic and lung function in children living near motorways," *Epidemiology*, vol. 8, no. 3, pp. 298–303, 1997.

[74] A. A. Karner, D. S. Eisinger, and D. A. Niemeier, "Near-roadway air quality: Synthesizing the findings from real-world data," *Environmental Science & Technology*, vol. 44, no. 14, pp. 5334–5344, 2010.

[75] C. Monn, V. Carabias, M. Junker, R. Waeber, M. Karrer, and H. U. Wanner, "Small-scale spatial variability of particulate matter <10 μm (PM10) and nitrogen dioxide," *Atmospheric Environment*, vol. 31, no. 15, pp. 2243–2247, 1997.

[76] L. B. Westover, J. C. Tou, and J. H. Mark, "Novel mass spectrometric sampling device-hollow fiber probe," *Analytical Chemistry*, vol. 46, no. 4, pp. 568–571, 1974.

[77] M. E. Cisper, C. G. Gill, L. E. Townsend, and P. H. Hemberger, "On-line detection of volatile organic compounds in air at parts-per-trillion levels by membrane introduction mass spectrometry," *Analytical Chemistry*, vol. 67, no. 8, pp. 1413–7, 1995.

[78] M. Soni, S. Bauer, J. W. Amy, P. Wong, and R. G. Cooks, "Direct determination of organic compounds in water at parts-per-quadrillion levels by membrane introduction mass spectrometry," *Analytical Chemistry*, vol. 67, no. 8, pp. 1409–12, 1995.

[79] N. G. Davey, E. T. Krogh, and C. G. Gill, "Membrane introduction mass spectrometry (MIMS)," *Trends in Analytical Chemistry*, vol. 30, no. 9, pp. 1477–1485, 2011.

[80] A. Feilberg, A. P. S. Adamsen, S. Lindholst, M. Lyngbye, and A. Schafer, "Evaluation of biological air filters for livestock ventilation air by membrane inlet mass spectrometry," *Journal of Environmental Quality*, vol. 39, no. 3, pp. 1085–1096, 2010.

[81] A. W. Norgaard, K. A. Jensen, C. Janfelt, F. R. Lauritsen, P. A. Clausen, and P. Wolkoff, "Release of VOCs and particles during use of nanofilm spray products," *Environmental Science & Technology*, vol. 43, no. 20, pp. 7824–7830, 2009.

[82] . USEPA, 1999 National-Scale Air Toxics Assessment: 1999 Data Tables http://www.epa.gov/ttn/atw/nata1999/tables.html (accessed April 20 government document, 1999.

[83] . USEPA, 2009 Areas Designated under the 2006 Air Quality Standards http://www.epa.gov/pmdesignations/2006standards/rec/region10R.htm (accessed April 20, 2009.

[84] T. Larson, S. B. Henderson, and M. Brauer, "Mobile monitoring of particle light absorption coefficient in an urban area as a basis for land use regression," *Environmental Science & Technology*, vol. 43, no. 13, pp. 4672–4678, 2009.

[85] M. Gilroy and M. Yost, "Tacoma and Seattle area air toxics evaluation," 2010.

[86] Y. Liu, M. Shao, L. L. Fu, S. H. Lu, L. M. Zeng, and D. G. Tang, "Source profiles of volatile organic compounds (VOCs) measured in ChinaPart I," *Atmospheric Environment*, vol. 42, no. 25, pp. 6247–6260, 2008.

[87] I. J. Simpson, N. J. Blake, B. Barletta, G. S. Diskin, H. E. Fuelberg, K. Gorham, L. G. Huey, S. Meinardi, F. S. Rowland, S. A. Vay, A. J. Weinheimer, M. Yang, and D. R. Blake, "Characterization of trace gases measured over Alberta oil sands mining operations: 76 speciated C_2–C_{10} volatile organic compounds (VOCs), CO_2, CH_4, CO, NO, NO_2, NO_y, O_3 and SO_2," *Atmospheric Chemistry and Physics*, vol. 10, no. 23, pp. 11931–11954, 2010.

[88] "Joint community update: Reporting on our environmental activities to the community, Wood Buffalo Environmental Association, cummulative environmental management association and regional aquatics monitoring program, Edmonton, Alberta, Canada," report, 2008.

[89] "An assessment of the environmental implications of oil and gas production: A regional case study, United States Environmental Protection Agency, 2008.," report, 2008.

[90] L. M. McKenzie, R. Z. Witter, L. S. Newman, and J. L. Adgate, "Human health risk assessment of air emissions from development of unconventional natural gas resources," *Science of the Total Environment*, vol. 424, pp. 79–87, 2012.

[91] A. K. Chambers, M. Strosher, T. Wootton, J. Moncrieff, and P. McCready, "Direct measurement of fugitive emissions of hydrocarbons from a refinery," *Journal of the Air & Waste Management Association*, vol. 58, no. 8, pp. 1047–1056, 2008.

[92] R. Camilli and A. N. Duryea, "Characterizing spatial and temporal variability of dissolved gases in aquatic environments with in situ mass spectrometry," *Environmental Science & Technology*, vol. 43, no. 13, pp. 5014–5021, 2009.

[93] E. N. Kelly, J. W. Short, D. W. Schindler, P. V. Hodson, M. S. Ma, A. K. Kwan, and B. L. Fortin, "Oil sands development contributes polycyclic aromatic compounds to the athabasca river and its tributaries," *Proceedings of the National Academy of Sciences of the United States of America*, vol. 106, no. 52, pp. 22346–22351, 2009.

[94] C. Groat and T. Grimshaw, "Fact based regulation for environmental protection in shale gas development, the energy institute, austin, texas, 2012," report, 2012.

[95] D. A. Lane, "Mobile mass-spectrometry," *Environmental Science & Technology*, vol. 16, no. 1, pp. A38–A46, 1982.

[96] S. Taylor and V. M. Bierbaum, "Focus on harsh environment mass spectrometry," *Journal of the American Society for Mass Spectrometry*, vol. 19, no. 10, pp. 1375–1376, 2008.

[97] S. C. Herndon, J. T. Jayne, M. S. Zahniser, D. R. Worsnop, B. Knighton, E. Alwine, B. K. Lamb, M. Zavala, D. D. Nelson, J. B. McManus, J. H. Shorter, M. R. Canagaratna, T. B. Onasch, and C. E. Kolb, "Characterization of urban pollutant emission fluxes and ambient concentration distributions using a mobile laboratory with rapid response instrumentation," *Faraday Discussions*, vol. 130, pp. 327–339, 2005.

[98] C. Guimbaud, V. Catoire, S. Gogo, C. Robert, M. Chartier, F. Laggoun-Defarge, A. Grossel, P. Alberic, L. Pomathiod, B. Nicoullaud, and G. Richard, "A portable infrared laser spectrometer for flux measurements of trace gases at the geosphere-atmosphere interface," *Measurement Science & Technology*, vol. 22, no. 7, 2011.

[99] G. Petron, G. Frost, B. R. Miller, A. I. Hirsch, S. A. Montzka, A. Karion, M. Trainer, C. Sweeney, A. E. Andrews, L. Miller, J. Kofler, A. Bar-Ilan, E. J. Dlugokencky, L. Patrick, C. T. Moore, T. B. Ryerson, C. Siso, W. Kolodzey, P. M. Lang, T. Conway, P. Novelli, K. Masarie, B. Hall, D. Guenther, D. Kitzis, J. Miller, D. Welsh, D. Wolfe, W. Neff, and P. Tans, "Hydrocarbon emissions characterization in the Colorado Front Range: A pilot study," *Journal of Geophysical Research-Atmospheres*, vol. 117, 2012.

[100] R. G. Cooks and T. Mueller, "Through a glass darkly: glimpses into the future of mass spectrometry," *Mass Spectrom (Tokyo)*, vol. 2, no. Spec Iss, p. S0001, 2013.

[101] N. G. Davey, C. T. E. Fitzpatrick, J. M. Etzkorn, M. Martinsen, R. S. Crampton, G. D. Onstad, T. V. Larson, M. G. Yost, E. T. Krogh, M. Gilroy, K. H. Himes, E. T. Saganic, C. D. Simpson, and C. G. Gill, "Measurement of spatial and temporal variation in volatile hazardous air pollutants in tacoma, wa using a mobile membrane introduction mass spectrometry (MIMS) system," *Journal of Environmental Science and Health Part a-Toxic/Hazardous Substances & Environmental Engineering*, vol. 49, pp. 1199–1208, 2014.

[102] W. Lindinger, A. Hansel, and A. Jordan, "Proton-transfer-reaction mass spectrometry (PTR-MS): on-line monitoring of volatile organic compounds at pptv levels," *Chemical Society Reviews*, vol. 27, no. 5, pp. 347–354, 1998.

[103] Z. Ouyang, R. J. Noll, and R. G. Cooks, "Handheld miniature ion trap mass spectrometers," *Analytical Chemistry*, vol. 81, no. 7, pp. 2421–2425, 2009.

[104] R. Camilli, C. M. Reddy, D. R. Yoerger, B. A. S. Van Mooy, M. V. Jakuba, J. C. Kinsey, C. P. McIntyre, S. P. Sylva, and J. V. Maloney, "Tracking hydrocarbon plume transport and biodegradation at deepwater horizon," *Science*, vol. 330, no. 6001, pp. 201–204, 2010.

[105] B. Brkic, N. France, and S. Taylor, "Oil-in-water monitoring using membrane inlet mass spectrometry," *Analytical Chemistry*, vol. 83, no. 16, pp. 6230–6, 2011.

[106] F. L. Overney and C. G. Enke, "A mathematical study of sample modulation at a membrane inlet mass spectrometer - potential application for the analysis of mixtures," *J Am Soc Mass Spectrom*, vol. 7, pp. 93–100, 1996.

[107] A. Jordan, S. Haidacher, G. Hanel, E. Hartungen, J. Herbig, L. Mark, R. Schottkowsky, H. Seehauser, P. Sulzer, and T. D. Mark, "An online ultra-high sensitivity proton-transfer-reaction mass-spectrometer combined with switchable reagent ion capability (PTR+SRI-MS)," *International Journal of Mass Spectrometry*, vol. 286, no. 1, pp. 32–38, 2009.

[108] B. J. Prince, D. B. Milligan, and M. J. McEwan, "Application of selected ion flow tube mass spectrometry to real-time atmospheric monitoring," *Rapid Communications in Mass Spectrometry*, vol. 24, no. 12, pp. 1763–1769, 2010.

[109] D. Smith and P. Spanel, "Selected ion flow tube mass spectrometry (SIFT-MS) for on-line trace gas analysis," *Mass Spectrometry Reviews*, vol. 24, no. 5, pp. 661–700, 2005.

[110] C. H. Yang, N. A. Khan, and H. F. Wu, "Differentiation and quantification of xylene by combining headspace solid-phase microextraction/gas chromatography and self-ion molecule reaction in an ion trap tandem mass spectrometry," *Journal of Separation Science*, vol. 31, no. 16-17, pp. 3050–3057, 2008.

[111] J. H. Nelson, D. A. Friesen, C. G. Gill, and E. T. Krogh, "On-line measurement of oxidative degradation kinetics for trace gasoline contaminants in aqueous solutions and natural water by membrane introduction tandem mass spectrometry," *J Environ Sci Health A Tox Hazard Subst Environ Eng*, vol. 45, no. 13, pp. 1720–31, 2010.

[112] R. Schwarzenbach, P. Gschwend, and D. Imboden, *Environmental Organic Chemistry*. New York: John Wiley & Sons, 1993.

[113] "National institute of standards and technology," 2012.

[114] J. Kaspar, P. Fornasiero, and N. Hickey, "Automotive catalytic converters: current status and some perspectives," *Catalysis Today*, vol. 77, no. 4, pp. 419–449, 2003.

[115] E. Gasthauer, M. Maze, J. P. Marchand, and J. Amouroux, "Characterization of asphalt fume composition by gc/ms and effect of temperature," *Fuel*, vol. 87, no. 7, pp. 1428–1434, 2008.

[116] G. M. Huang, L. Gao, J. Duncan, J. D. Harper, N. L. Sanders, Z. Ouyang, and R. G. Cooks, "Direct detection of benzene, toluene, and ethylbenzene at trace levels in ambient air by atmospheric pressure chemical ionization using a handheld mass spectrometer," *Journal of the American Society for Mass Spectrometry*, vol. 21, no. 1, pp. 132–135, 2010.

[117] R. Atkinson, "Atmospheric chemistry of VOCs and NO(x)," *Atmospheric Environment*, vol. 34, no. V, pp. 2063–2101, 2000.

[118] M. L. Wesely and B. B. Hicks, "A review of the current status of knowledge on dry deposition," *Atmospheric Environment*, vol. 34, pp. 2261–2282, 2000.

[119] E. Woolfenden, "Monitoring VOCs in Air Using Sorbent Tubes Followed by Thermal Desorption-Capillary GC Analysis: Summary of Data and Practical Guidelines," *Journal of the Air & Waste Management Association*, vol. 47, no. 1, pp. 20–36, 1997.

[120] G. Ouyang and J. Pawliszyn, "Recent developments in SPME for on-site analysis and monitoring," *TrAC Trends in Analytical Chemistry*, vol. 25, no. 7, pp. 692–703, 2006.

[121] F. R. Lauritsen and T. Kotiaho, "Advances in membrane inlet mass spectrometry (MIMS)," *Reviews in Analytical Chemistry*, vol. 15, pp. 237–264, 1996.

[122] I. J. Simpson, J. E. Marrero, S. Batterman, S. Meinardi, B. Barletta, and D. R. Blake, "Air quality in the Industrial Heartland of Alberta, Canada and potential impacts on human health," *Atmospheric Environment*, vol. 81, pp. 702–709, 2013.

[123] K. Badjagbo, S. Moore, and S. Sauve, "Real-time continuous monitoring methods for airborne VOCs," *Trac-Trends in Analytical Chemistry*, vol. 26, no. 9, pp. 931–940, 2007.

[124] R. J. Bell, N. G. Davey, M. Martinsen, C. Collin-Hansen, E. T. Krogh, and C. G. Gill, "A field-portable membrane introduction mass spectrometer for real-time quantitation and spatial mapping of atmospheric and aqueous contaminants," *Journal of the American Society for Mass Spectrometry*, vol. 26, no. 2, pp. 212–223, 2015.

[125] R. J. Bell, N. G. Davey, M. Martinsen, R. Short, C. G. Gill, and E. T. Krogh, "The Effect of the Earths and Stray Magnetic Fields on Mobile Mass Spectrometer Systems," *Journal of The American Society for Mass Spectrometry*, vol. 26, no. 2, pp. 201–211, 2015.

[126] N. G. Davey, R. J. Bell, E. T. Krogh, and C. G. a. Gill, "A membrane introduction mass spectrometer utilizing ion-molecule reactions for the on-line speciation and quantitation of volatile organic molecules," *Rapid Communications in Mass Spectrometry*, vol. 29, pp. 2187–2194, 2015.

[127] R. J. Bell, R. T. Short, F. H. W. Van Amerom, and R. H. Byrne, "Calibration of an in situ membrane inlet mass spectrometer for measurements of dissolved gases and volatile organics in seawater," *Environmental Science & Technology*, vol. 41, no. 23, pp. 8123–8128, 2007.

[128] R. J. Bell, R. T. Short, and R. H. Byrne, "In situ determination of total dissolved inorganic carbon by underwater membrane introduction mass spectrometry," *Limnology and Oceanography-Methods*, vol. 9, pp. 164–175, 2011.

[129] J. A. Diaz, D. Pieri, C. R. Arkin, E. Gore, T. P. Griffin, M. Fladeland, G. Bland, C. Soto, Y. Madrigal, D. Castillo, E. Rojas, and S. Achi, "Utilization of in situ airborne MS-based instrumentation for the study of gaseous emissions at active volcanoes," *International Journal of Mass Spectrometry*, vol. 295, no. 3, pp. 105–112, 2010.

[130] R. T. Short, D. P. Fries, and M. L. Kerr, "Influence of the earths magnetic field on portable mass spectrometers," *Proceedings of the 12th Sanibel Conference on Mass Spectrometry*, Sanibel Island, Florida, 22-25 Jan, 2000.

[131] O. M. N. D. Teodoro, J. A. M. C. Silva, and A. M. C. Moutinho, "Multitechnique surface-analysis system - apparatus description," *Vacuum*, vol. 46, no. 8-10, pp. 1205–1209, 1995.

[132] F. Poppenk, R. Amini, and G. Brouwer, "Design and application of a helmholtz cage for testing nano-satellites," 2007.

[133] S. Goldwasser, "TV and monitor CRT (picture tube) information (v2.02)," Samuel M. Goldwaser, 1998.

[134] R. T. Short, D. P. Fries, S. K. Toler, C. E. Lembke, and R. H. Byrne, "Development of an underwater mass-spectrometry system for in situ chemical analysis," *Measurement Science & Technology*, vol. 10, no. 12, pp. 1195–1201, 1999.

[135] R. O. Jenkins, "A review of thermionic cathodes," *Vacuum*, vol. 19, no. 8, pp. 353–359, 1969.

[136] R. Kiser, *Introduction to Mass Spectrometry and Its Applicaitons*. Prentice-Hall, Inc., second ed., 1965.

[137] R. E. Honig, "Ionization potentials of some hydrocarbon series," *Journal of Chemical Physics*, vol. 16, no. 2, pp. 105–112, 1948.

[138] H. Orsnes, S. Bohatka, and H. Degn, "Reaction of water at hot filament interferes with measurements of dissolved gases by membrane inlet mass spectrometry," *Rapid Communications in Mass Spectrometry*, vol. 11, no. 15, pp. 1736–1738, 1997.

[139] N. Karellas and Q. Chen, "Real-time air monitoring of trichloroethylene and tetrachloroethylene using mobile taga mass spectrometry," *Journal of Environmental Protection*, vol. 4, p. 99, 2013.

[140] M. A. LaPack, J. C. Tou, and C. G. Enke, "Membrane mass spectrometry for the direct trace analysis of volatile organic compounds in air and water," *Analytical Chemistry*, vol. 62, pp. 1265–1271, 1990.

[141] R. A. Ketola, T. Mansikka, M. Ojala, T. Kotiaho, and R. Kostiainen, "Analysis of volatile organic sulfur compounds in air by membrane inlet mass spectrometry," *Analytical Chemistry*, vol. 69, no. 22, pp. 4536–4539, 1997.

[142] J. Gross, *Mass Spectrometry: A Textbook*. Springer Science & Business Media, 2004.

[143] J. S. Brodbelt and R. G. Cooks, "An exceedingly simple mass spectrometer interface with application to reaction monitoring and environmental analysis," *Analytical Chemistry*, vol. 57, pp. 1153–1155, 1985.

[144] F. R. Lauritsen, T. K. Choudhury, L. E. Dejarme, and R. G. Cooks, "Microporous membrane introduction mass-spectrometry with solvent chemical ioniza-

tion and glow-discharge for the direct detection of volatile organic compounds in aqueous solution," *Analytica Chimica Acta*, vol. 266, no. 1, pp. 1–12, 1992.

[145] F. R. Lauritsen, T. Kotiaho, T. K. Choudhury, and R. G. Cooks, "Direct detection and identification of volatile organic compounds dissolved in organic solvents by reversed-phase membrane introduction tandem mass spectrometry," *Analytical Chemistry*, vol. 64, no. 11, pp. 1205–1211, 1992.

[146] M. E. Cisper, A. W. Garrett, and P. H. Hemberger, "Analysis of polar organic compounds using charge exchange ionization and membrane introduction mass spectrometry," *Analytical Chemistry*, vol. 68, p. 2097, 1996.

[147] A. Colorado, D. J. J. Barket, J. M. Hurst, and P. B. Shepson, "A fast-response method for determination of atmospheric isoprene using quadrupole ion trap mass spectrometry," *Analytical Chemistry*, vol. 70, pp. 5129–5135, 1998.

[148] F. Wedian and D. B. Atkinson, "Ozone modulation of volatile hydrocarbons using membrane introduction mass spectrometry," *Environmental Science & Technology*, vol. 36, no. 19, pp. 4152–4155, 2002.

[149] E. Louarn, A. Hamrouni, C. Colbeau-Justin, L. Bruschi, J. Lemaire, M. Heninger, and H. Mestdagh, "Characterization of a membrane inlet interfaced with a compact chemical ionization FT-ICR for real-time and quantitative voc analysis in water," *International Journal of Mass Spectrometry*, vol. 353, pp. 26–35, 2013.

[150] J. S. Brodbelt, "Analytical applications of ion-molecule reactions," *Mass Spectrometry Reviews*, vol. 16, no. 2, pp. 91–110, 1997.

[151] R. J. Eismin, M. K. Fu, S. Yem, F. Widjaja, and H. I. Kenttamaa, "Identification of epoxide functionalities in protonated monofunctional analytes by using ion/molecule reactions and collision-activated dissociation in different ion trap tandem mass spectrometers," *Journal of the American Society for Mass Spectrometry*, vol. 23, no. 1, pp. 12–22, 2012.

[152] M. S. B. Munson and F. H. Field, "Chemical ionization mass spectrometry .i. general introduction," *Journal of the American Chemical Society*, vol. 88, no. 12, p. 2621, 1966.

[153] E. S. Eichmann and J. S. Brodbelt, "Functional group-selective ion molecule reactions of ethylene-glycol and its monomethyl and dimethyl ethers," *Journal of the American Society for Mass Spectrometry*, vol. 4, no. 2, pp. 97–105, 1993.

[154] S. Lias, J. Bartmess, J. Liebman, J. Holmes, R. Levin, and E. Mallard, "Ion energetics data," in *NIST Chemistry WebBook* (P. Linstrom and W. Mallard, eds.).

[155] G. I. Nemeth, H. L. Selzle, and E. W. Schlag, "Magnetic ZEKE experiments with mass analysis," *Chemical Physics Letters*, vol. 215, pp. 151–155, 1993.

[156] S. Fujisawa, K. Ohno, S. Masuda, and Y. Harada, "Penning ionization electron-spectroscopy of monohalogenobenzenes - C_6H_5F, C_6H_5Cl, C_6H_5Br, and C_6H_5I," *Journal of the American Chemical Society*, vol. 108, no. 21, pp. 6505–6511, 1986.

[157] C. Z. Wang, Y. Su, H. Y. Wang, and Y. L. Guo, "Gas chromatographic-ion trap mass spectrometric analysis of volatile organic compounds by ion-molecule reactions using the electron-deficient reagent ion CCl_3^+," *Journal of the American Society for Mass Spectrometry*, vol. 22, no. 10, pp. 1839–1850, 2011.

[158] F. A. Londry, R. L. Alfred, and R. E. March, "Computer-simulation of single-ion trajectories in Paul-type ion traps," *Journal of the American Society for Mass Spectrometry*, vol. 4, no. 9, pp. 687–705, 1993.

[159] R. K. Julian, M. Nappi, C. Weil, and R. G. Cooks, "Multiparticle simulation of ion motion in the ion-trap mass-spectrometer - resonant and direct-current pulse excitation," *Journal of the American Society for Mass Spectrometry*, vol. 6, no. 1, pp. 57–70, 1995.

[160] G. C. Stafford, P. E. Kelley, J. E. P. Syka, W. E. Reynolds, and J. F. J. Todd, "Recent improvements in and analytical applications of advanced ion trap technology," *International Journal of Mass Spectrometry and Ion Processes*, vol. 60, pp. 85–98, 1984.

[161] R. E. March and J. F. Todd, *Quadrupole Ion Trap Mass Spectrometry*. John Wiley & Sons, INC., 2005.

[162] J. Thomson, *Rays Of Positive Electricity and Their Application to Chemical Analysis*. London: Longman's Green and Company, 1913.

[163] F. Aston, "LXXIV. a positive ray spectrograph," *Philosophical Magazine Series 6*, vol. 38, no. 228, pp. 707–714, 1919.

[164] W. Johnson and A. Nier, "Atomic masses in the region Xenon to Europium," *Physical Review*, vol. 105, no. 3, pp. 1014–1023, 1957.

[165] E. Lawrence, "Method and apparatus for the acceleration of ions," Feb. 20 1934. US Patent 1,948,384.

[166] M. Dole, L. L. Mack, R. L. Hines, R. C. Mobley, L. D. Ferguson, and M. B. Alice, "Molecular beams of macroions," *The Journal of Chemical Physics*, vol. 49, no. 5, pp. 2240–2249, 1968.

[167] M. B. Comisarow and A. G. Marshall, "Fourier transform ion cyclotron resonance spectroscopy," *Chemical Physics Letters*, vol. 25, no. 2, pp. 282 – 283, 1974.

[168] J. B. Fenn, M. Mann, C. K. Meng, S. F. Wong, and C. M. Whitehouse, "Electrospray ionization for mass spectrometry of large biomolecules," *Science*, vol. 246, no. 4926, pp. 64–71, 1989.

[169] A. Makarov, "Electrostatic axially harmonic orbital trapping: a high-performance technique of mass analysis," *Analytical Chemistry*, vol. 72, no. 6, pp. 1156–1162, 2000.

[170] R. G. Cooks, Z. Ouyang, Z. Takats, and J. Wiseman, "Ambient mass spectrometry.," *The Analyst*, vol. 135, no. 4, pp. 659–660, 2010.

[171] R. E. March, "Quadrupole ion traps," *Mass Spectrometry Reviews*, vol. 28, no. 6, pp. 961–989, 2009.

[172] G. E. Patterson, A. J. Guymon, L. S. Riter, M. Everly, J. Griep-Raming, B. C. Laughlin, Z. Ouyang, and R. G. Cooks, "Miniature cylindrical ion trap mass spectrometer," *Analytical Chemistry*, vol. 74, no. 24, pp. 6145–6153, 2002.

[173] M. Baasandorj, D. B. Millet, L. Hu, D. Mitroo, and B. J. Williams, "Measuring acetic and formic acid by proton-transfer-reaction mass spectrometry: sensitivity, humidity dependence, and quantifying interferences," *Atmospheric Measurement Techniques*, vol. 8, no. 3, pp. 1303–1321, 2015.

[174] J. de Gouw and C. Warneke, "Measurements of volatile organic compounds in the earth's atmosphere using proton-transfer-reaction mass spectrometry.," *Mass Spectrometry Reviews*, vol. 26, no. 2, pp. 223–257, 2007.